

**Magnesium hydroxide derivatives as
stabilisers and flame retardants for
plasticised poly(vinyl chloride)**

by

DANIEL MATLHOMOLA MOLEFE



**Magnesium hydroxide derivatives as stabilisers and flame
retardants for plasticised poly(vinyl chloride)**

by

DANIEL MATLHOMOLA MOLEFE

A thesis submitted in partial fulfilment of the requirements for the degree

Doctor of Philosophy

In the

Department of Chemistry

Faculty of Natural and Agricultural Science

University of Pretoria

Pretoria

September 2015

Supervisor: Dr F.J.W.J Labuschagné

Co-Supervisor: Prof W.W. Focke

DECLARATION BY CANDIDATE

I, the undersigned, declare that the thesis that I hereby submit for the degree Doctor of Philosophy, at the University of Pretoria, is my contribution to research work done under the guidance of my two supervisors with assistance of others in generating the experimental data and has not previously been submitted for a degree or examination at this or any other institution of higher education.

Daniel Matlhomola Molefe

DEDICATIONS

This work is dedicated to my wife, Lebo, three children, Lesedi, Marang and Nhlanhla for their love continued support under, sometimes, very demanding circumstances.

My late parents, especially my mother Doreen, my late sister Lindi, for their never ending love and support, *may their soul rest in peace!*

Further, to my three brothers. Happy, Michael, Patrick and sister, Jabo for their unrelinquished faith in the primary purpose of our being and ever nearing metathesis in our lives that kept me focused on this objective. We all learnt a great deal over the past couple of years, which was dominated by the utmost of faith, determination and endurance.

Lastly, my in laws, Hosia “Tagolo”, Isabella “Koko”, Tselane, Valentine “Vali”, Carold “Carrey” Pheto and my inseparable friend Rainy Dladla. Thank you for recognising this opportunity that changed my whole life. I must say I was doing this whole research just to motivate and encourage our children, brothers and sisters that one should not give up in studying, it does not matter how old you are!

Without any one of you, this research would have been impossible.

Magnesium hydroxide derivatives as stabilisers and flame retardants for plasticised poly(vinyl chloride)

By

DANIEL MATLHOMOLA MOLEFE

Supervisor: Dr F.J.W.J. Labuschagné

Co-Supervisor: Prof W.W. Focke

Department of Chemistry

University of Pretoria

Doctor of Philosophy

September 2015

SYNOPSIS

The potential of magnesium hydroxide, hydromagnesite and layered double hydroxides (LDHs) as heat stabilisers and flame retardants for plasticised poly (vinylchloride) (PVC) was studied. These inorganic hydrated fillers feature flake-shaped particles with a strong tendency to agglomerate. Filler particles must be homogeneously distributed and individually dispersed in the polymer matrix in order to attain the best performance. For this reason the first step in the investigation was to explore the use of a stearic acid coating in order to improve the dispersability of these fillers in liquids. The platelet morphology-type flame retardants were coated with approximately a monolayer of stearic acid using a solvent technique. Compared to the uncoated powders, the BET surface area was lower, the powder packing density was improved, and the thickening effect on white oil was significantly reduced. The latter two observations were rationalised in terms of a reduction in the attractive interactions between the powder particles.

The viscosity of white oil slurries containing 25 wt.% solids showed shear-thinning non-Newtonian behaviour. The coated powders showed significantly lower viscosities at low shear rates although the difference diminished at high shear rates. The lower viscosities shown by the coated powders indicate that the surface modification facilitated the break-up of agglomerates and aided the dispersion of individual particles in the fluid.

The thermal decomposition of these hydrated fillers is central to their flame retardant action. At elevated temperatures they endothermically release inert gases. The latter dilute the atmosphere surrounding the burning sample while the endothermic decomposition cools the substrate. These two effects are responsible for

the flame retardant action of these fillers. The detailed behaviour of the present samples was studied using thermogravimetric analysis and spectroscopic methods. The decomposition mechanisms, proposed in the literature for these flame retardants, were confirmed. This includes the mass loss, enthalpy of decomposition, and the nature of evolved gases for temperatures up to 1 000 °C. The magnesium hydroxide decomposed endothermically at temperatures well above 250 °C releasing only steam. The LDH decomposed between 225 °C and 450 °C and the hydromagnesite between about 220 °C and 500 °C. Both initially released water vapour followed by carbon dioxide.

Next the utility of the magnesium hydroxide, hydromagnesite and LDH as combination heat stabilisers and flame retardants for plasticised PVC was studied. Emulsion grade PVC was plasticised with 100 parts per hundred parts of resin (phr) diisononyl phthalate (DINP) and filled with 30 parts per hundred parts of resin (phr) filler additive. Thermomat static heat stabilities were determined at 200 °C by following the time dependence of hydrogen chloride evolution. Fire retardancy was studied using a cone calorimeter at a radiant flux of 35 kW m⁻². The layered double hydroxide outperformed the other fillers with regard to improving heat stabilisation and also with respect to most fire retardancy indices.

Since the layered double hydroxide performed best it was decided to see whether slight composition variations could improve performance. Derivatives of the standard LDH compound ($[Mg_{0.667}Al_{0.333}(OH)_2](CO_3)_{0.167} \cdot 0.44H_2O$) were synthesised using a hydrothermal method. Again, emulsion grade PVC was plasticised with 100 phr diisononyl phthalate and stabilised with 30 phr of the LDH filler additive derivatives. The heat stability and fire resistance of these compounds were studied.

Heat stabilities were determined at 200 °C. The dynamic heat stability tests were performed on the plastisols using the torque rheometer method. Static heat stability was evaluated on the fused compounds. It was evaluated from discoloration profiles of strips exposed for various lengths of time to high heat in a Metrastat oven. The time dependence of hydrogen chloride evolution was followed with a Metrohm Thermomat instrument. The conventional LDH provided the best dynamic heat stability. However, partial replacement of the magnesium with copper significantly delayed the release of volatile HCl. If instead the replacement was done using zinc, better colour retention was achieved.

The fire performance was determined at a radiant flux of 35 kWm⁻² in a cone calorimeter. The conventional magnesium-aluminium LDH lowered the peak heat release rate of the plasticised PVC from 623 ± 8 kW m⁻² to 389 ± 9 kW m⁻² and reduced the smoke release by 37 %. Partial replacement of the aluminium with iron resulted in a red pigmented additive that was more effective as a flame retardant reducing the peak heat release rate (*pHRR*) to as little as 253 ± 5 kW m⁻². This additive also showed better smoke suppression (reduction of 44 %) but the best smoke suppression was achieved by replacing part of the magnesium with copper (reduction by 49 %).

Keywords: Layered double hydroxide; poly(vinyl chloride); heat stabiliser; thermal analysis; flame retardants; cone calorimeter.

ACKNOWLEDGEMENTS

I would like to thank several people, without whose support this work would not have been possible:

My supervisor, Dr F.J.W.J Labuschagné, for giving me input and guidance throughout the experiment and work. Thank you so much.

Other appreciations and gratitude go to my co-supervisor Prof WalterW Focke for his constructive ideas and support regarding this research. Thank you so much for not giving up on me. Please allow me to say this to you, **Walter** you are truly a **Motivator!**

My studymates at the Institute of Applied Materials (*IAM*), University of Pretoria, Herminio “Zapiro” Muiambo, Daniel Afonso Macheca, Dr Pedro Masinga Jr, Shephard Tichapondwa, Dr Mthokozisi Sibanda, Washington Mhike, Dr Shatish “Morewa” Ramjee. “Bro” Joel Lekitima, Dr Paul Ejikeme, Mr Katlego Makgopa from Chemistry department, I’ll forever treasure your inputs. Thanks guys! The microscopy, XRD, XPS, PSD, and Cone Calorimeter staff to name but a few for allowing us access to their instruments. Thank you for your support!

Chamotte Holdings (Pty.) Ltd. for their contributions of hydromagnesite and hydrotalcite powders and the financial assistance of Pretoria University towards this research is hereby acknowledged.

Finally, I owe special thanks to my wife, **Lebo**, for believing in me all the way through.

TABLE OF CONTENTS

DECLARATION BY CANDIDATE.....	ii
DEDICATIONS	iii
SYNOPSIS.....	v
ACKNOWLEDGEMENTS	viii
TABLE OF CONTENTS	ix
ORGANISATION OF THE THESIS	xv
LIST OF FIGURES	xviii
LIST OF TABLES.....	xxiii
LIST OF EQUATIONS.....	xxiv
SCHEME OF REACTIONS.....	xxiv
LIST OF ABBREVIATIONS.....	xxiv
LIST OF SYMBOLS	xxvi
LIST OF GREEK SYMBOLS.....	xxvi
Chapter 1: Outline of the thesis	1
1.1 Introduction	1
1.2 Scope and focus of the work	1
1.2.1 Research objective.....	1
1.2.2 Problems related to hydrated inorganic filler-type additives	2
1.2.3 Methodology	3
1.3 References	5

Chapter 2: The influence of stearic acid coating on the properties of magnesium hydroxide, hydromagnesite and hydrotalcite powders	8
2.1 Introduction	8
2.2 Experimental	12
2.2.1 Materials	12
2.2.2 Stearic acid coating	12
2.3 Characterization.....	13
2.3.1 Particle size and BET surface area	13
2.3.2 Oil absorption	13
2.3.3 Tap density	13
2.3.4 Scanning electron microscopy (SEM).....	14
2.3.5 Thermal analysis.....	14
2.3.6 X-Ray diffraction (XRD)	14
2.3.7 Diffuse Reflectance Infra-red Fourier Transform (DRIFT) analysis	14
2.3.8 Rheology	15
2.3.9 X-ray Photoelectron Spectroscopy (XPS).....	15
2.4 Results	15
2.5 Discussion	30
2.6 Conclusion.....	33
2.7 Acknowledgements	34
2.8 References	35
Chapter 3: The effect of magnesium hydroxide, hydromagnesite and layered double hydroxide on the heat stability and fire performance of plasticised PVC	40
3.1 Introduction	40
3.2 Experimental	42

3.2.1	Materials	42
3.2.2	Synthesis of LDH and hydromagnesite	43
3.2.3	Surface coating of the fillers	44
3.2.4	Preparation of PVC-composites	44
3.3	Characterisation	45
3.3.1	Particle size and BET surface area determination	45
3.3.2	Scanning Electron Microscopy (SEM)	45
3.3.3	X-ray diffraction (XRD)	45
3.3.4	X-ray fluorescence (XRF)	45
3.3.5	Inductively coupled plasma optical emission spectrometry (ICP-OES)	46
3.3.6	Fourier transform infrared spectroscopy (FTIR)	46
3.3.7	Thermogravimetric Analysis (TGA)	46
3.3.8	Heat stability assessment	47
3.3.9	Cone calorimeter fire testing	47
3.4	Results	49
3.4.1	Characterisation of the hydrated fillers	49
3.4.2	Characterisation of the PVC composites	53
3.4.3	Heat stability of the PVC composites	55
3.4.4	Fire testing	57
3.5	Discussion	63
3.6	Conclusion	65
3.7	References	67
Chapter 4: Layered double hydroxide derivatives as flame retardant for flexible PVC		73
4.1	Introduction	73

4.2	Experimental	75
4.2.1	Materials	75
4.3	Characterisation	76
4.3.1	Mechanical Properties	76
4.3.2	Thermogravimetric Analysis (TGA)	76
4.3.3	Cone calorimeter test	76
4.4	Results	77
4.4.1	Physical appearance	77
4.4.2	Mechanical Properties	77
4.4.3	Thermogravimetric Analysis (TGA) of the LDH-PVC composites	78
4.4.4	Flammability	80
4.5	Discussion	89
4.6	Conclusions	92
4.7	Acknowledgements	92
4.8	References	93
Chapter 5: Heat stabilising flexible PVC with layered double hydroxide derivatives		97
5.1	Introduction	97
5.2	Experimental	100
5.2.1	Materials	100
5.2.2	Synthesis of LDH-derivatives	100
5.2.3	Surface coating of the LDH-derivatives	101
5.2.4	Preparation of PVC-composites	101
5.3	Characterisation	102
5.3.1	Particle size and BET surface area determination	102

5.3.2	Scanning Electron Microscopy (SEM).....	102
5.3.3	X-ray diffraction (XRD).....	103
5.3.4	Inductively coupled plasma optical emission spectrometry (ICP-OES)...	103
5.3.5	Fourier transform infrared spectroscopy (FTIR).....	103
5.3.6	Thermogravimetric Analysis (TGA).....	104
5.4	Heat stability assessment.....	104
5.4.1	Dynamic heat stability (Rheomix)	104
5.4.2	Metrastat thermal stability	104
5.4.3	Thermomat thermostability	105
5.5	Results	106
5.5.1	LDH Particle size and BET surface area.....	106
5.5.2	Heat stability of the PVC composites.....	110
5.5.3	TGA of the LDH-PVC composites	112
5.5.4	Dynamic heat stability test (Rheomix).....	114
5.5.5	Metrastat thermal stability.....	116
5.5.6	Thermomat heat stability.....	117
5.6	Discussion	119
5.7	Conclusion.....	123
5.8	Acknowledgements	124
5.9	References	125
Chapter 6:	Conclusions and Recommendations	129
6.1	Overall conclusions	129
6.2	Future Research.....	132
	APPENDICES	133

ORGANISATION OF THE THESIS

The work done for this study has been divided into six Chapters altogether (Chapters 1-5) highlighting different aspects of the research.

Chapter 1 is an introduction to the work with a brief outline of the objectives of this study, as well as some problems relating to inorganic fillers.

Chapter 2 reports on the influence of a stearic acid coating on the properties of magnesium hydroxide, hydromagnesite and hydrotalcite powders. The main issue addressed here was to find a way to improve the dispersability of the fillers into liquids. While ultimately dispersion in the plasticiser and in a PVC melt was the objective, mineral oil was chosen instead. It represents a worst case scenario for the hydrophilic fillers owing to its non-polar nature. Furthermore, this model compound is a Newtonian fluid. This means that any non-Newtonian behaviour of the dispersions had to be due to the microstructure of the fillers present. It was found that a monolayer coating of stearic acid was an effective modification that significantly improved the flow behaviour of dispersions because it facilitated deagglomeration of the powder particles in the liquid phase. As a result, and wherever possible, such coatings were employed in further investigations that followed this study. This Chapter was published as a research paper titled “The influence of stearic acid coating on the properties of magnesium hydroxide, hydromagnesite and hydrotalcite powders” published in *J Mater Sci* (2009) 44: 6100–6109 and authored by Walter W Focke, Dan Molefe, FJW Labuschagne and Shatish Ramjee.

Chapter 3 reports on the effect of magnesium hydroxide, hydromagnesite and layered double hydroxide on the heat stability and fire performance of plasticised PVC. Thermogravimetric analysis, heat stability and fire performance properties were assessed with a cone calorimeter. It turned out that the layered double hydroxide outperformed the other hydrated filler with respect to both heat stability and fire retardant properties. This Chapter was published as a research paper titled “The effect of magnesium hydroxide, hydromagnesite and layered double hydroxide on the heat stability and fire performance of plasticized PVC” published in *Journal of Fire Sciences* (2015) 33 (6): 493-510 and authored by Dan Matlhomola Molefe, FJWJ (Johan) Labuschagne, Walter W Focke, Isbé van der Westhuizen and Osei Ofosu.

Chapter 4 discusses layered double hydroxide derivatives as flame retardant for flexible PVC. It was found that partial substitution of either the magnesium or aluminium in the standard product can have a profound effect on fire performance. This Chapter was submitted as a research paper to *Journal of Thermal Analysis and Calorimetry*. The manuscript was titled “Fire retarding flexible PVC with layered double hydroxide derivatives” and was authored by Dan Matlhomola Molefe, FJWJ Labuschagne, WW Focke and Osei Ofosu.

Chapter 5 reports on the heat stabilising effect of the layered double hydroxide derivatives in flexible PVC. Several techniques were employed, i.e. thermogravimetric analysis, Thermomat and Metrastat static thermostability and dynamic heat stability using the Rheomix instrument. This Chapter was submitted as a research paper titled “Heat stabilising flexible PVC with layered double hydroxide derivatives” published in *Polymer Degradation and Stability* (2015) 113: 46–54

authored by F Labuschagne, DM Molefe, WW Focke, I van der Westhuizen, HC Wright and MD Royeppen.

Chapter 6 provides overall conclusions and recommendations for future research.

The **Appendices** provide additional information on the equipment used in this research.

LIST OF FIGURES

Figure	Description	Page
Figure 2.1:	SEM pictures showing the morphology of the neat powders: A. Hydrotalcite. B. Hydromagnesite. C. Magnesium hydroxide.....	15
Figure 2.2:	XRD spectra of the various powders. Key: hydromagnesite (□), dypingite (Δ) and magnesite (+).....	16
Figure 2.3:	DRIFT spectra for magnesium hydroxide, hydrotalcite and hydromagnesite.....	17
Figure 2.4:	DRIFT spectra for neat and 2.5 g/L stearic acid solution treated hydromagnesite compared to those for magnesium stearate and neat stearic acid.....	18
Figure 2.5:	TGA curves for hydromagnesite, magnesium hydroxide and hydrotalcite powders obtained in air at a scan rate of 10°C/min.....	19
Figure 2.6:	Effect of stearic acid dosage level on the BET surface area of the powders.	22
Figure 2.7:	Schematic of surface-adsorbed close-packed monolayer of stearic acid on a mineral surface.	22
Figure 2.8:	Effect of stearic acid dosage level on the ratio of the C/O atomic ratio as estimated from XPS.	25
Figure 2.9	Specific maximum filler volume fractions determined from tap density (for uncoated filler only) and oil absorption experiments (uncoated and treated with 2.5 g/L stearic acid).....	26
Figure 2.10:	Effect of stearic acid coating on the viscosity of 25 wt.% suspensions of hydromagnesite, magnesium hydroxide and hydrotalcite powders in white oil at 30	

°C. Open symbols indicate neat powders while solid symbols are for powders treated with 2.5 g/L stearic acid solution in acetone. The arrows indicate the reduction in apparent viscosity facilitated by the surface coatings.....27

Figure 3.1: SEM micrographs of (A) Layered double hydroxide (LDH); (B) Magnesium hydroxide (MH) and (C) Hydromagnesite (HM). The size bar indicates a length of 200 nm.47

Figure 3.2: X-ray diffraction patterns for magnesium hydroxide (MH), hydromagnesite (HM) and layered double hydroxide (LDH).49

Figure 3.3: FTIR spectra of the hydrated fillers.50

Figure 3.4: TGA traces in air for the LDH derivatives. Temperature was scanned from 25 °C to 900 °C at a scan rate of 10 °C min⁻¹ with air flowing at a rate of 50 mL min⁻¹.51

Figure 3.5: TGA traces for the PVC-LDH composites in (A) nitrogen and (B) air atmospheres. The temperature was scanned from 25 °C to 900 °C at a scan rate of 10 °C min⁻¹ with gas flowing at a rate of 50 mL min⁻¹.....52

Figure 3.6: The induction and stability times were obtained by tracking the evolution of hydrochloric acid. A. Representative conductivity curves for the PVC compounds. B. Thermomat static heat stability at 200 °C. Key: PVC = no additive; HM= hydromagnesite; MH = magnesium hydroxide, and LDH= layered double hydroxide.....53

Figure 3.7: Representative cone calorimeter heat release rate curves for the plasticized PVC compound and its composites with the hydrated fillers.....59

Figure 3.8: The effect of the hydrated fillers on the *FIGRA* and *pHRR/t_{ign}* of PVC composites. The sample sheets were backed by aluminium foil and their dimensions

were 100 mm × 100 mm × 3.5 ± 0.1 mm. They were exposed horizontally to an external heat flux of 35 kW m⁻²60

Figure 3.9: Cone calorimeter smoke production rates for the plasticized PVC compound and its composites with LDH derivatives. The sample sheets were backed by aluminium foil and their dimensions were 100 mm × 100 mm × 3.5 ± 0.1 mm.60

Figure 3.10: Comparing the smoke production of the plasticized PVC compound with that from its composites with LDH derivatives. The sample sheets were backed by aluminium foil and their dimensions were 100 mm × 100 mm × 3.5 ± 0.1 mm. They were exposed horizontally to an external heat flux of 35 kW m⁻²61

Figure 4.1: Physical appearance of the pressed PVC sheets.....76

Figure 4.2: TGA traces for the PVC-LDH composites in (A) nitrogen and (B) air atmospheres. The temperature was scanned from 25 °C to 900 °C at a scan rate of 10 °C min⁻¹ with gas flowing at a rate of 50 mL in⁻¹78

Figure 4.3: Cone calorimeter time to ignition and flame out for the plasticized PVC compound and its composites with LDH derivatives.....80

Figure 4.4: Representative cone calorimeter mass loss curves for the plasticized PVC compound and its composites with LDH derivatives. The sample sheets were backed by aluminium foil and their dimensions were 100 mm × 100 mm × 3.5 ± 0.1 mm. They were exposed horizontally to an external heat flux of 35 kW m⁻².....81

Figure 4.5: Representative cone calorimeter heat release rate curves for the plasticised PVC compound and its composites with LDH derivatives. The sample sheets were backed by aluminium foil and their dimensions were 100 mm × 100 mm × 3.5 ± 0.1 mm. They were exposed horizontally to an external heat flux of 35 kW m⁻²82

Figure 4.6: Cone calorimeter peak heat release rates and total heat release for the plasticised PVC compound and its composites with LDH derivatives. The sample sheets were backed by aluminium foil and their dimensions were 100 mm × 100 mm × 3.5 ± 0.1 mm. They were exposed horizontally to an external heat flux of 35 kW m⁻².....83

Figure 4.7: The effect of the LDH derivatives on the *FIGRA* and *pHRR*/tign of PVC composites. The sample sheets were backed by aluminium foil and their dimensions were 100 mm × 100 mm × 3.5 ± 0.1 mm. They were exposed horizontally to an external heat flux of 35 kW m⁻².....85

Figure 4.8: Cone calorimeter smoke production rates for the plasticized PVC compound and its composites with LDH derivatives. The sample sheets were backed by aluminium foil and their dimensions were 100 mm × 100 mm × 3.5 ± 0.1 mm. They were exposed horizontally to an external heat flux of 35 kW m⁻².....86

Figure 4.9: Comparing the smoke production of the plasticized PVC compound with that from its composites with LDH derivatives. The sample sheets were backed by aluminium foil and their dimensions were 100 mm × 100 mm × 3.5 ± 0.1 mm. They were exposed horizontally to an external heat flux of 35 kW m⁻².....86

Figure 5.1: SEM micrographs of (A) MgZnAl-LDH; (B) MgFeAl-LDH; (C) MgCuAl-LDH, and (D) CaAl-LDH. The size bar indicates a length of 200 nm....104

Figure 5.2: X-ray diffraction patterns for the various LDH derivatives.....105

Figure 5.3: FTIR spectra of the various LDH derivatives.....107

Figure 5.4: TGA traces in air for the LDH derivatives. Temperature was scanned from 25 °C to 900 °C at a scan rate of 10 °C min⁻¹ with air flowing at a rate of 50 mL min⁻¹.....108

Figure 5.5: TGA traces in air for the PVC-LDH composites. Temperature was scanned from 25 °C to 900 °C at a scan rate of 10 °C min⁻¹ with nitrogen flowing at a rate of 50 mL min⁻¹111

Figure 5.6: Representative torque vs. time curves obtained with the Rheomix. The mixing chamber temperature was set at 200 °C and the rotor speed was set at 60 rpm.....112

Figure 5.7: Metrastat sample appearances. (A) Neat PVC; (B) MgAl-LDH; (C) CaAl-LDH; (D) MgCuAl-LDH; (E) MgFeAl-LDH, and (F) MgZnAl-LDH.....113

Figure 5.8: “Normalized” Metrastat grey value test results. (A) Neat PVC; (B) MgAl-LDH; (C) CaAl-LDH; (D) MgZnAl-LDH. The broken horizontal line defines the failure criterion that was adopted.....114

Figure 5.9: Representative Thermomat conductivity curves for the PVC compounds: Neat PVC; 2. MgZnAl-LDH; 3. MgFeAl-LDH; 4. MgAl-LDH; 5. CaAl-LDH; 6. MgCuAl-LDH. The broken horizontal line defines the failure criterion.....115

Figure 5.10: Static and dynamic heat stability times measured at 200 °C using the torque rheometer technique (Rheomix); following the development of colour with heating time (Metrastat), and tracking the evolution of hydrochloric acid (Thermomat)116

Figure 5.11: Thermomat conductivity curves showing typical curve fits of equation...120

Figure 5.12: The correlation between the parameters of equation (5) for the LDH-stabilised PVC compounds. The solid line is described by the relation $k = 0.196 e^{\theta/4}$ 121

LIST OF TABLES

Table	Description	Page
Table 2.1:	Stearic acid coating levels expressed in wt.% as calculated from the residual level in the solvent and from TG data.....	23
Table 2.2:	Consistency index K and the flow behaviour index n for the slurries...	28
Table 3.1:	LDH particle sizes, BET surface area and d-spacing from XRD result.	48
Table 3.2:	XRF composition analysis data of samples roasted at 1 000 °C.....	48
Table 3.3:	Cone calorimeter data summary.....	57
Table 4.1:	LDH derivatives: Apparent elemental composition calculated from ICP-OES, TGA residue at 900 °C and d-spacing from XRD result.....	74
Table 4.2:	Mechanical properties (tensile strength, Young's modulus and elongation to break) of the PVC compounds filled with the LDH derivatives.....	76
Table 4.3:	Cone calorimeter data summary.....	79
Table 5.1:	LDH particle sizes and BET surface area.....	103
Table 5.2:	LDH derivatives: Apparent elemental composition calculated from ICP-OES, BET surface area and particle size.....	104

LIST OF EQUATIONS

The stearic acid equivalent to a monolayer amount equation.....	24
Power-law model.....	28
Krieger-Dougherty expression.....	29
Krieger-Dougherty model.....	29
Porosity (ϵ).....	31
Autocatalytic reaction mechanism.....	127

SCHEME OF REACTIONS

Scheme I: Thermal decomposition of magnesium hydroxide.....	20
Scheme II: Thermal decomposition of the synthetic hydrotalcite.....	20
Scheme III: Degradation pathway for hydromagnesite.....	20

LIST OF ABBREVIATIONS

ASTM	American Society for Testing and Materials
Al(OH) ₃	aluminium trihydroxide
ATR	Attenuated total reflection
BET	Brunauer Emmett Teller
CaAl-LDH	calcium aluminum double layered hydroxide
CaO	calcium oxide
DINP	diisononyl phthalate
DRIFT	Diffuse reflectance infra-red Fourier transform
DTG	derivative thermogravimetry
FEG SEM	field emission gun scanning electron microscope
FIGRA	fire growth rate ($\text{kW m}^{-2} \text{s}^{-1}$)
FPI	fire performance index ($\text{kW m}^2 \text{s}^{-1}$)

FTIR	Fourier transform infrared spectroscopy
HM	hydromagnesite
HRR	heat release rate (kW m^{-2})
HT	hydrotalcite
ICP-OES	Inductively Coupled Plasma Optical Emission Spectroscopy
IR	Infra-red
ISO	International Organisation for Standardization
K	consistency index (Pa s)
$K\alpha$	X-ray spectroscopy emission line
LDH	layered double hydroxide
LOI	limited oxygen index
M	water molecules
MAHRE	maximum average rate of heat emission (kW m^{-2})
MgAl-LDH	magnesium and aluminum based LDH
MgCO_3	magnesium carbonate
MgCuAl-LDH	magnesium copper aluminium double layered hydroxide
MgO	magnesium oxide
MgZnAl-LDH	magnesium zinc aluminium double layered hydroxide
MH	magnesium hydroxide
NaHCO_3	sodium bicarbonate
phr	parts per hundred of resin
pHRR	peak heat release rate (kW m^{-2})
$\text{pHRR}/t_{\text{ign}}$	peak heat release rate over time to ignition ($\text{kW m}^{-2} \text{s}^{-1}$)
PSD	particle size distribution
PVC	poly (vinyl chloride)
RH	relative humidity

SEM	scanning electron microscopy
TGA	thermogravimetric analysis
tHR	total heat released (MJ m^{-2})
XPS	X-ray photoelectron spectroscopy
XRD	X-ray diffraction

LIST OF SYMBOLS

d_{10}	the tenth percentile particle size
d_{50}	fiftieth percentile particle size
d_{90}	the ninetieth percentile particle size
k	rate constant (s^{-1})
K-value	a measure of the molecular mass of PVC resins
M	dimensionless constant
n	dimensionless constant defining the reaction order
rpm	revolutions per minute
t_{ign}	time to ignition (s)
mol.%	molar percentage (% mol)
vol.%	volume percent (%)
wt.%	weight percent (%)

LIST OF GREEK SYMBOLS

∞	Infinity
α	degree of conversion (-)
ε	porosity (-)
η	viscosity of the suspension (Pa s)
φ_{max}	maximum random packing density (-)
θ	angle between incident and scattered X-rays ($^{\circ}$)
η_0	viscosity of the neat fluid in the absence of suspended solids (Pa s)
η_r	relative viscosity (-)
$\dot{\gamma}$	shear rate (s^{-1})

- k particle shape factor (-)
- θ reaction order parameter of the conversion function (-)
- τ apparent time constant (s)

Chapter 1: Outline of the thesis

1.1 Introduction

The overall focus and the general objectives of this study, as well as some problems related to inorganic filler-type additives used as heat stabilisers and flame retardants are described. Specific objectives are addressed in the individual Chapters.

1.2 Scope and focus of the work

1.2.1 Research objective

PVC is fundamentally unstable at elevated temperature and if plasticised its inherent flame retardance is compromised. Hence the main aim and objective of this thesis was to investigate the effectiveness of a set of inorganic materials, i.e. hydrated filler-type flame retardant materials and their use as heat stabilisers and flame retardants for plasticised PVC. These included layered double hydroxides, i.e. synthetic variants of the mineral hydrotalcite (HT), hydromagnesite (HM) and magnesium hydroxide (MH). According to the literature, these hydrated filler additives may offer fire retardancy performance (Laoutid et al., 2009, Rigolo and Woodhams, 1992, Haurie et al., 2006, Morgan et al., 2007). The focus was given to these materials basically because of their clay-like layered crystalline structure and metal hydroxide-like chemistry that offers many options for modification and optimisation. Towards this goal limited syntheses of layered double hydroxides (LDHs) derivatives was attempted. A specific objective was to explore limited substitution of the magnesium and aluminium present in LDH with other metal cations (Fe, Zn, Ca and Cu). The target was to use these materials to improve the heat stability and fire performance of plasticised PVC.

1.2.2 Problems related to hydrated inorganic filler-type additives

There are some problems that are encountered when these endothermic flame retardants are used. The decomposition of $Mg(OH)_2$ in particular, results in a powdery residue with a high surface area (Hornsby and Watson, 1990). It tends to catalyse oxidation of char residues leading to an afterglow effect. As a result, effective barrier formation is realised only when additional additives are incorporated (Hornsby, 2001, Carpentier et al., 2000, Burns et al., 2008, Genovese and Shanks, 2007). Secondly, high loadings are required to achieve adequate flame resistance (Hornsby, 2001). The high filler loadings impair the fluidity of the corresponding polymer melts (Hornsby, 2001, Wang et al., 2006, Zhang et al., 2007) and adversely affects mechanical properties of the solid compounds (Hornsby, 2001, Wang et al., 2006). Since these fillers are pulverised bulk materials, they tend to agglomerate during conveying and storage as a result of adhesive hydrogen bonding interactions. The compounding process must succeed in breaking down the agglomerates and thoroughly disperse the individual particles in the polymer melt (Potente and Flecke, 1997). Well-mixed homogeneous dispersions are required to minimize melt viscosity. The mechanical integrity of the compound is also compromised by the hydrophilic nature of the filler surfaces. Suitable surface modifications can improve the compatibility of inorganic fillers with hydrophobic polymer matrices (Wang et al., 2006). Stearic acid is widely used to coat basic fillers such as calcium carbonate (Papirer et al., 1984, Gilbert and Petiraksakul, 1997, Osman and Suter, 2002), magnesium hydroxide (Wang et al., 2006) and hydromagnesite (Haurie et al., 2006). Compounds containing stearate coated fillers show better processing behaviour, increased elongation to break, improved impact properties at the cost of reduced tensile strength (Wang et al., 2006,

Gilbert and Petiraksakul, 1997, Rigolo and Woodhams, 1992, Hornsby, 1994, Huang et al., 2008).

Levchik and Weil (2005) and Weil *et al.* (2006) reviewed the chemical additives that have provide acceptable fire properties in the principal PVC application areas. The hydrated filler additives magnesium hydroxide (MH), hydromagnesite (HM) and layered double hydroxide (LDH) have utility as endothermic flame retardants and smoke suppressants for PVC as well as other polymers (Xu et al., 2006, Wang and Zhang, 2004, Gao et al., 2014). Their flame retardant action relies on endothermic decomposition reactions that absorb heat and release inert gases, e.g. steam and carbon dioxide (Hornsby, 2001, Hornsby and Watson, 1990, Laoutid et al., 2009). The cooling of the polymer substrate inhibits solid phase decomposition reactions. Simultaneously the steam and/or carbon dioxide released by the reaction dilutes the surrounding atmosphere with an inert gas. Finally, the residues may form an ash-char barrier layer at the surface that reduces heat transfer from the flame to the remaining polymer substrate.

1.2.3 Methodology

Considering the problems outlined above, the following research programme was formulated:

- (a) Modify the fillers by coating with stearic acid to improve their dispersion and improving the compatibility with polymer matrices. Use mineral oil as model liquid to study the rheological behaviour of the surface coating of the filler/oil melts.

- (b) Characterise the modified compounds using microscopy (SEM), spectroscopic techniques, thermogravimetric analysis (TGA), X-ray diffraction (XRD)
- (c) Prepare and characterise plasticised PVC compounds using the fillers as heat stabilisers and flame-retardants.
- (d) Evaluate the fillers for their heat stabilising effect in these compound using both static and dynamic methods.

1.3 References

BURNS, M., WAGENKNECHT, U., KRETZSCHMAR, B. & FOCKE, W. W. 2008. Effect of hydrated fillers and red phosphorus on the limiting oxygen index of poly (ethylene-co-vinyl acetate) - poly (vinyl butyral) and low density polyethylene - poly (ethylene-co-vinyl alcohol) blends. *Journal of Vinyl and Additive Technology*, 14, 113-119.

CARPENTIER, F., BOURBIGOT, S., LE BRAS, M., DELOBEL, R. & FOULON, M. 2000. Charring of fire retarded ethylene vinyl acetate copolymer—magnesium hydroxide/zinc borate formulations. *Polymer degradation and stability*, 69, 83-92.

GAO, Y., WU, J., WANG, Q., WILKIE, C. A. & O'HARE, D. 2014. Flame retardant polymer/layered double hydroxide nanocomposites. *Journal of Materials Chemistry A*, 2, 10996-11016.

GENOVESE, A. & SHANKS, R. A. 2007. Structural and thermal interpretation of the synergy and interactions between the fire retardants magnesium hydroxide and zinc borate. *Polymer degradation and stability*, 92, 2-13.

GILBERT, M. & PETIRAKSAKUL, P. 1997. Stearate coatings on particulate fillers: the effects on resulting compound properties. *Polymers & polymer composites*, 5, 535-539.

HAURIE, L., FERNÁNDEZ, A. I., VELASCO, J. I., CHIMENOS, J. M., LOPEZ CUESTA, J.-M. & ESPIELL, F. 2006. Synthetic hydromagnesite as flame retardant. Evaluation of the flame behaviour in a polyethylene matrix. *Polymer Degradation and Stability*, 91, 989-994.

HORNSBY, P. R. & WATSON, C. L. 1990. A study of the mechanism of flame retardance and smoke suppression in polymers filled with magnesium hydroxide. *Polymer Degradation and Stability*, 30, 73-87.

HORNSBY, P. R. 1994. The application of magnesium hydroxide as a fire retardant and smoke-suppressing additive for polymers. *Fire and materials*, 18, 269-276.

HORNSBY, P. R. 2001. Fire retardant fillers for polymers. *International Materials Reviews*, 46, 199-210.

HUANG, H., TIAN, M., YANG, J., LI, H., LIANG, W., ZHANG, L. & LI, X. 2008. Stearic acid surface modifying Mg(OH)₂: Mechanism and its effect on properties of ethylene vinyl acetate/Mg(OH)₂ composites. *Journal of applied polymer science*, 107, 3325-3331.

LAOUTID, F., BONNAUD, L., ALEXANDRE, M., LOPEZ-CUESTA, J.-M. & DUBOIS, P. 2009. New prospects in flame retardant polymer materials: from fundamentals to nanocomposites. *Materials Science and Engineering: R: Reports*, 63, 100-125.

LEVCHIK, S. V. & WEIL, E. D. 2005. Overview of the recent literature on flame retardancy and smoke suppression in PVC. *Polymers for Advanced Technologies*, 16, 707-716.

MORGAN, A. B., COGEN, J. M., OPPERMAN, R. S. & HARRIS, J. D. 2007. The effectiveness of magnesium carbonate-based flame retardants for poly (ethylene-co-vinyl acetate) and poly (ethylene-co-ethyl acrylate). *Fire and Materials*, 31, 387-410.

OSMAN, M. A. & SUTER, U. W. 2002. Surface treatment of calcite with fatty acids: structure and properties of the organic monolayer. *Chemistry of materials*, 14, 4408-4415.

PAPIRER, E., SCHULTZ, J. & TURCHI, C. 1984. Surface properties of a calcium carbonate filler treated with stearic acid. *European Polymer Journal*, 20, 1155-1158.

- POTENTE, H. & FLECKE, J. 1997. The breaking down and agglomerating of fillers in polymer melt: A physical model for mathematical description. *Journal of reinforced plastics and composites*, 16, 1281-1292.
- RIGOLO, M. & WOODHAMS, R. 1992. Basic magnesium carbonate flame retardants for polypropylene. *Polymer Engineering & Science*, 32, 327-334.
- WANG, X. & ZHANG, Q. 2004. Effect of hydrotalcite on the thermal stability, mechanical properties, rheology and flame retardance of poly(vinyl chloride). *Polymer International*, 53, 698-707.
- WANG, Z., CHEN, Z., FAN, W. & NIE, W. 2006. Effects of surface modifiers on mechanical and rheological properties of halogen-free flame retarded polyethylene composites. *Polymer-Plastics Technology and Engineering*, 45, 191-196.
- WEIL, E. D., LEVCHIK, S. & MOY, P. 2006. Flame and smoke retardants in vinyl chloride polymers - Commercial usage and current developments. *Journal of Fire Sciences*, 24, 211-236.
- XU, Z. P., SAHA, S. K., BRATERMAN, P. S. & D'SOUZA, N. 2006. The effect of Zn, Al layered double hydroxide on thermal decomposition of poly(vinyl chloride). *Polymer Degradation and Stability*, 91, 3237-3244.
- ZHANG, F., ZHANG, H. & SU, Z. 2007. Surface treatment of magnesium hydroxide to improve its dispersion in organic phase by the ultrasonic technique. *Applied Surface Science*, 253, 7393-7397.

Chapter 2: The influence of stearic acid coating on the properties of magnesium hydroxide, hydromagnesite and hydrotalcite powders¹

2.1 Introduction

Polymers find increasing use as structural and functional materials. Owing to their combustible, organic nature, they pose a fire risk in some applications. This risk can be reduced by incorporating flame retardant additives. Laoutid et al. [1] provide a recent review of flame retardants for polymers. Hydrated fillers, e.g. aluminium trihydrate and magnesium hydroxide, have utility as endothermic flame retardants [2-4].

The candle model for polymer burning assumes independent pyrolysis and flame zones [5]. Heat transfer from the flame provides coupling between the gas and condensed phases. It drives the thermal degradation reactions that produce volatile fuel fragments that, in turn, feed the flame. This model suggests three possible strategies for flame proofing combustible polymers [5, 6]: (i) interference with the gas phase combustion and (ii) with the substrate pyrolysis reactions or (iii) their decoupling via a physical barrier to heat and mass transport. With endothermic flame retardants this may correspond to (i) dilution of the flammable gas with inert gases; (ii) the cooling of the substrate and promotion of charring; and (iii) the formation of an ash-char barrier layer. The endothermic decomposition reaction absorbs heat and releases inert gases [1, 4, 7]. The cooling of the polymer substrate inhibits the solid

¹ This Chapter was published as *J Mater Sci* (2009) 44:6100–6109 and the contents are reproduced here in full in the publication format.

phase decomposition reactions. Simultaneously the steam and/or carbon dioxide released by the reaction dilutes the surrounding atmosphere with an inert gas.

The use of endothermic flame retardants is associated with some problems. In particular, on decomposition, $\text{Mg}(\text{OH})_2$ forms a powdery residue with a high surface area [8]. It tends to catalyse oxidation of char residues leading to an afterglow effect. As a result, effective barrier formation is realized only when additional additives are incorporated [4, 9-11]. Secondly, high loadings are required to achieve adequate flame resistance [4]. The high filler loadings impair the fluidity of the corresponding melts [4, 14-16] and the mechanical properties of the solid compounds [4, 14]. Since these fillers are pulverized bulk materials, they tend to agglomerate during conveying and storage as a result of adhesive forces. When these agglomerates are added to a polymer, it is necessary that the compounding process succeeds in breaking down the agglomerates and thoroughly disperses the individual particles in the polymer melt [16]. A well-mixed homogeneous dispersion is required to minimize melt viscosity. The mechanical integrity of the compound is also compromised by the hydrophilic nature of these filler surfaces. Suitable surface modifications can improve the compatibility of inorganic fillers with hydrophobic polymer matrices [14]. Stearic acid is widely used to coat basic fillers such as calcium carbonate [17-20], magnesium hydroxide [14, 18, 21-23] and hydromagnesite [24]. Compounds containing stearate coated fillers show better processing behaviour, increased elongation to break and improved impact properties at the cost of reduced tensile strength [12-14, 18, 25-26].

The degradation onset temperature for aluminium trihydrate is about 210 °C and it absorbs ca. 1.05 MJ kg⁻¹ of heat [1]. Magnesium hydroxide is significantly more stable. Thermal decomposition occurs in the temperature range 280 °C to 350 °C and

the enthalpy of decomposition is 1.2 - 1.3 MJ kg⁻¹ [1, 27]. This allows magnesium hydroxide to be used in polymers requiring higher processing temperatures, e.g. nylon and polypropylene [28].

Magnesium carbonate and magnesium hydroxide (Mg(OH)₂) occur in nature as the minerals magnesite and brucite. Magnesium hydroxide has a layered structure composed of stacked trioctahedral metal hydroxide sheets. Hydrotalcite is a natural anionic clay mineral with the structural formula: Mg₆Al₂(OH)₁₆CO₃·4H₂O. However, in this study we consider a synthetic hydrotalcite-like compound with nominal composition Mg₄Al₂(OH)₁₂CO₃·3H₂O. Such synthetic analogues are commonly referred to as layered double hydroxides (LDH) [29-30]. They also feature the brucite-like stacked sheet structure of magnesium hydroxide [30]. The difference is that a portion of the magnesium ions in the sheets have been replaced with aluminium ions. This substitution imparts a net positive charge that is balanced by an equal negative charge from the interlayer carbonate anions [31]. Water molecules also occupy the interlayer space.

Hydrous carbonates and basic magnesium hydroxycarbonates are intermediate phases located between magnesium hydroxide and magnesium carbonate. Forms that occur as minerals [32] include nesquehonite (MgCO₃·3H₂O) and lansfordite (MgCO₃·5H₂O) [33], artinite (MgCO₃·Mg(OH)₂·3H₂O), hydromagnesite (4MgCO₃·Mg(OH)₂·4H₂O) and dypingite (4MgCO₃·Mg(OH)₂·5H₂O) [34]. At a unit cell level, these minerals also have a layer structure [33]. Magnesium hydroxide and magnesium carbonate are readily synthesized but it is very difficult to prepare pure, single phase basic magnesium carbonate forms. Nevertheless, Hayek and Gleispach

[35] showed that pure hydromagnesite can be prepared by homogeneous precipitation and complex-acidolysis.

Camino et al. [27] compared the flame retardant effect of various inorganic hydroxides with that of hydrotalcite in poly (ethylene-co-vinyl acetate) (EVA). They found that EVA filled with 50 wt.% flame retardant; the hydrotalcite-based compound featured the slowest heat release rate and the lowest evolved gas temperature. The basic carbonates, e.g. hydromagnesite, may offer fire retardancy performance comparable to magnesium hydroxide [1, 3, 25, 36-37]. While the enthalpy of decomposition is lower at ca. 0.80 MJ kg^{-1} [24], a greater quantity of inert gases including carbon dioxide is released.

This study is a first step in a project designed to explore the utility of magnesite ore-derived compounds as potential flame retardants for polymers. Powders were prepared on a pilot plant using proprietary processes and yielded small crystals in a profusely agglomerated state. Powders composed of such small agglomerated crystals are not suitable for compounding into polymer melts. They adversely affect the melt viscosity and the required loading levels can often not be achieved. However, owing to their high surface area, they are ideal for studying the effect of stearic acid coatings on physical properties. This investigation considers the effect of stearic acid coatings on the properties of such hydromagnesite and hydrotalcite powders as well as a magnesium hydroxide reference material. Finally, we follow Zhang et al. [15] and use mineral oil as model liquid to study the effect of the surface coating on the rheology of the particle suspensions.

2.2 Experimental

2.2.1 Materials

Hydromagnesite (grade HMH) and hydrotalcite (grade HT5) were supplied by Chamotte Holdings. The hydromagnesite was manufactured using a proprietary procedure based on the methods described by Botha and Strydom [38]. The hydrotalcite is a layered double hydroxide with the approximate composition $[\text{Mg}_{0.66}\text{Al}_{0.34}(\text{OH})_2](\text{CO}_3)_{0.17} \cdot \frac{1}{2}\text{H}_2\text{O}$. Both materials contained silica and magnesium carbonate as minor impurities. Magnesium hydroxide was obtained from Aldrich (Cat. No. 31,009-3 magnesium hydroxide 95 %). Distilled water was used in all experiments. White oil, with a density of 0.831 g cm^{-3} at $20 \text{ }^\circ\text{C}$ and a viscosity of 13.8 mPa s at $40 \text{ }^\circ\text{C}$, was obtained from Akulu Marchon. Acetone (99.5 %) and stearic acid were supplied by Saarchem UnivAR and Bio-Zone Chemicals respectively. Potassium bromide (Uvasol KBr, Merck) was used to prepare samples for the recording of infrared spectra.

2.2.2 Stearic acid coating

Stearic acid surface coatings were applied using a solution method. A predetermined amount of stearic acid was weighed out into a 500 mL Schott Duran bottle. To this was added 400 mL of acetone. The sealed bottle was suspended in a water bath and shaken at regular intervals until all the stearic acid was fully dissolved. Then 20 g of inorganic filler (hydromagnesite, hydrotalcite or magnesium hydroxide) was added. The mixture was shaken manually for about one minute. Thereafter the contents were stirred for 30 min using a magnetic stirrer. The mixture was then allowed to stand for 3 days before recovering the filler and the solvent by filtering. The filtrates were dried at ambient temperature. In this way, the powders were exposed to solutions containing

0, 0.25, 0.50, 1.00, 2.50 and 5.00 g L⁻¹ stearic acid in acetone. This corresponds to total stearic acid dosage levels corresponding to 0, 0.5, 1, 2, 5 and 10 wt.% based on the mass of neat filler added. The actual amount of stearate absorbed on or by the fillers treated with the 2.5 g L⁻¹ and 5 g L⁻¹ solutions was determined by evaporating the recovered acetone solutions and weighing the residues.

2.3 Characterization

2.3.1 Particle size and BET surface area

Particle size distributions were determined using a Malvern Mastersizer Hydro 2000MU instrument. Single point BET surface area measurements were done using a Micromeritics Flowsorb II 2300 instrument.

2.3.2 Oil absorption

The oil absorption of neat powders, as well as powders treated with the 2.5 g L⁻¹ stearic acid solution, was determined using the spatula rub-out method described in ASTM D 281-95.

2.3.3 Tap density

Tap density was determined by adding small amounts of powder to a 50 mL measuring cylinder. After each addition, the cylinder was exhaustively tapped against a wooden board at an angle of ca. 25° from the vertical to consolidate the column of powder. The mass of powder corresponding to a tapped volume of 50 mL was determined. The average of triplicate determinations is reported.

2.3.4 Scanning electron microscopy (SEM)

Small quantities of powder were placed onto carbon tape on a metal sample holder. Excess powder was removed using a single compressed air blast. The samples were then coated with gold under argon gas using a SEM autocoating unit E5200 (Polaron equipment LTD). They were viewed on a JEOL 840 SEM scanning electron microscope under low magnification.

2.3.5 Thermal analysis

About 15 mg powder was placed in open 70 μL alumina pans. Thermogravimetric analysis was performed using the dynamic method on a Mettler Toledo A851 TGA/SDTA instrument in air flowing at a rate of 50 mL min^{-1} . Temperature was scanned from 25 to 900 $^{\circ}\text{C}$ at a rate of 10 $^{\circ}\text{C min}^{-1}$.

2.3.6 X-Ray diffraction (XRD)

XRD analysis on a PANalytical X-pert Pro powder diffractometer was used for phase identification. The instrument featured variable divergence and receiving slits and an X'celerator detector using Fe filtered $\text{CoK}\alpha$ radiation (0.17901 nm). X'Pert High Score Plus software was used for data manipulation.

2.3.7 Diffuse Reflectance Infra-red Fourier Transform (DRIFT) analysis

Infrared spectra were recorded using a DRIFT accessory on a Perkin-Elmer Spectrum 2000GX FTIR spectrometer. The ratio of sample mass to KBr mass was set at 1:20. Thirty scans were recorded over the frequency range 400 – 4 000 cm^{-1} and Fourier transformed at a resolution of 4 cm^{-1} .

2.3.8 Rheology

The white oil suspensions containing 25 wt.% inorganic filler were prepared as follows: 2.250 g neat powder or 2.368 g of the 5 % stearic acid coated sample were mixed with 6.750 g and 6.632 g white oil respectively. The powders were thoroughly mixed into the liquid using an agate mortar and pestle. The viscosities of these white oil suspensions were measured at a temperature of 30 °C on an Anton Paar Physica UDS 200 rheometer using the parallel plate geometry. The disk diameter was 25 mm and the gap between the two plates was set at 1.1 mm.

2.3.9 X-ray Photoelectron Spectroscopy (XPS)

XPS spectra were obtained on a PHI spectrometer (Model 5400) equipped with an Mg/Al dual mode source and a small area analyser with PSD detector. An achromatic Mg K α X-ray (1253.6 eV) source was operated at 300 W. The vacuum pressure was 10⁻⁸ torr during spectra acquisition. Survey spectra were obtained at take-off angles of 15°C, 45°C and 80°C. Before analysis, samples were dried over P₂O₅ in a vacuum desiccator.

2.4 Results

Figure 2.1 shows the morphology of the neat filler particles as observed by SEM. It shows that the hydrotalcite and the magnesium hydroxide powders comprise copiously agglomerated flake-like particles. The hydromagnesite consists of well-formed, dice-shaped crystals that appear glued-together by a less well-defined phase. The Malvern particle size analysis of all the powders revealed bimodal particle size distributions (PSD). The peak corresponding to the larger particle size is attributed to the presence of large agglomerates. The locations of the peaks at smaller particles

sizes in the PSD probably give a better indication of primary particle dimensions. These were 1.5 μm , 1.0 μm and 5.8 μm for magnesium hydroxide, hydrotalcite and hydromagnesite respectively.

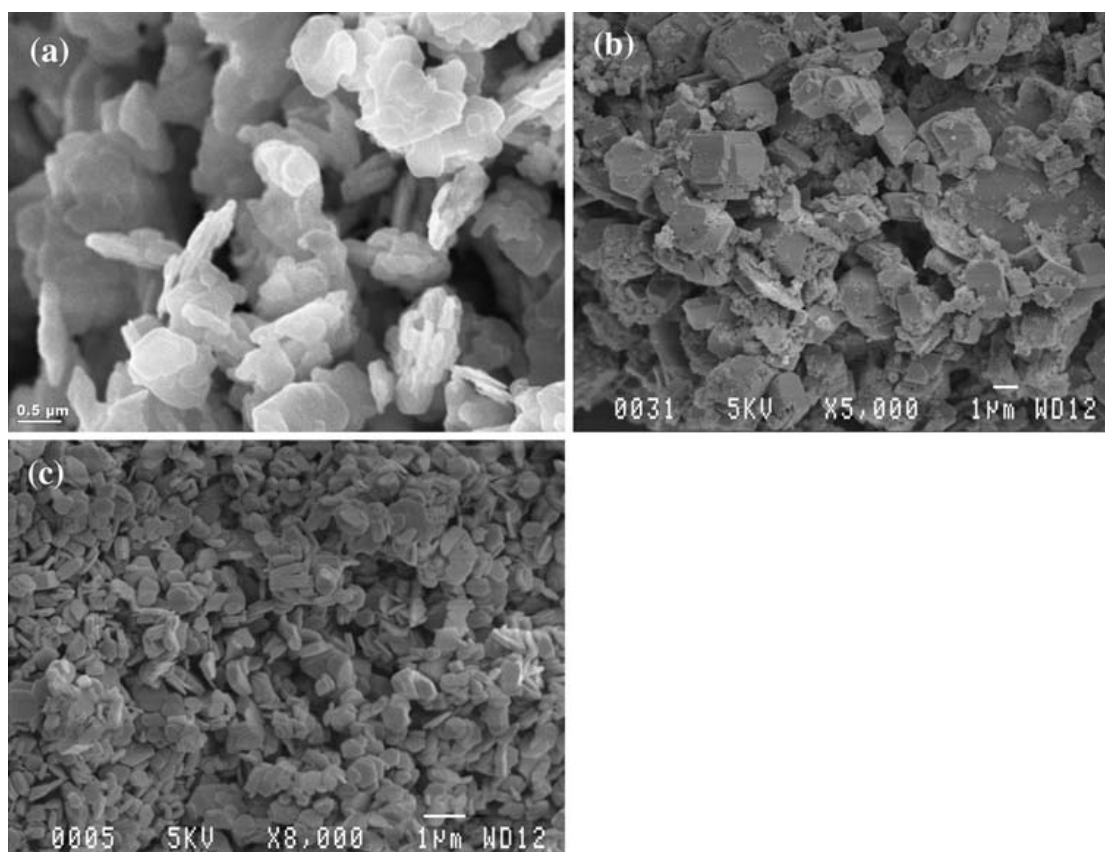


Figure 2.1: SEM pictures showing the morphology of the neat powders: (a) Hydrotalcite, (b) Hydromagnesite, (c) Magnesium hydroxide

The XRD spectra in Figure 2.2 and the DRIFT spectra in Figure 2.3 confirm the chemical nature of the three powders. The sharp peaks in the XRD spectrum for $\text{Mg}(\text{OH})_2$ and hydrotalcite point to high crystallinity of the corresponding powders. The peaks at $2\theta = 21.6^\circ$ and $2\theta = 13.5^\circ$ in the XRD spectra for magnesium hydroxide and hydrotalcite are consistent with the expected brucite layer basal spacings of 0.477 nm and 0.763 nm respectively. The XRD spectrum for the hydromagnesite

shows additional reflections that indicate the presence of dypingite and magnesite as impurity phases.

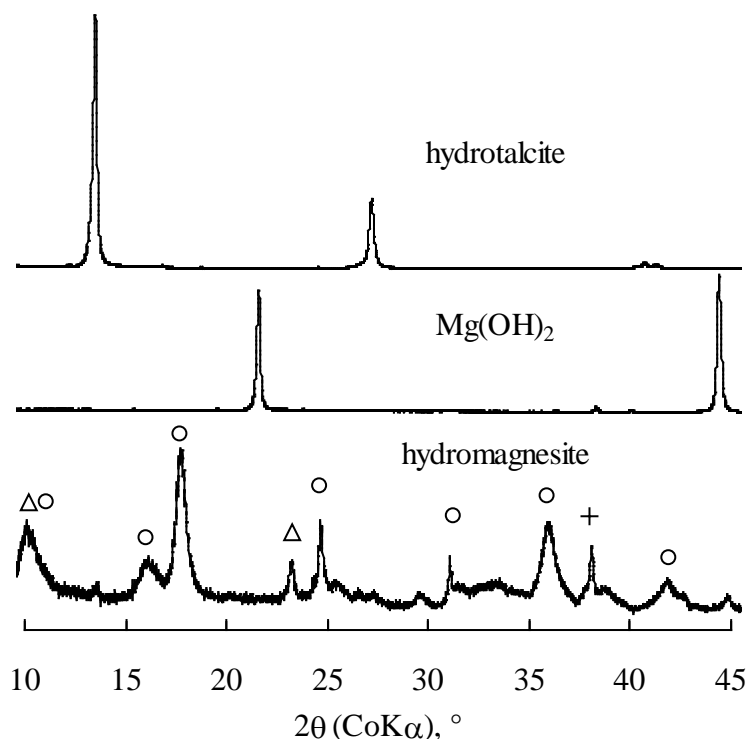


Figure 2.2: XRD spectra of the various powders. Key: hydromagnesite (\circ), dypingite (Δ), and magnesite (+)

The $\text{Mg}(\text{OH})_2$ DRIFT spectrum shown in Figure 2.3 is characterized by a sharp and intense $-\text{OH}$ stretching vibration peak at ca. 3700 cm^{-1} . This sharp peak is also observed in the hydromagnesite at about 3650 cm^{-1} but in the hydrotalcite it is much broader and it is centred at a lower wavenumber (ca. 3450 cm^{-1}). The hydrotalcite features a single carbonate peak at 1367 cm^{-1} while in the hydromagnesite the carbonate asymmetric stretching vibration band is split with peaks at 1420 cm^{-1} and 1480 cm^{-1} . The latter also features a carbonate symmetric stretch band at ca. 1120 cm^{-1} and three bending bands at 800 cm^{-1} . The presence of the water of crystallization is indicated by the bands at ca. 3510 and 3450 cm^{-1} [32].

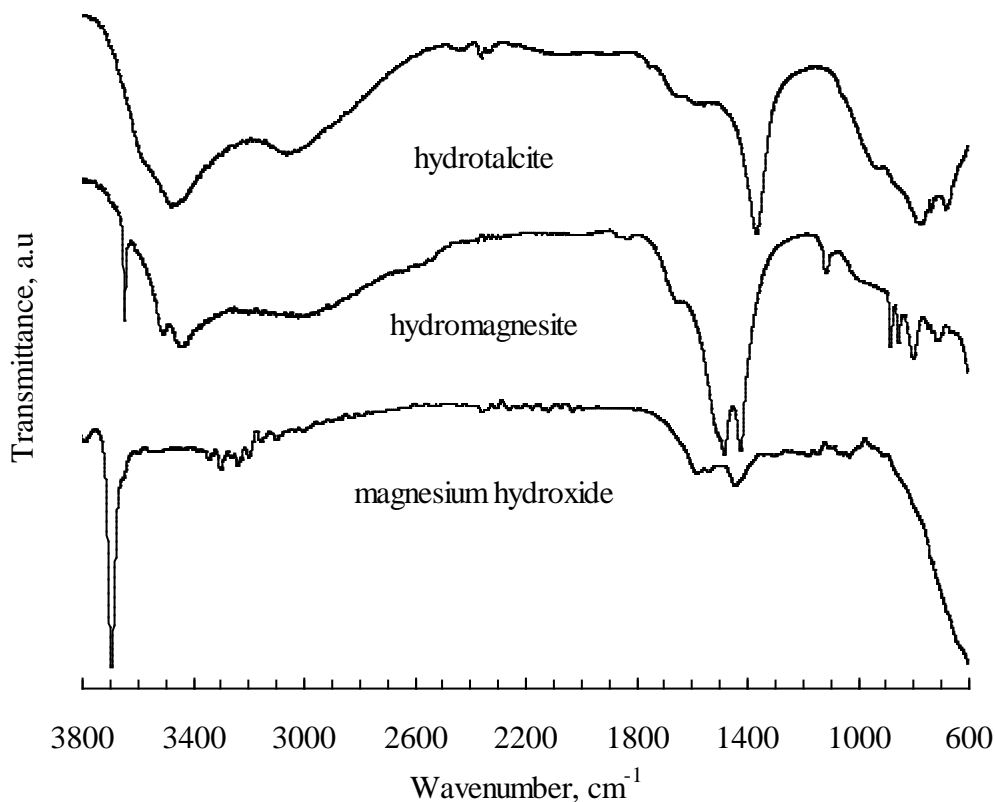


Figure 2.3: DRIFT spectra for magnesium hydroxide, hydrotalcite and hydromagnesite.

Figure 2.4 compares the infrared spectra of hydromagnesite, with and without a stearic acid coating, with those for stearic acid and magnesium stearate. The small peaks at ca. 2915 and 2855 cm^{-1} (due to symmetric and asymmetric stretching vibration of aliphatic groups $-\text{CH}_2-$ groups) confirms the presence of stearic acid in the coated sample. The spectrum for stearic acid shows the carbonyl stretching vibration at ca. 1700 cm^{-1} . Unfortunately the low intensity of the absorption bands in the present hydromagnesite spectrum makes it impossible to establish the nature of the absorbed stearic acid, i.e. whether neutral or ionised.

Comparison of the DRIFT spectra for the stearic acid coated and uncoated magnesium hydroxide and hydrotalcite samples showed similar small peaks at ca. 2915 and

2855 cm^{-1} for the stearic acid solution treated samples. The absence of such peaks for the uncoated samples, confirms the presence of stearic acid on the surface of the coated samples.

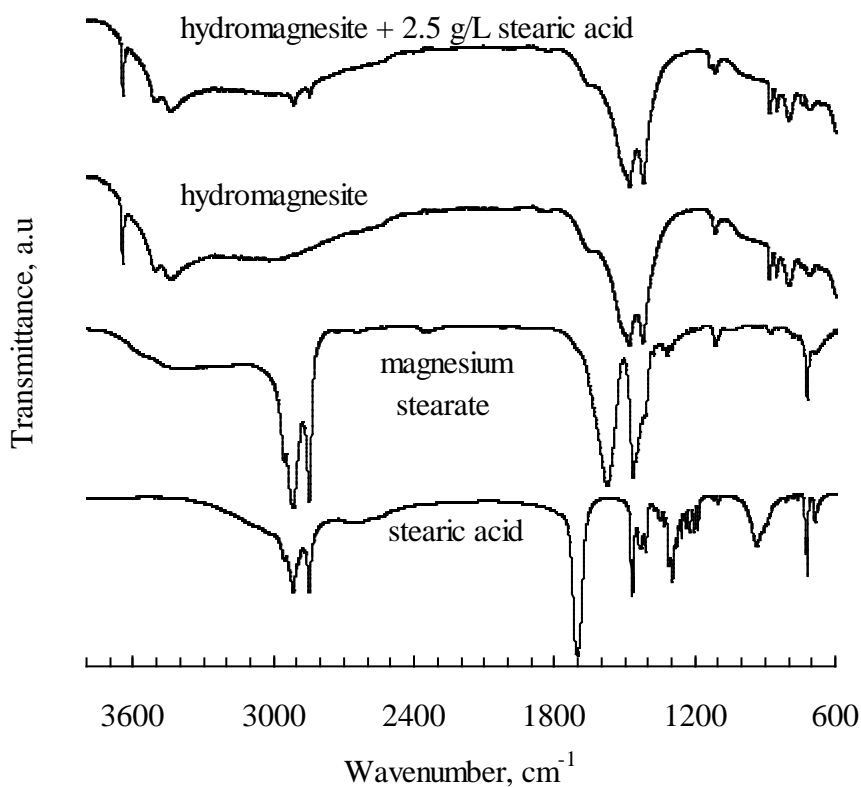


Figure 2.4: DRIFT spectra for neat and 2.5 g L^{-1} stearic acid solution treated hydromagnesite compared to those for magnesium stearate and neat stearic acid.

Figure 2.5 shows mass loss curves for hydromagnesite, magnesium hydroxide and hydrotalcite powders obtained in air. The degradation pathways for these three compounds are given in Schemes I to III. In each case water, or water and carbon dioxide are released in gaseous form and inert oxides remain.

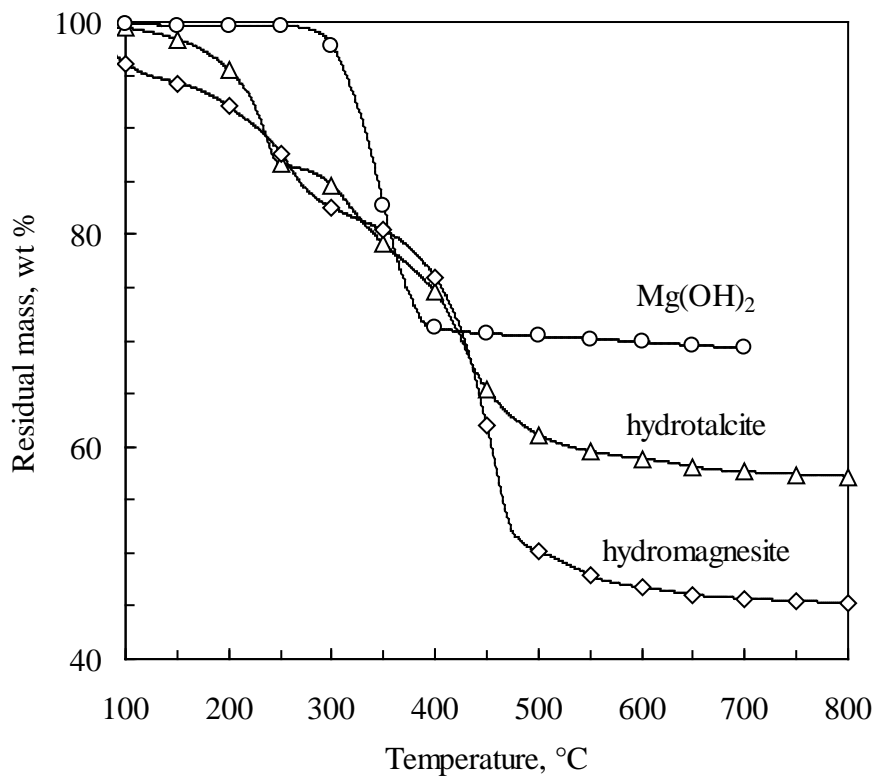
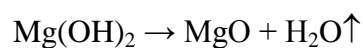
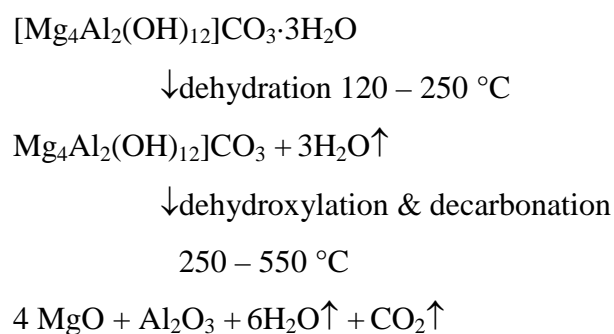


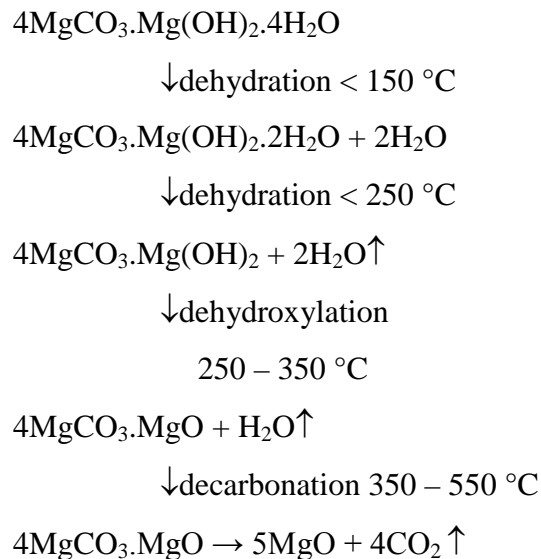
Figure 2.5: TGA curves for hydromagnesite, magnesium hydroxide and hydrotalcite powders obtained in air at a scan rate of $10\text{ }^{\circ}\text{C min}^{-1}$.



Scheme I: Thermal decomposition of magnesium hydroxide. The theoretical mass loss is 30.9 wt.%.



Scheme II: Thermal decomposition of the synthetic hydrotalcite [39-40].



Scheme III: Degradation pathway for hydromagnesite [41-44].

The mass loss of the hydrotalcite sample proceeds stepwise with three distinct but overlapping peaks in the DTG trace. These events are commonly attributed to the loss of interlayer water, dehydroxylation and a combination dehydroxylation-decarbonation reaction respectively [40].

The endothermic decomposition of hydromagnesite occurs in three steps over the temperature range 200 °C to 550 °C as shown in Scheme III [43]. The first step entails the removal of water of crystallisation. Water is also released in the second step owing to the decomposition of magnesium hydroxide layers. Finally carbon dioxide is released when the MgCO₃ decomposes to form MgO.

The residual masses at the end temperatures indicated in Figure 2.5 were 69.3 wt.%, 58.1 wt.% and 45.3 wt.% for Mg(OH)₂, hydrotalcite and hydromagnesite respectively. The corresponding theoretically expected values are 69.1 wt.%, 56.1 wt.% and 43.1 wt.% for Mg(OH)₂, hydrotalcite and hydromagnesite respectively. The small discrepancies are attributed to the presence of impurities.

TGA was also used to estimate the amount of stearate absorbed on the powders that were treated with 2.5 g L^{-1} and 5 g L^{-1} stearic acid solutions. The method assumes that the stearate is completely lost at elevated temperatures. The calculation procedure compared the relative mass loss of the coated sample to that of the neat powder at high temperature (e.g. $800 \text{ }^\circ\text{C}$), but adjusted with respect to the mass loss observed at $150 \text{ }^\circ\text{C}$ to correct for the possibility of variable moisture contents. The results are presented in Table 2.1.

Figure 2.6 shows the effect of stearic acid coating on the measured BET surface areas. A decrease in BET surface area is observed as the stearic acid concentration in the solution is increased. However, above 1 g L^{-1} the BET surface areas reached plateau values of $6.9 \text{ m}^2 \text{ g}^{-1}$, $10 \text{ m}^2 \text{ g}^{-1}$ and $23 \text{ m}^2 \text{ g}^{-1}$ for magnesium hydroxide, hydrotalcite and hydromagnesite respectively. This reduction is probably caused by the stearic acid filling in some narrow crevice defects in the plate-like crystals.

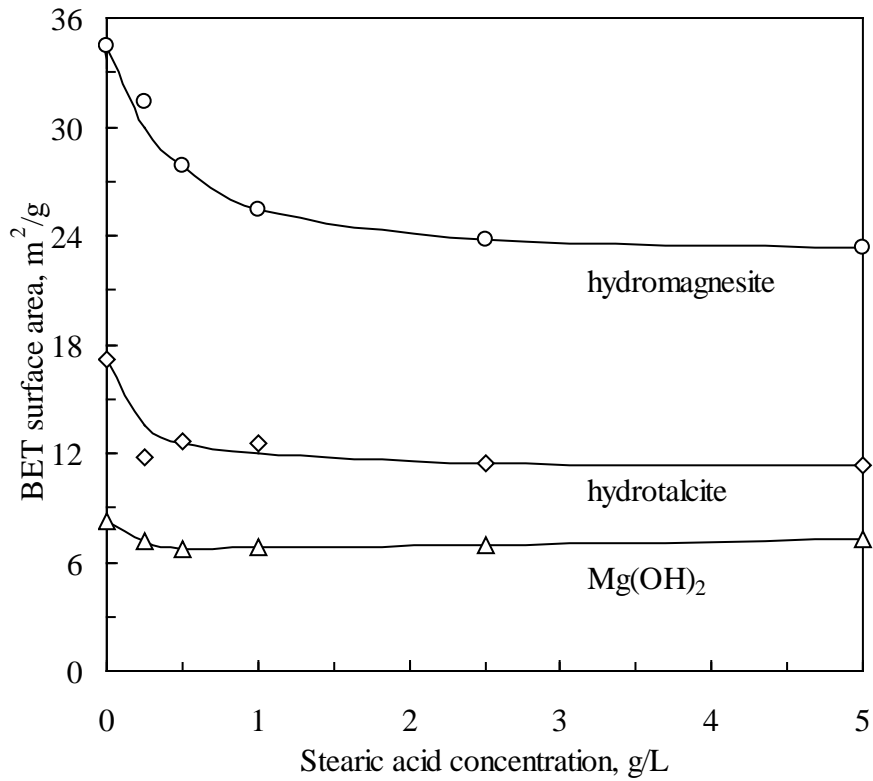


Figure 2.6: Effect of stearic acid dosage level on the BET surface area of the powders.

Close-packed stearic acid chains assume a hexagonal arrangement with the extended chains oriented at an angle 29° to the vertical [45]. The projected surface area per stearate chain is approximately equal to 0.22 nm^2 [46].

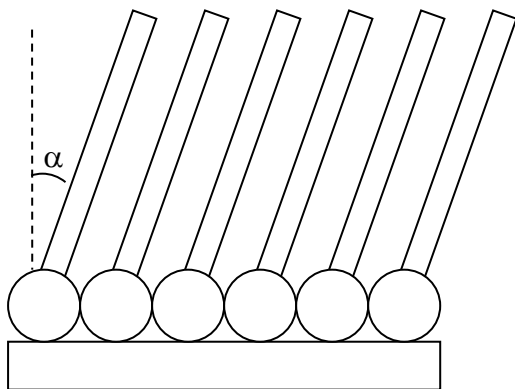


Figure 2.7: Schematic of surface-adsorbed close-packed monolayer of stearic acid on a mineral surface.

Figure: 2.7 shows the surface-adsorbed close-packed monolayer of stearic acid on a mineral surface with close packed chains oriented at an angle α to the vertical. This means that the actual projected area will be $A_{\text{BET}}/\cos \alpha$, α taken as the slant angle.

Table 2.1: Stearic acid coating levels expressed in wt.% as calculated from the residual level in the solvent and from TGA data.

Powder:	hydrotalcite		Mg(OH) ₂		Hydromagnesite	
Stearic acid solution concentration, g L ⁻¹	solvent analysis	TGA	solvent analysis	TGA	solvent analysis	TGA
2.5	2.5 ± 0.3	2.8	3.3 ± 0.2	2.9	5.1 ± 0.0	-
5.0	3.6 ± 0.4	3.2	2.8 ± 0.1	2.1	5.6 ± 0.0	6.4
Monolayer estimate						
BET	3.7		1.8		7.3	

Let the surface area of the powder be $A_{\text{BET}} \text{ m}^2 \text{ g}^{-1}$. The molar mass of stearic acid is $284.48 \text{ g mol}^{-1}$ and number $N_{\text{Avo}} = 6.022169 \times 10^{23}$. Thus the stearic acid equivalent to a monolayer amount equals:

$$100 \frac{a_{\text{solid}} M_{\text{st}} \cos \alpha}{A_{\text{st}} N_{\text{Avo}}} = 0.247 A_{\text{BET}} \cos \alpha \quad \text{wt \%} \quad (1)$$

If the available surface area of the powder is completely covered by such a monolayer, and assuming a value of 30° for the slant angle, the amount absorbed is given by $0.215 A_{\text{BET}} \text{ wt.}\%$. The measured BET surface areas (A_{BET}) for the neat powders were $8.2 \text{ m}^2 \text{ g}^{-1}$, $17.3 \text{ m}^2 \text{ g}^{-1}$ and $34.5 \text{ m}^2 \text{ g}^{-1}$ for Mg(OH)₂, hydrotalcite and hydromagnesite respectively. This implies monolayer coverage would be attained at 1.8 wt.%, 3.7 wt.% and 7.3 wt.% respectively. These values are compared to

measured values in Table 2.1. The results indicate that the actual amount absorbed from solutions containing 2.5 g L^{-1} or more stearic acid was slightly below the value expected for monolayer coverage in the case of hydrotalcite and hydromagnesite. The results also suggest that the coverage on the magnesium hydroxide exceeded monolayer absorption.

Figure 2.8 shows the carbon to oxygen (C/O) atomic ratio calculated from the peak areas of the C1s (285-295 eV) and O1s (530-545 eV) signals as measured by XPS. The XPS technique samples the composition of matter at the surface to a depth of a few nanometres. Stearic acid has a theoretical C/O atomic ratio of 9.0. The value obtained by XPS analysis for the grade stearic acid used presently was actually 9.5. These values are much higher than the theoretical ratios for the neat hydrotalcite (0.056) and neat hydromagnesite (0.222). The ratios measured for coated samples thus provide an indication of the amount of stearic acid absorbed on the surfaces of the powders. The C/O atomic ratio initially increases rapidly with the stearic acid solution concentration but then levels off above 2.5 g L^{-1} . Values similar to that expected for neat stearic acid were attained for the hydromagnesite and hydrotalcite samples treated with a solution containing 2.5 g L^{-1} stearic acid. This suggests that close to monolayer coverage was achieved and it was therefore decided to use these samples in the rheology experiments. The XPS data indicates a value for the C/O atomic ratio that is approximately equivalent to two thirds of that for stearic acid for the $\text{Mg}(\text{OH})_2$ treated with the 2.5 g L^{-1} solutions and equivalent to nine tenths of that for stearic acid for the $\text{Mg}(\text{OH})_2$ treated with the 5.0 g L^{-1} solution. This is at odds with the TG and solution depletion estimates shown in Table 1. Both these techniques suggest that the stearic acid adsorbed about 50 % more than a monolayer equivalent (with the

Mg(OH)₂ treated with the 2.5 g L⁻¹ solution having a higher organic content). The reason for these discrepancies is not understood at present. It is possible that the “missing” stearic acid was incorporated as a bulk phase in crevices internal to the Mg(OH)₂ particles.

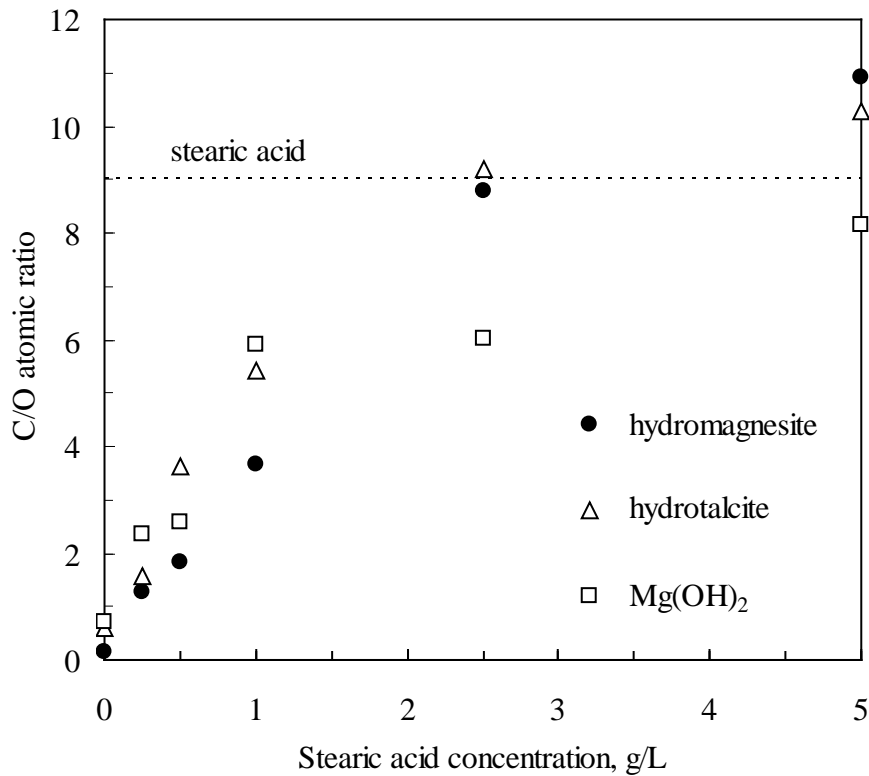


Figure 2.8: Effect of stearic acid dosage level on the ratio of the C/O atomic ratio as estimated from XPS.

Figure 2.9 shows specific filler volume fractions measured using the tap density techniques and the oil absorption technique. The values determined using the tap density method, are significantly lower than those calculated from oil absorption measurements. This is understandable as in the tap method the particles are compacted in a virtually shear-free manner. The oil absorption procedure involves application of significant shear with the oil acting as a lubricant. This helps to break-up loose particle agglomerates allowing the particles to pack more efficiently. The

presence of a stearic acid coating is clearly beneficial yielding significantly higher packing densities compared to the neat fillers. The improvement was greatest in the case of the hydrotalcite and least for the magnesium hydroxide.

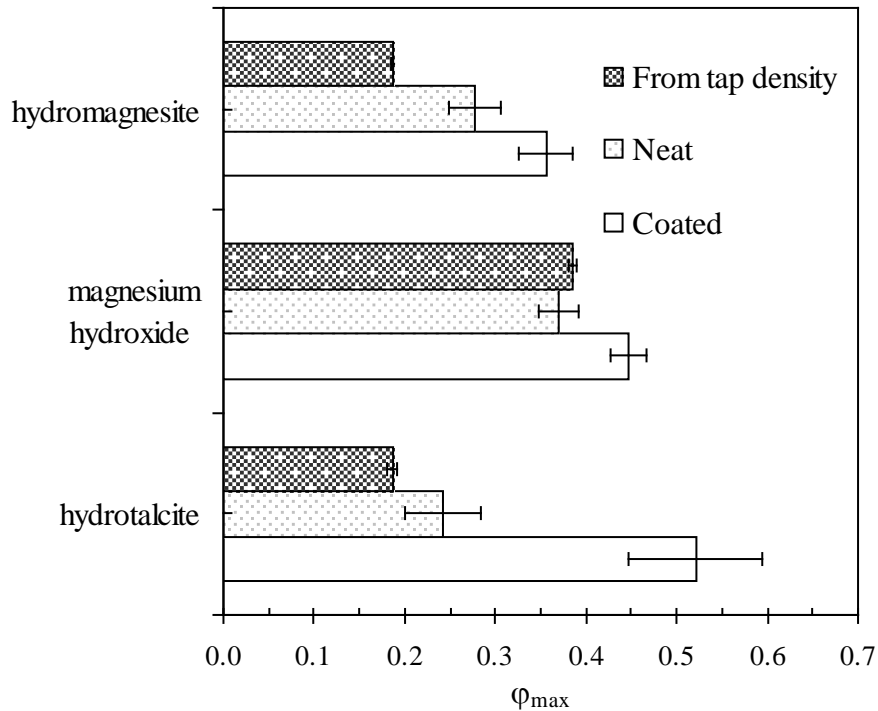


Figure 2.9: Specific maximum filler volume fractions determined from tap density (for uncoated filler only) and oil absorption experiments (uncoated and treated with 2.5 g/L stearic acid).

Figure 2.10 shows the viscosity of the white oil and suspensions containing 25 wt.% inorganic filler as measured at a temperature of 30 °C. Note that the indicated filler content refers to the purely inorganic part, i.e. the stearic acid coating was deemed to form part of the organic liquid phase. Owing to the large difference in densities between the solids and the liquid medium, the volume fraction filler in the suspensions amounted to only 10.3, 11.0 and 11.9 vol.% for Mg(OH)₂, hydromagnesite and hydrotalcite respectively.

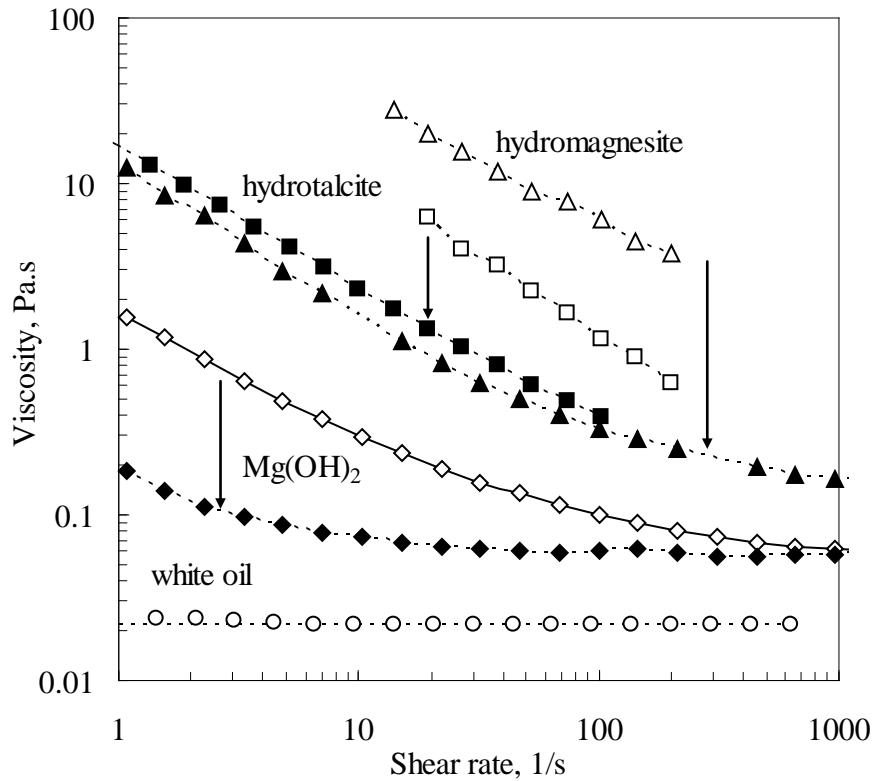


Figure 2.10: Effect of stearic acid coating on the viscosity of 25 wt.% suspensions of hydromagnesite, magnesium hydroxide and hydrotalcite powders in white oil at 30 °C. Open symbols indicate neat powders while solid symbols are for powders treated with 2.5 g/L stearic acid solution in acetone. The arrows indicate the reduction in apparent viscosity facilitated by the surface coatings.

The white oil shows the expected Newtonian behaviour with a shear-independent viscosity of 21.7 mPa s. The viscosities of the slurries are much higher, by several orders of magnitude, when compared at a shear rate of 1 s^{-1} . However, the slurry viscosities also show strong shear-thinning behaviour. The relative viscosity for the Mg(OH)_2 slurry decreases to about 3.0 at a shear rate of $1\ 000 \text{ s}^{-1}$. Shear thinning non-Newtonian behaviour is well known for concentrated suspensions but in this instance such behaviour is observed at the relatively low solid phase volume fraction of 0.10 to 0.12. This implies that the fine powders considered here are very effective

thickening agents for white oil. This is especially true for the uncoated hydromagnesite and hydrotalcite powders.

Furthermore, close to identical data were generated for a decrease in shear rate. A plot (not shown) of the values for a decreasing shear rate (reverse) fit the increasing shear rate (forward) plots in Figure 2.9 almost identically; showing no form of hysteresis. This implies that the mechanism for the reduction in viscosity due to an increase in shear rate is reversible and not permanent.

The shear thinning behaviour of the hydromagnesite and hydrotalcite suspensions follow the power-law model with:

$$\eta = K\dot{\gamma}^{n-1} \quad (2)$$

where η is the viscosity of the suspension and $\dot{\gamma}$ is the shear rate.

Values for the consistency index K and the flow behaviour index n were calculated and are presented in Table 2. Both parameters change when a stearic acid coating is applied. The consistency index decreases by about an order of magnitude for the hydrotalcite and the hydromagnesite. These changes reflect the decrease in slurry viscosity for the coated powders compared to the neat uncoated versions.

Table 2.2: Consistency index K and the flow behaviour index n for the slurries

Powder:	Hydrotalcite		Mg(OH) ₂		Hydromagnesite	
Treatment	K	n	K	n	K	n
Neat	105	0.03	1.64	0.24	165	0.28
Coated (2.5 g L ⁻¹)	16.3	0.17			12.7	0.18

2.5 Discussion

The viscosity of particle suspensions depends on the nature of the flow units present [47]. The flow units may comprise individually dispersed powder particles or particle agglomerates that act in unison with occluded liquid. Any such associated liquid contributes to the effective volumetric concentration of the flow units in the remaining liquid. In other words, the occluded liquid behaves in such a way that it becomes part of the “solid” phase. The Newtonian viscosity of such suspensions is adequately described by the Krieger-Dougherty [47-49] expression:

$$\eta_r = \frac{\eta}{\eta_o} = \left(1 - \frac{\phi}{\phi_{\max}}\right)^{-2.5k\phi_{\max}} \quad (3)$$

Here η_o represents the viscosity of the pure fluid; η that of the suspension, and η_r is the relative viscosity. k is a particle shape factor that assumes the value unity for spheres [47]. ϕ is the volume fraction of the flow units and ϕ_{\max} is the maximum attainable volume fraction. At this level an abrupt transition to elastic solid-like behaviour is observed [50].

Eilers' [51-52] expression provides an alternative formulation that gives very similar results to the Krieger-Dougherty model [48-49]:

$$\eta_r = \left(1 + \frac{1.25k\phi}{1 - \phi / \phi_{\max}}\right)^2 \quad (4)$$

Real slurries show non-Newtonian flow characteristics with the apparent viscosity decreasing with increasing rate of shear [48]. This is commonly attributed to their agglomerative nature [53]. When the individual particles are suspended in a liquid,

they aggregate to form floc-like agglomerates or clusters. Newtonian behaviour is observed when the agglomerates, acting as individual flow units, retain their integrity. Non-Newtonian behaviour results when the application of shear induces changes in the effective volume of these flow units [47-49, 53]. Quemada [54] and Wildemuth and Williams [55] independently posed that the incorporation of a shear-dependent maximum packing fraction (ϕ_{\max}) in the rheological model for viscosity suffices to explain virtually all non-Newtonian effects over the entire concentration range. At low shear the agglomerates assume a loose floc structure that imbibes much of the fluid. The shear-thinning behaviour observed at intermediate deformation rates is then a manifestation of the shear induced reduction of the degree of aggregation and concomitant release of occluded fluid [56]. There are two distinct mechanisms for such agglomerate break-up: erosion and rupture [57, 58]. In erosion individual particles are removed from the cluster and dispersed into the fluid. In the rupture mechanism, the agglomerate breaks down into fragments of similar size. The critical stress for effecting erosion tends to be smaller than that required for rupture. When complete cluster break-up is achieved, the slurry viscosity coincides with the predictions of equations (2) or (3) with ϕ_{\max} defined by the maximum packing density of the individual particles [53] and this corresponds to a packed bed scenario. Experimental [50] and theoretical [59] studies indicate that the maximum three-dimensional random close packing density of monodisperse spheres corresponds to $\phi_{\max} = 0.64$.

Usui [60] argues that the clusters assume a spherical shape when the number of primary particles in the clusters becomes large. In addition, it is assumed here that the clusters are of similar size. It is then possible to estimate a lower limit for the porosity

of the agglomerates present at low shear rates using either equation (2) or equation (3). The hydrodynamic volume of the agglomerates depends on their porosity (ε), i.e. how loosely the particles are packed inside the flocs. For hydrotalcite and hydromagnesite the observed relative viscosities exceeded 500 at the lowest shear rates investigated. These values are so much higher than unity that for all practical purposes both equations indicate that the porosity can be estimated using:

$$\varepsilon = 1 - \phi/\phi_{\max} = 1 - \phi/0.64 \quad (5)$$

This yields values of 0.81 and 0.83 for the uncoated hydrotalcite and hydromagnesite samples respectively. These values are similar to the porosity value obtained for both samples using the tap density technique, i.e. 0.81. The implication is that the flocs, present at low shear, have a packing density similar to remnants of the original dry agglomerates. This is rather surprising given that the suspensions were prepared by a high shear process. Therefore the evidence suggests that, despite being well dispersed during the preparation step, they have a natural tendency to revert to an agglomerated floc structure with porosities similar to those of the solid dry powders. Further proof of this re-agglomeration tendency is the reversibility of the viscosity plots for an increase and decrease in the shear rate. Reducing the shear rate allows the particles to re-agglomerate to an agglomerated floc structure and manifests as an increase in viscosity.

The neat stearic acid coated magnesium hydroxide slurries attain a Newtonian viscosity plateau at shear rates exceeding 100 s^{-1} . It can be assumed that this state corresponds to the state where all the c individually dispersed so that the maximum packing is given by the oil absorption value, i.e. $\phi_{\max} = 0.447$. This allows one to

estimate the shape factor k to be estimated using either equation (2) or (3). The Krieger-Dougherty equation and Eilers' model yield similar values of $k = 3.39$ and $k = 3.86$ respectively.

The fact that the stearic acid coated powders yield slurries with significantly lower viscosities indicates that the surface treatment makes it easier for agglomerates to break-up under the influence of shear. This in turn suggests that the adhesive forces between particles have been weakened by the stearic acid coating.

2.6 Conclusion

The effect of a stearic acid coating on the properties of hydrated filler-type flame retardants was studied. The flame retardants comprised fine synthetic powders of magnesium hydroxide hydromagnesite and hydrotalcite. The surface coating was applied by treating the powders with dilute solutions of stearic acid in acetone. The presence of the coating was confirmed by DRIFT and quantified by XPS and TGA. It was found that the coating level approximately equivalent to monolayer coverage was achieved when the hydrotalcite and hydromagnesite powders were treated with 20 mL acetone per gram filler containing 2.5 g L^{-1} stearic acid.

Measured BET surface areas of the hydrotalcite and hydromagnesite powders decreased by as much as 33 % when coated with stearic acid. SEM showed that the hydrotalcite and magnesium hydroxide powders comprised small crystals that are profusely agglomerated. Owing to their fineness and tendency to agglomerate in high porosity structures, both the hydrotalcite and hydromagnesite powders are very effective thickening agents for white oil. The rheology of slurries containing 25 wt.%

solids (ca. 11 vol.%) was studied as a function of shear rate. The suspended powders increased the apparent low-viscosity by several orders of magnitude. This substantial thickening effect is attributed to a tendency of the particles to aggregate as high-porosity flocs in the oil. A lower limit for the porosity of the flocs is estimated at 81 vol.% on the assumption that the flocs are spherical in shape and similar in size.

The suspensions also showed considerable shear thinning. This is consistent with the idea that the application of shear causes break-up of the agglomerates and releases the occluded fluid. The significantly lower viscosities observed for the stearic acid treated samples indicate that the surface coating reduces the adhesive forces between the particles. This makes it easier to break-up the agglomerates and aids dispersion of individual particles. However, a reduction in the shear rate allows for the reformation of the agglomerates.

2.7 Acknowledgements

Financial support for this research, from the Institutional Research Development Programme (IRDP) and the National Research Foundation of South Africa (NRF) as well as the THRIP program of the Department of Trade and Industry (administered by the NRF), is gratefully acknowledged.

2.8 References

1. Laoutid F, Bonnaud L, Alexandre, M (2009) New prospects in flame retardant polymer materials: From fundamentals to nanocomposites. *Mater Sci Eng, R* 63(3):100-125
2. Delfosse L, Baillet C, Brault A, Brault, D (1989) Combustion of ethylene-vinyl acetate copolymer filled with aluminium and magnesium hydroxides. *Polym Degrad Stab* 23(4):337-347
3. Horn WE (2000) Inorganic hydroxides and hydroxycarbonates: Their function and use as flame-retardant additives. 293-294 In: Grand AF (ed), Wilkie CA (ed) *Fire Retardancy of Polymeric Materials*, 1st Ed. CRC Press, Boca Raton
4. Hornsby PR (2001) Fire retardant fillers for polymers. *Int Mater Rev* 46(4):199-210
5. Fenimore CP, Jones GW (1966) Modes of inhibiting polymer flammability. *Comb and Flame*, 10(2):295-301
6. Fenimore CP, Martin FJ (1966) Flammability of polymers. *Comb and Flame*, 10(2):135-139
7. Hornsby PR, Watson CL (1989) Mechanism of smoke suppression and fire retardancy in polymers containing magnesium hydroxide filler. *Plast Rubber Process Appl* 11(1):45-51
8. Hornsby PR, Watson CL (1990) A study of the mechanism of flame retardance and smoke suppression in polymers filled with magnesium hydroxide. *Polym Degrad Stab* 30(1):73-87
9. Carpentier F, Bourbigot S, Le Bras M, Delobel R, Foulon M (2000) Charring of fire retarded ethylene vinyl acetate copolymer - magnesium hydroxide/zinc borate formulations. *Polym Degrad Stab* 69(1):83-92
10. Genovese A, Shanks (2007) RA Structural and thermal interpretation of the synergy and interactions between the fire retardants magnesium hydroxide and zinc borate. *Polym Degrad Stab* 92(1):2-13
11. Burns M, Wagenknecht U, Kretzschmar B, Focke WW (2008) Effect of hydrated fillers and red phosphorus on the limiting oxygen index (LOI) of EVA-PVB and LDPE-EVAL blends. *J Vinyl Add Tech* 14:113-119
12. Hornsby PR (1999) Rheology, compounding and processing of filled thermoplastics. *Adv Polym Sci* 139:155-217

13. Hornsby PR (1994) Application of magnesium hydroxide as a fire retardant and smoke-suppressing additive for polymers. *Fire Mater* 18(5):269-276
14. Wang Z, Chen Z, Fan W, Nie W (2006) Effects of surface modifiers on mechanical and rheological properties of halogen-free flame retarded polyethylene composites. *Polymer Plast Tech Eng* 45(2):191-196
15. Zhang F, Zhang H, Su Z (2007) Surface treatment of magnesium hydroxide to improve its dispersion in organic phase by the ultrasonic technique. *Appl Surf Sci* 253(18):7393-7397
16. Potente H, Flecke J, (1997) The breaking down and agglomerating of fillers in polymer melt: A physical model for mathematical description. *J Reinf Plas Compos* 16(14) 1281-1292
17. Papirer E, Schultz J, Turchi C (1984) Surface properties of a calcium carbonate filler treated with stearic acid. *Eur Polym J* 20:1155-1158
18. Gilbert M, Petiraksakul P (1997) Stearate coatings on particulate fillers - The effects on resulting compound properties. *Polym and Polym Compos* 5(8):535-539
19. Osman M, Suter U (2002) Surface Treatment of Calcite with Fatty Acids: Structure and Properties of the Organic Monolayer. *Chem Mater* 14:4408-4415
20. Khanna, YP, Taylor DA, Paynter CD, Skuse DR (2009) Surface modification of calcium carbonate. I. Characterization of physico-chemical phases of stearic acid coating. Submitted to *J Mater Sci*
21. Liauw CM, Rothon RN, Hurst SJ, Lees GC (1998) The use of flow micro-calorimetry and FTIR techniques for characterising filler/organic acid interactions. *Compos Interfaces* 5(6):503-514
22. Gilbert M, Sutherland I, Guest A (2000) Characterization of coated particulate fillers. *J Mater Sci* 35(2):391-397
23. Gilbert M, Petiraksakul P, Mathieson I (2001) Characterisation of stearate/stearic acid coated fillers. *Mater Sci Technol* 17(11):1472-1478
24. Haurie L, Fernández AI, Velasco JI, Chimenos JM, Ticó-Grau JR, Espiell F (2005) Synthetic hydromagnesite as flame retardant. A study of the stearic coating process. *Macromol Symp* 221:165-174
25. Rigolo M, Woodhams RT (1992) Basic magnesium carbonate flame retardants for polypropylene. *Polym Eng Sci* 32:327-334

26. Huang H, Tian M, Yang J, Li H, Liang W, Zhang L, Li X (2008) Stearic acid surface modifying Mg(OH)₂: Mechanism and its effect on properties of ethylene vinyl acetate/Mg(OH)₂ composites. *J Appl Polym Sci* 107(5):3325-3331
27. Camino G, Maffezzoli A, Braglia M, De Lazzaro M, Zammarano M. (2001) Effect of hydroxides and hydroxycarbonate structure on fire retardant effectiveness and mechanical properties in ethylene-vinyl acetate copolymer. *Polym Degrad Stab* 74(3):457-464
28. Miyata S, Imahashi T, Anabuki H (1980) Fire-retarding polypropylene with magnesium hydroxide. *J Appl Polym Sci*, 25(3):415-425
29. Miyata S, Kumura, T. (1973) Synthesis of new hydrotalcite-like compounds and their physico-chemical properties, *Chem Lett* 843-848
30. Bellotto M, Rebours B, Clause, O Lynch J (1996) A re-examination of hydrotalcite crystal chemistry. *J Phys Chem* 100:8524-8527
31. De Roy A, Forano C, El Malki K, Besse J P (1992) In: Ocelli ML (ed), Robson HE (ed), *Expanded Clays and Other Microporous Solids*, 1st edn. Van Nostrand Reinhold, New York, 2:108
32. White W B (1971) Infrared characterization of water and hydroxyl ion in the basic magnesium carbonate minerals. *Am Mineral* 56:46-53
33. Hales MC, Frost RL, Martens, WN (2008) Thermo-Raman spectroscopy of synthetic nesquehonite implication for the geosequestration of greenhouse gases. *J Raman Spectrosc* 39:1141-1149
34. Raade G (1970) Dypingite, a new hydrous basic carbonate of magnesium, from Norway. *Am Mineral* 55(9-10):1457-1465
35. Hayek E, Gleispach H (1966) Hydroxidcarbonate von Magnesium und Zink – (Präparative Homogenfällung durch Komplexacidolyse, 5. Mitt.) *Monatsh Chem* 97(4):1059-1063
36. Haurie L, Fernández AI, Velasco JI, Chimenos JM, Lopez Cuesta JM, Espiell F (2006) Synthetic hydromagnesite as flame retardant. Evaluation of the flame behaviour in a polyethylene matrix. *Polym Degrad Stab* 91(5): 989-994
37. Morgan AB, Cogen JM, Opperman RS, Harris JD (2007) The effectiveness of magnesium carbonate-based flame retardants for poly (ethylene-co-vinyl acetate) and poly (ethylene-co-ethyl acrylate). *Fire and Mater* 3(6):387-410
38. Botha A, Strydom CA (2001) Preparation of a magnesium hydroxy carbonate from magnesium hydroxide. *Hydrometallurgy* 62(3):175-183

39. Rey F, Fornés V, Rojo JM (1992) Thermal decomposition of hydrotalcites. An infrared and nuclear magnetic resonance spectroscopic study. *J Chem Soc, Faraday Trans* 88:2233-2238
40. Bera P, Rajamathi M, Hegde MS, Kamath PV (2000) Thermal behavior of hydroxides, hydroxysalts and hydrotalcites. *Bull Mater Sci* 23:141-145
41. Sawada Y, Yamaguchi J, Sakurai O, Uematsu K, Mizutani N, Kato M (1979) Thermogravimetric study on the decomposition of hydromagnesite $4\text{MgCO}\cdot\text{Mg}(\text{OH})\cdot 4\text{H}_2\text{O}$. *Thermochim Acta* 33:127-140
42. Sawada Y, Yamaguchi J, Sakurai O, Uematsu K, Mizutan N, Kato M (1979) Thermal decomposition of basic magnesium carbonates under high-pressure gas atmospheres. *Thermochim Acta* 32(1-2):277-291
43. Choudhary VR, Pataskar SG, Gunjkar VG, Zope GB (1994) Influence of preparation conditions of basic magnesium carbonate on its thermal analysis. *Thermochim Acta* 232:95-110
44. Vágvölgyi V, Frost RL, Hales M, Locke A, Kristóf J, Horváth E (2008) Controlled rate thermal analysis of hydromagnesite. *J Therm Anal Calorim* 92(3):893-897
45. Itoh T, Ohta N, Shichi T, Yui T Takagi K (2003) The self-assembling properties of stearate ions in hydrotalcite clay composites, *Langmuir* 19:9120-9126
46. He JX, Yamashita S, Jones W, Yamagishi A (2002) Templating effects of stearate monolayer on formation of Mg-Al-hydrotalcite, *Langmuir* 18:1580-1586
47. Mandersloot WGB, Scott KJ (1990) Rheology of particle suspensions. *S Afr J Chem Eng* 2:53-69
48. Krieger IM, Dougherty TJ (1959) A Mechanism for Non-Newtonian Flow in Suspensions of Rigid Spheres. *Trans of the Soc Rheol* 3:137-152
49. Krieger (1972) Rheology of monodisperse lattices. *Adv Colloid Interface Sci* 3(2):111-136
50. Jones DAR, Leary B, Boger DV (1991) The rheology of a concentrated colloidal suspension of hard spheres. *J Colloid Interface Sci*, 147(2):479-495.
51. Eilers H (1941) Die Viskosität von Emulsionen hochviskoser Stoffe als Funktion der Konzentration. *Kolloid-Z* 97(3): 313-321
52. Eilers H (1943) Die Viskositäts-Konzentrationsabhängigkeit kolloider Systeme in organischen Lösungsmitteln. *Kolloid-Z* 102(2):154-169

53. Usui H, Kishimoto K Suzuki H (2001) Non-Newtonian viscosity of dense slurries prepared by spherical particles. *Chem Eng Sci* 56(9):2979-2989
54. Quemada D (1986) Comments on the paper “Viscosity of suspensions modeled with a shear-dependent maximum packing fraction” by Wildemuth CR, Williams MC *Rheol Acta* 25(6):647-649
55. Wildemuth CR, Williams MC (1984) Viscosity of suspensions modeled with a shear-dependent maximum packing fraction. *Rheol Acta* 23(6):627-635
56. Tsenoglou C (1990) Scaling concepts in suspension rheology. *J. Rheol.* 34(1):15-24
57. Rwei SP, Manas-Zloczower I, Feke DL (1990) Observation of carbon black agglomerate dispersion in simple shear flows. *Polym Eng Sci* 30(12):701-706
58. Hansen S, Khakhar DV, Ottino JM (1998) Dispersion of solids in nonhomogeneous viscous flows. *Chem Eng Sci* 53(10):1803-1817
59. Jalali P, Li M (2004) An estimate of random close packing density in monodisperse hard spheres. *J Chem Phys* 120(2):1138-1139
60. Usui H (2002) Prediction of dispersion characteristics and rheology in dense slurries. *J Chem Eng Jpn* 35(9):815-829

Chapter 3: The effect of magnesium hydroxide, hydromagnesite and layered double hydroxide on the heat stability and fire performance of plasticised PVC²

3.1 Introduction

Magnesium hydroxide [Mg(OH)₂] (MH) occurs in nature as the mineral brucite. It has a layered structure composed of stacked trioctahedral metal hydroxide sheets. Hydrotalcite is a natural anionic clay mineral [Mg₆Al₂(OH)₁₆CO₃·4H₂O]. Layered double hydroxides (LDHs) are synthetic analogues (1-3). LDHs also feature the stacked sheet structure of brucite (3). The difference is that a portion of the magnesium ions in the sheets have been replaced with aluminium ions. This substitution imparts a net positive charge that is balanced by an equal negative charge from the interlayer carbonate anions. Water molecules also occupy the interlayer space. Hydromagnesite [4MgCO₃·Mg(OH)₂·4H₂O] (HM) is a basic magnesium hydroxycarbonate mineral that also has a layered structure (4).

PVC is a very versatile polymer with diverse applications. Neat PVC features a relatively high chlorine content of 56.7 wt.%. That makes it more resistant to ignition and burning than most organic polymers (5). Furthermore, pyrolysis of PVC yields an isotropic carbon char residue (6) and this contributes to the mechanisms of flame retardant action (7). However, the conventional plasticisers used in the manufacture of

² This Chapter was published as Journal of Fire Sciences (2015) Vol. 33(6) 493–510 and the contents are reproduced here in the format used for submission.

flexible PVC detract from this outstanding fire resistance. Therefore, flame-retardant (FR) and smoke-suppressant (SS) additives must be incorporated in order to meet product test specifications such as oxygen index, heat release rate, smoke evolution, etc. (5).

Levchik and Weil (8) and Weil *et al.* (9) reviewed the chemical additives that have been considered to achieve acceptable fire properties in the principal PVC application areas. The hydrated filler additives aluminium trihydrate, magnesium hydroxide (MH), hydromagnesite (HM) and layered double hydroxide (LDH) have utility as endothermic flame retardants and smoke suppressants for PVC as well as other polymers.(10-14). Their flame retardant action relies on endothermic decomposition reactions that absorb heat and release inert gases, e.g. steam and carbon dioxide (11, 15, 16). The cooling of the polymer substrate inhibits solid phase decomposition reactions. Simultaneously the steam and/or carbon dioxide released by the decomposition reactions dilutes the surrounding atmosphere with an inert gas. Finally, the residues may form an ash-char barrier layer at the surface that reduces heat transfer from the flame to the remaining polymer substrate.

Neat PVC is thermally unstable (17) and prone to autocatalytic dehydrochlorination (18). The hydrogen chloride assumes a catalytic role in the degradation mechanism (19). In practice the thermal instability associated with the use of PVC is overcome through the use of heat stabiliser additives.(17) Scavenging the liberated HCl generated by the degradation reaction is one way to retard the degradation. Layered double hydroxides (LDHs) provide heat stabilisation to PVC owing to their intrinsically high capacity to react with HCl (20-23). The thermal stabilisation action

of LDH involves two steps. Initially, HCl formed during thermal dehydrochlorination, displaces the carbonate interlayer anions to afford LDHs with Cl^- anions in the interlayer. As further dehydrochlorination takes place, the HCl reacts with the clay itself, ultimately destroying its structure and forming metal chlorides, metal hydroxy-chlorides and hydrates of MgCl_2 and AlCl_3 (21).

This communication reports on the performance of magnesium hydroxide, hydromagnesite and LDH on the thermal stability, fire retardancy and smoke suppression of plasticized PVC. Static heat stability was determined using the Thermomat technique and fire performance was determined with a cone calorimeter. The objective was to determine whether LDH-based heat stabiliser can impart fire retardant properties comparable to those provided by magnesium hydroxide and hydromagnesite.

3.2 Experimental

3.2.1 Materials

Reagent grade (95 %) magnesium hydroxide and magnesium oxide (light, 95 %) was obtained from Sigma-Aldrich. Industrial grades magnesium oxide and $\text{Al}(\text{OH})_3$ were supplied by Chamotte Holdings. All other chemicals were analytical grade reagents supplied by Merck. TPC Paste Resin Co., Ltd. supplied PG680, an emulsion grade poly(vinyl chloride). It was a free flowing powder with a K-value of 69. The diisononyl phthalate (DINP) plasticiser was supplied by Isegen.

3.2.2 Synthesis of LDH and hydromagnesite

The layered double hydroxide (LDH) $[Mg_{0.667}Al_{0.333}(OH)_2](CO_3)_{0.167} \cdot mH_2O$ was synthesised according to the method described by Labuschagné *et al.* (24). The procedure was as follows: The $Al(OH)_3$ and light MgO powders were mixed in the required 2:1 stoichiometric ratio. The powder mix was slowly added, while stirring, to one litre of distilled water in a 1.6 L Parr autoclave. The final solids concentration of the slurry was 15 wt.%. A 60 mol.% excess of $NaHCO_3$ was added to the mixture as the source for the intercalate anion. The reaction was conducted under vigorous stirring at a temperature of 180 °C and a pressure of approximately 14 bar. The autoclave was kept at this temperature and pressure for approximately 5 h. Thereafter heating was discontinued and the reaction mixture was allowed to cool overnight while stirring. The solid product was removed from the autoclave, filtered and washed several times with distilled water to remove residual Na_2CO_3 . Finally it was dried in an oven at 80 °C for at least 48 h.

The hydromagnesite was also synthesised according to the method described by Labuschagné *et al.* (24) as follows. Magnesium oxide stock from Chamotte Holdings was calcined at 800 °C for 10 min. A total of 100 g of the cooled MgO was suspended in 1.5 L distilled water using a Silverson disperser at 6700 rpm. An ice bath was used to keep the temperature of the mixture at approximately 23 °C. Carbon dioxide was bubbled through the mixture to form hydromagnesite. The pH gradually dropped and stabilised at 8.2. It was maintained at this value for another 30 min. The mixture was filtered and the precipitate dried in an oven at 140 °C for approximately 12 h. Finally the dry sample was ground to a fine powder.

3.2.3 Surface coating of the fillers

All samples were coated with stearic acid as follows: The dried solids were milled to a fine powder using a coffee grinder. They were then suspended in 1 L distilled water and heated to 75 °C. The solids content of all the slurries was less than 20 wt.%. The slurries were vigorously agitated with a Silverson disperser. Stearic acid, equivalent to 2.0 wt.% based on the total dry uncoated solid sample, was added to the hot slurry. The suspension was stirred for 15 min at 6 000 rpm. The coated powders were recovered by filtering. They were dried in a convection oven set at 60 °C and ground to a fine powder.

3.2.4 Preparation of PVC-composites

DINP plasticiser (130 g) was weighed into a 600 mL beaker. Next small portions of the PVC powder (up to a total of 130 g) were added and mixed using a high-speed Anvil milkshake mixer. The dispersion was de-aerated for about 30 min in a Speedvac vacuum chamber. Then the LDH filler powder (39 g) was incorporated. The dispersion was again de-aerated but this time for about 1 h.

Cast PVC composite sheets were made in a three-step pressing process. The paste mixture was poured into a mould measuring 100 mm × 100 mm × 3.5 ± 0.1 mm. The mould was closed and placed in a convection oven set at a temperature of 130 °C for 10 min. Then it was hot pressed at a pressure of 10 MPa at 150 °C for 5 min. The mould was then removed from the press and a heavy weight placed on the top plate. The moulding was allowed to cool down at ambient conditions before it was removed.

3.3 Characterisation

3.3.1 Particle size and BET surface area determination

The particle size distributions were determined with a Mastersizer Hydrosizer 2000MY (Malvern Instruments, Malvern, UK). The specific surface areas of the powders were measured on a Nova 1000e BET instrument in N₂ at 77 K.

3.3.2 Scanning Electron Microscopy (SEM)

A small quantity of powder was placed onto carbon tape on a metal sample holder. Excess powder was removed using a single compressed air blast. The samples were then coated five times with carbon under argon gas using the Polaron Equipment E5200 SEM auto-coating sputter system. The powder samples were viewed on a Zeiss Ultra plus FEG SEM scanning electron microscope.

3.3.3 X-ray diffraction (XRD)

X-ray diffraction analysis was performed on a PANalytical X-pert Pro powder diffractometer fitted with an X'celerator detector using Fe filtered CoK α radiation (0.17901 nm). The instrument featured variable divergence and receiving slits. X'Pert High Score Plus software was used for data manipulation and phase identification.

3.3.4 X-ray fluorescence (XRF)

Chemical composition was determined by the X-ray fluorescence method. Milled samples (< 75 μ m) of the materials were roasted at 1 000 °C for at least 3 hours to oxidize Fe²⁺. Glass disks were prepared by fusing 1 g roasted sample and 8 g of a flux (consisting of 35 % LiBO₂ and 64.71 % Li₂B₄O₇) at 1 050 °C. The glass disks were

analysed by a PANalytical Axios X-ray fluorescence spectrometer equipped with a 4 kW Rh tube.

3.3.5 Inductively coupled plasma optical emission spectrometry (ICP-OES)

The elemental composition of the LDH was determined with a Spectro Arcos model inductively coupled plasma optical emission spectrometer (ICP-OES). First about 0.5 g of the clay was dissolved in 50 mL Aqua Regia. After cooling down, the reaction mixture was diluted with 50 mL of distilled water and filtered through ashless filter paper. Before performing the ICP-OES analysis, 1 mL of solution was added to 99 mL of distilled water. The analysis was then performed, analysing for copper, magnesium, aluminium, calcium, zinc, iron and sodium. The insoluble fraction was determined by ashing the filter paper.

3.3.6 Fourier transform infrared spectroscopy (FTIR)

FTIR spectra were recorded on a PerkinElmer 100 Spectrophotometer. Powder samples were pressed onto the Zn/Se plate of a MIRacle ATR attachment. The spectra were obtained over the range $650 - 4\,000\text{ cm}^{-1}$ and represent the average of 32 scans at a resolution of 2 cm^{-1} .

3.3.7 Thermogravimetric Analysis (TGA)

Thermogravimetric analysis (TGA) was performed using the dynamic method on a Mettler Toledo A851 TGA/SDTA instrument. About 11-15 mg sample was placed in an open $150\text{ }\mu\text{L}$ alumina pan. Temperature was scanned from $25\text{ }^{\circ}\text{C}$ to $900\text{ }^{\circ}\text{C}$ at a scan rate of $10\text{ }^{\circ}\text{C min}^{-1}$ with air or nitrogen flowing at a rate of 50 mL min^{-1} .

3.3.8 Heat stability assessment

The heat stability of the PVC compounds was evaluated on a Metrohm 895 Professional PVC Thermomat according to ISO 182 Part 3 (25). The method is based on the fact that PVC releases HCl when it decomposes at high temperatures. The evolved hydrochloric acid is flushed with a stream of nitrogen gas and passed through a measuring vessel where it is absorbed in purified water. The progress of the decomposition is tracked by measuring the change in the conductivity of this water. Performance is quantified in terms of either the induction time (i.e. the time that is required to reach the break point in the conductivity curve) or a stability time, i.e. the time until a conductivity difference of $50 \mu\text{S cm}^{-1}$ is reached. The PVC compound sample amount tested was 0.50 ± 0.05 g. The samples were cut into small pieces less than 1 mm in size. The stability was determined in triplicate at 200°C . Nitrogen flow was controlled at 7 L h^{-1} and 50 mL deionised water was used to trap the HCl.

3.3.9 Cone calorimeter fire testing

The ISO 5660 standards (26-28) were followed in performing the cone calorimeter tests using a Dual Cone Calorimeter (Fire Testing Technology (UK) Ltd.). Three specimens of each composition were tested. The sheet dimensions were $100 \text{ mm} \times 100 \text{ mm} \times 3.5 \pm 0.1 \text{ mm}$. They were placed on aluminium foil and exposed horizontally to an external heat flux of 35 kW m^{-2} . This heat flux was chosen on the basis of the study conducted by Wang *et al.* (29). They studied 3 mm to 10 mm thick PVC sheets at heat fluxes of 25, 35 and 50 kW m^{-2} . They found that the time to ignition varied linearly with the inverse of the cone calorimeter heat flux. Furthermore, the minimum heat flux for ignition of sheets in this thickness range was

found to be about 19 kW m^{-2} . The smoke photometer used a helium-neon (He-Ne) laser that emits red light with a wavelength of 632.8 nm.

3.4 Results

3.4.1 Characterisation of the hydrated fillers

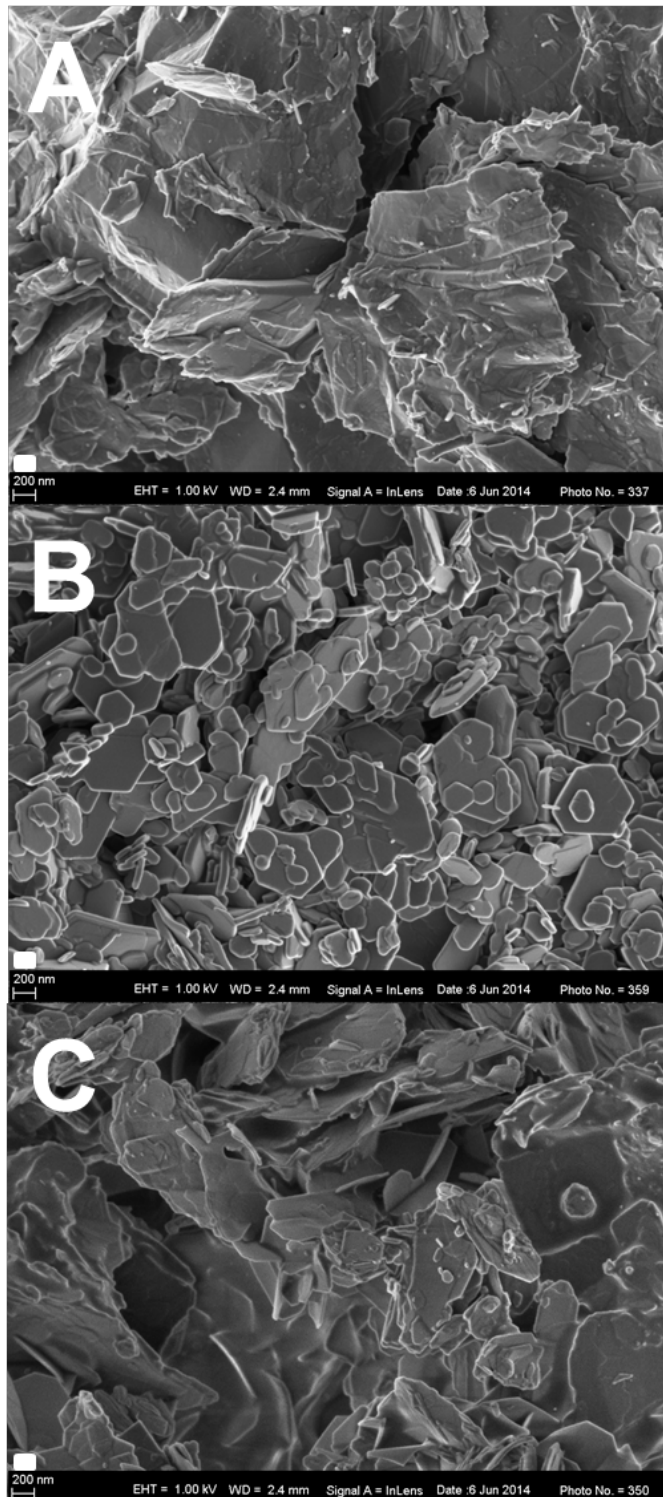


Figure 3.1: SEM micrographs of (A) Hydromagnesite (HM); (B) Layered double hydroxide (LDH); and (C) Magnesium hydroxide (MH). The size bar indicates a length of 200 nm.

Figure 3.1 shows FEG SEM micrographs of the hydrated filler powders. The individual powder particles are made up of highly agglomerated flake-shaped crystals. The primary flakes were smallest for the LDH and largest for the hydromagnesite.

Table 3.1 reports the particle sizes and the BET specific surface areas for the filler additives. The median (d_{50}) particle size varied from 3.1 μm to 9.8 μm . BET surface was highest for the hydromagnesite ($24.8 \text{ m}^2\text{g}^{-1}$) and lowest for the magnesium hydroxide ($9.4 \text{ m}^2\text{g}^{-1}$).

Table 3.1: LDH particle sizes, BET surface area and d-spacing from XRD results

Sample	Surface area	d-spacing	Particle size, μm		
	$\text{m}^2 \text{g}^{-1}$	nm	d_{10}	d_{50}	d_{90}
MgAl-LDH	18.3	0.761	0.68 ± 0.00	3.08 ± 0.03	13.1 ± 0.3
Mg(OH) ₂	9.4	0.478	0.93 ± 0.01	3.78 ± 0.12	43.2 ± 2.4
Hydromagnesite	24.8	0.924	2.96 ± 0.08	9.75 ± 0.16	29.7 ± 1.5

Table 3.2: XRF composition analysis data of samples roasted at 1 000 °C

Concentration, wt.%	SiO ₂	Al ₂ O ₃	Fe ₂ O ₃	MnO	MgO	CaO	NiO
MgAl-LDH	1.59	36.85	0.15	0.00	60.51	0.72	0.18
Hydromagnesite	3.53	0.19	0.21	0.07	94.92	0.89	0.18
Mg(OH) ₂	0.54	0.30	0.00	0.00	99.16	0.00	0.00
MgO*	7.89	0.79	0.80	0.03	89.38	0.92	0.18
Std dev (%)	0.04	0.30	0.15	0.00	60.51	0.72	0.18

*Ex Chamotte

Table 3.2 shows the chemical composition data obtained for the various samples. The XRF chemical composition results for the LDH, expressed in terms of the general formula $[Mg_{2+\alpha}Al_{1-\alpha}(OH)_6](CO_3)_{(1-\alpha)/2} \cdot xH_2O$, indicated an apparent α value of 0.025. The magnesium hydroxide contained aluminium and silica as impurities. The other samples contained, in addition, minor amounts of iron, manganese nickel and calcium as impurities.

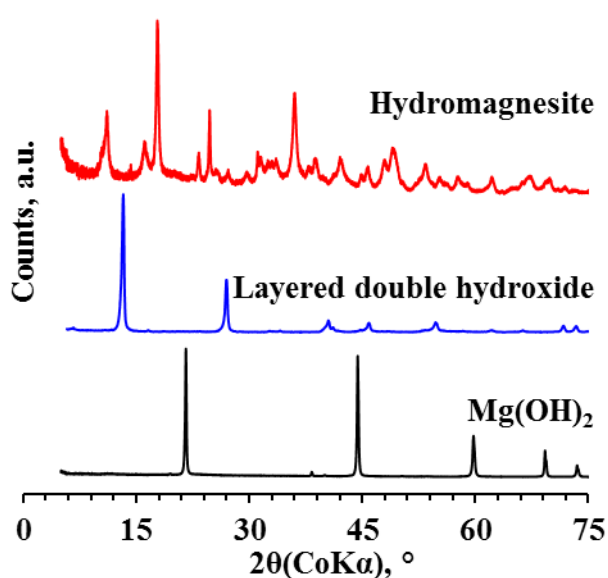


Figure 3.2: X-ray diffraction patterns for magnesium hydroxide (MH), hydromagnesite (HM) and layered double hydroxide (LDH).

The XRD patterns for the hydrated fillers are shown in Figure 2. The reflections at $2\theta = 13.474^\circ$ and $2\theta = 27.125^\circ$ in the XRD diffractogram for LDH are consistent with a brucite layer basal spacing of 0.761 nm. The d-spacing values for the other compounds are listed in Table 1. It was larger (0.924 nm) for the hydromagnesite and lower (0.478 nm) for the $Mg(OH)_2$. There are additional reflections appearing in the XRD spectrum for the hydromagnesite indicating the presence of impurity phases dypingite ($Mg_5(CO_3)_4(OH)_2 \cdot 5H_2O$) and magnesite (MgO). The sharp nature of the reflections points to a high crystallinity of the corresponding powders.

The $\text{Mg}(\text{OH})_2$ spectrum shown in Figure 3.3 is characterised by a sharp and intense $-\text{OH}$ stretching vibration peak at ca. 3700 cm^{-1} . This peak is also observed in the hydromagnesite but in the LDH it is much broader and it is centred at a lower wavenumber (ca. 3450 cm^{-1}). It is attributed to $-\text{OH}$ stretching vibrations in the octahedral layer and the free and hydrogen bonded water molecules present in the interlayer. The shoulder observed at 3000 cm^{-1} for LDH arises from interactions between carbonate (CO_3^{2-}) and H_2O in the interlayer region (30). The LDH features a single carbonate peak at 1367 cm^{-1} while in the hydromagnesite the carbonate asymmetric stretching vibration band is split with peaks at 1420 cm^{-1} and 1480 cm^{-1} . The latter also features a carbonate symmetric stretch band at ca. 1120 cm^{-1} and three bending bands at 800 cm^{-1} . The presence of the water of crystallisation is indicated by the bands at ca. 3510 cm^{-1} and 3450 cm^{-1} (4).

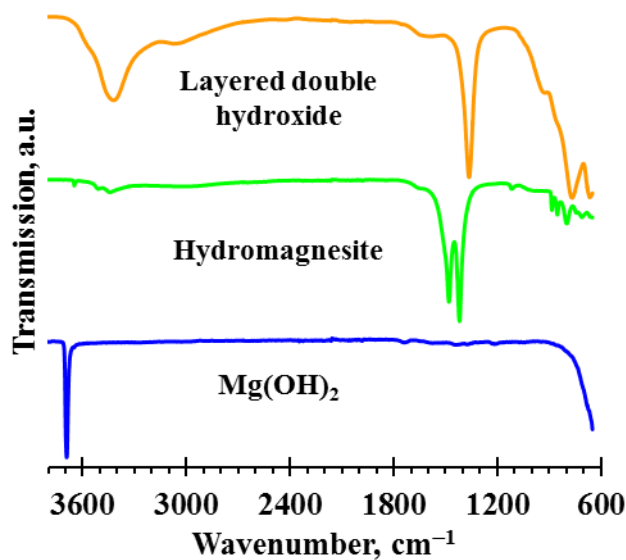


Figure 3.3: FTIR spectra of the hydrated fillers.

Figure 3.4 summarises the TGA mass loss curves for the LDH, magnesium hydroxide and hydromagnesite samples as obtained in an air atmosphere. The nature of the degradation steps for these three compounds was elucidated in previous studies (31-

36). In each case water, or water and carbon dioxide are released in gaseous form and inert oxides remain. The residual masses at 900 °C were 67.3 wt.%, 56.8 wt.% and 43.1 wt.% for Mg(OH)₂, hydrotalcite and hydromagnesite respectively. The corresponding theoretically expected values are 69.1 wt.%, 56.1 wt.% and 43.1 wt.% for Mg(OH)₂, hydrotalcite and hydromagnesite respectively. The small discrepancies are attributed to the presence of the indicated impurities and slight deviations from the idealized compositions of the fillers.

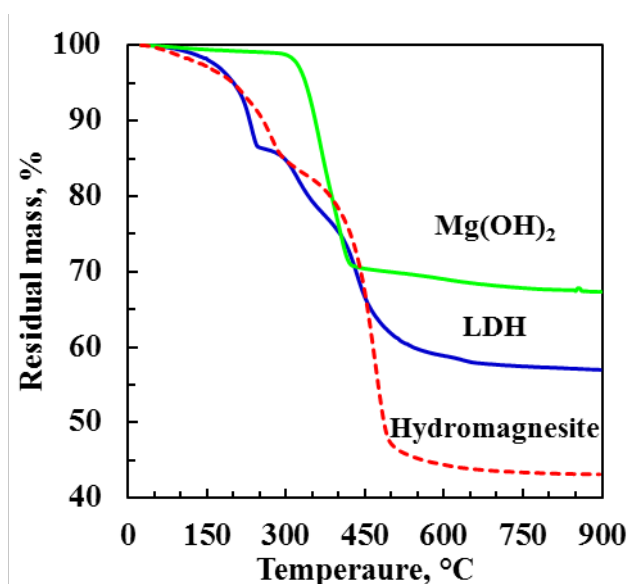


Figure 3.4: TGA traces in air for the hydrated fillers. Temperature was scanned from 25 °C to 900 °C at a scan rate of 10 °C min⁻¹ with air flowing at a rate of 50 mL min⁻¹.

3.4.2 Characterisation of the PVC composites

Figure 3.5 shows TGA traces for the LDH-PVC compounds recorded in air and in nitrogen atmospheres. In nitrogen atmosphere the flexible PVC apparently suffers major mass loss in two main steps. The first stage commences at 240 °C, reaches a maximum rate at 315 °C and ends at 370 °C. At this point the residue is 20.7 wt.%. The second stage starts as 420 °C reaches a maximum rate at 467 °C and ends at

510 °C with a residue of 7.0 wt.% remaining. The initial mass loss is due a combination of PVC degradation (mainly dehydrochlorination) events and volatilization of the plasticiser. The second stage is attributed to pyrolysis reactions that ultimately lead to a carbonaceous char residue (4.3 wt.% at 900 °C). The shape of the mass loss curves for the LDH-PVC composite mirrors that of PVC. The mass loss onset temperatures are similar but mass loss occurs over a narrower temperature range and the residue after each stage is greater than found for the neat PVC.

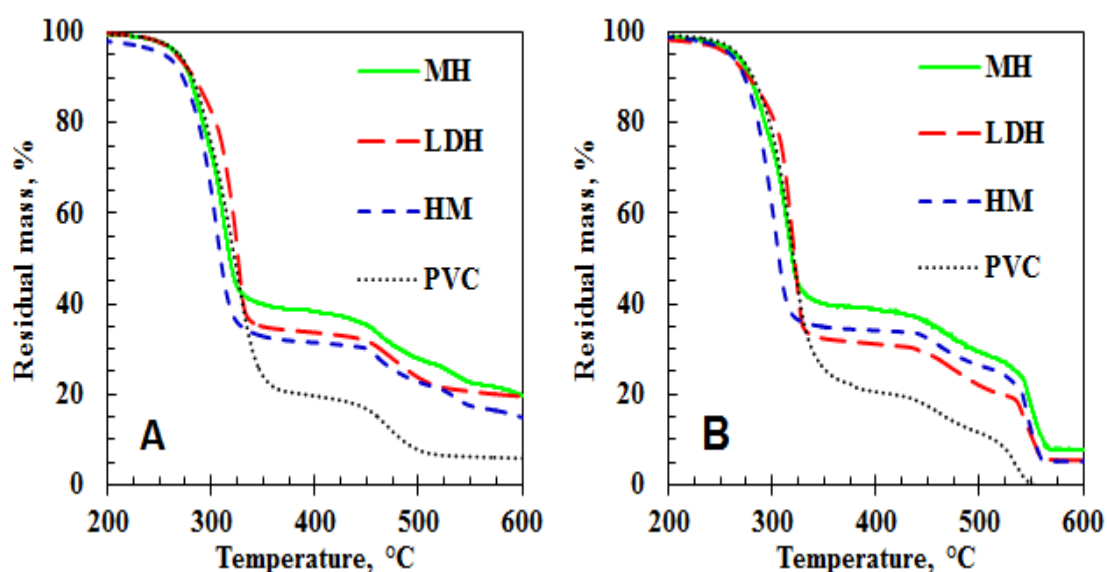


Figure 3.5: TGA traces for the PVC-LDH composites in (A) nitrogen and (B) air atmospheres. The temperature was scanned from 25 to 900 °C at a scan rate of 10 °Cmin⁻¹ with gas flowing at a rate of 50 mL min⁻¹. Key: PVC = no additive; HM= hydromagnesite; MH = magnesium hydroxide, and LDH = layered double hydroxide.

The initial part of the mass loss curves (below 300 °C) found in an air atmosphere is similar to that in a nitrogen atmosphere. However, at higher temperatures additional mass loss occurs owing to the oxidation of the carbonaceous char. The PVC sample residue decreases to zero at ca. 550 °C. The other samples show a greater residue but this represents non-volatile inorganic matter.

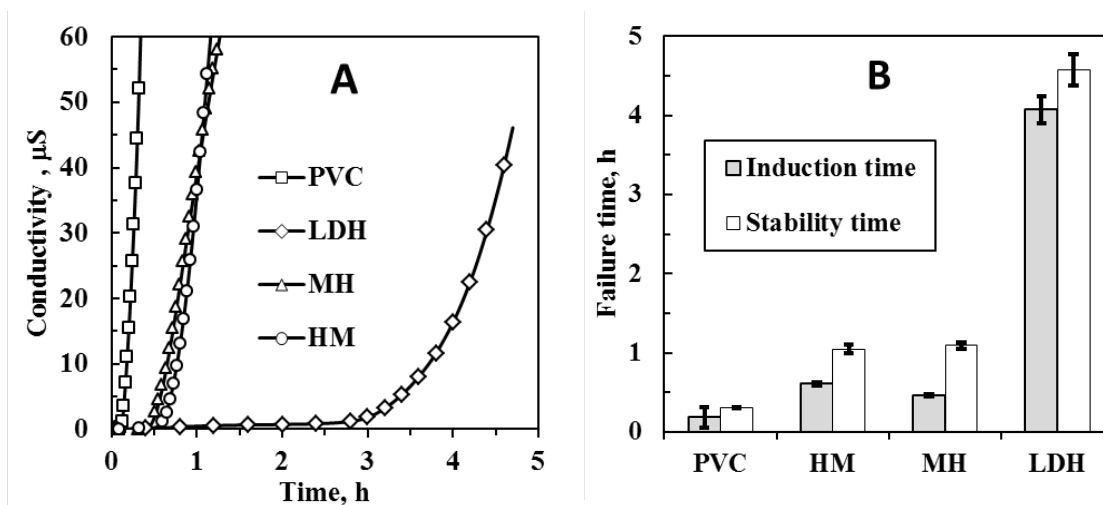
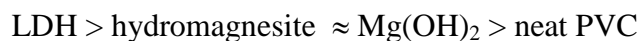


Figure 3.6: The induction and stability times were obtained by tracking the evolution of hydrochloric acid. A. Representative conductivity curves for the PVC compounds. B. Thermomat static heat stability at 200 °C. Key: PVC = no additive; HM= hydromagnesite; MH = magnesium hydroxide, and LDH = layered double hydroxide.

3.4.3 Heat stability of the PVC composites

During the primary stage of degradation discoloration of the PVC is observed. It is caused by the formation of conjugated polyene sequences of double bonds along the polymer chain. These defects are highly reactive and they undergo secondary reactions that lead to crosslinking or cleavage of the polymer chains (37). The thermogravimetric analysis performed on the PVC compounds provided basic information on the intrinsic heat stability of the PVC compounds. However, in the present study the progression of PVC degradation was quantified by following the evolution of HCl with the Thermomat method. Representative Thermomat conductivity response curves are shown in Figure 3.6A.

The induction time corresponds to the onset time while the stability time is defined by the time required to reach a conductivity of $50 \mu\text{S cm}^{-1}$. The ranking of the stabilisers in terms of the induction times was as follows:



The effect of the LDH derivatives on the Thermomat stability times of the flexible PVC compounds is shown in the Figure 3.6B. The neat PVC compound had a stability time of 0.31 ± 0.01 h. Only the LDH provided a significant improvement in both the induction time and the stability time (4.07 ± 0.17 h and 4.57 ± 0.20 h respectively). PVC degradation and stabilisation processes occur via multiple primitive reaction steps, each with their own characteristic temperature-dependent rate constant. In addition, mass transfer effects play a significant role. In view of these complications it is convenient to model the degradation using the single step reaction approximation (38-42). A central feature of PVC degradation is its autocatalytic nature (18, 19). This implies that an autocatalytic reaction mechanism (43, 44) should be considered, e.g.:

$$\frac{d\alpha}{dt} = k\alpha^{1-1/\theta} (1-\alpha)^{1+1/\theta} \quad (1)$$

where α is the degree of conversion that defines the extent of degradation of the PVC polymer [-]; t is the time [s]; k is the rate constant [s^{-1}] and θ is a dimensionless constant [-] defining the reaction order. This differential equation provides a parametric interpolation formula between the predictions of the logistic equation ($\theta \rightarrow \infty$) describing classic autocatalytic behaviour and second order kinetics ($\theta = 1$). For $1 \leq \theta < \infty$ and initial condition $\alpha = 0$ at $t = 0$, the general solution for isothermal conditions is (44):

$$\alpha = 1 - \left[1 + (t/\tau)^\theta \right]^{-1} \quad (2)$$

where the time constant is defined by $\tau = \theta/k$.

This equation predicts a rate maximum at a time equal to $[\theta/k][(\theta-1)/\theta+1]^{1/\theta}$.

Furthermore, the predicted S-shaped conversion curve shifts to higher times with increasing θ and lower values for the rate constant k . In order to apply equation (2) to the Thermomat data, it was assumed that the conductivity is directly proportional to the degree of degradation of the polymer sample. The parameters τ and θ were then obtained by least squares fitting of Equation (2) to the conductivity vs. time curves.

The order parameter for the neat PVC was found to be $\theta = 2.92 \pm 0.12$ and the degradation rate constant was $k = 5.07 \pm 0.26$ h. With LDH as the stabilizer the reaction order parameter was higher ($\theta = 7.06 \pm 0.47$) than that found for the neat PVC. It was also higher for hydromagnesite ($\theta = 5.81 \pm 0.06$ h) while for the magnesium hydroxide it was lower ($\theta = 4.77 \pm 0.15$ h). The LDH stabiliser caused a significant lowering of the degradation rate constant to a value of $k = 1.13 \pm 0.12$ h. However, the deviations, of the rate constants for magnesium hydroxide and hydromagnesite from this value, were not statistically significant. This means that these additives did not affect the intrinsic rate at which the PVC matrix degraded. The longer induction times that were observed were thus simply due to scavenging of the hydrochloric acid by the basic additives in the initial phase of the PVC degradation.

3.4.4 Fire testing

The cone calorimeter results are summarized in Table 3.3 and presented in Figure 3.7 to Figure 3.10. All the samples ignited after a short induction period and they all

burned producing large amounts of smoke. The time to ignition (t_{ign}) was 23 ± 2 s for the neat PVC compound. It was longer for the $\text{Mg}(\text{OH})_2$ and LDH containing compounds but shorter for hydromagnesite (19.3 ± 1.2 s). The TGA results shown in Figure 3.5 suggest that the hydromagnesite destabilises the PVC matrix as mass loss proceeds at lower temperatures. This may explain the reduced ignition time for this additive. In effect combustible organic fuel residues are released at an earlier time compared to the other compounds. The time to flame out was 306 ± 137 s for the neat PVC compound. On average, it increased by 68 %, 71 % and 114 % when $\text{Mg}(\text{OH})_2$, hydromagnesite and LDH respectively were added. Directly after ignition, the neat PVC compound showed rapid mass loss and this was virtually complete by 200 s. Thereafter there was a very slow steady decline in the residue amount with a char yield of 4.0 wt.% at the end of the test. The filled compounds lost mass at a much slower rate over a longer time. The apparent char yields were 15.9 wt.%, 13.8 wt.% and 11.3 wt.% for the LDH, magnesium hydroxide and hydromagnesite respectively. These values reflect the higher ash content due to the fillers rather than improved carbon yield. It is likely that these ash residues comprise complex mixtures of metal chlorides and oxides.

Figure 3.7 shows representative heat release rate (*HRR*) curves obtained from the cone calorimeter tests. The heat release curves for the neat plasticised PVC compound exhibited the shape characteristic of a thermally thin sample (45). Thermally thin samples are identified by a sharp peak in their *HRR* curves as the whole sample is pyrolyzed nearly at once. The *HRR* curves for the filled compounds were flatter and broader than that for the neat PVC. *HRR* curves characteristic of thermally thick, char-producing samples show a sudden rise to a plateau value (45). However, the

HRR curves for the sample containing hydrated filler were more complex. They showed a sudden rise to a peak value with a slow but steady decline over a longer period. The *pHRR* for the neat PVC compound was $623 \pm 8 \text{ kW m}^{-2}$. Incorporating LDH derivatives at the 13 wt.% level caused a significant lowering of the *pHRR*. LDH lowered the *pHRR* value to $389 \pm 9 \text{ kW m}^{-2}$ and the other two additives produced a similar reduction. The CO_2 and CO release rates (not shown graphically) curves mirrored those observed for the *HRR* (Figure 3.7) almost perfectly.

Table 3.3: Cone calorimeter data summary

Parameter	Units	PVC	LDH	Mg(OH) ₂	Hydromagnesite
Time to ignition (<i>t</i> _{ign})	s	23.0 ± 2.1	27.7 ± 1.2	28.3 ± 1.2	19.3 ± 1.2
Time to flame out	s	306 ± 137	654 ± 51	516 ± 16	527 ± 54
Time to <i>pHRR</i>	s	103 ± 10	105 ± 1	98 ± 3	132 ± 6
Peak heat release rate (<i>pHRR</i>)	kW m ⁻²	623 ± 8	389 ± 9	419 ± 9	406 ± 12
Total heat release (<i>tHR</i>)	MJ m ⁻²	68 ± 2	72 ± 3	74 ± 2	69 ± 3
Effective heat of combustion	MJ kg ⁻¹	16.7 ± 0.1	18.2 ± 0.2	16.6 ± 0.4	16.6 ± 0.4
Relative heat of combustion [#]	-	1.00 ± 0.01	1.25 ± 0.01	1.14 ± 0.03	1.14 ± 0.03
<i>FIGRA</i>	kW m ⁻² s ⁻¹	6.1 ± 0.6	3.7 ± 0.1	4.3 ± 0.2	3.1 ± 0.2
<i>MARHE</i>	kW m ⁻²	367 ± 11	208 ± 2	231 ± 5	252 ± 2
<i>pHRR/t</i> _{ign}	kW m ⁻² s ⁻¹	26.0 ± 0.8	14.4 ± 0.3	14.5 ± 0.3	21.1 ± 1.8
Smoke release	m ² m ⁻²	4413 ± 97	2780 ± 121	3181 ± 64	3000 ± 101
Char & ash @ 600 °C	wt.%	4.1 ± 0.8	18.4 ± 1.4	15.7 ± 1.7	11.1 ± 0.0

[#]Heat of combustion scaled with respect to PVC plus plasticiser content and relative to the value for the neat PVC compound

An important index used to interpret cone calorimeter data is the maximum average rate of heat emission (*MARHE*) (45, 46). The *MARHE* parameter is defined as the peak value of the cumulative heat emission divided by time (46). It provides a measure of the propensity for fire development under full scale conditions. The *MARHE* for the neat PVC was $367 \pm 11 \text{ kW m}^{-2}$ and this was reduced to

$202 \pm 2 \text{ kW m}^{-2}$ with the LDH as stabiliser-flame retardant. The addition of the other two filler additives also reduced the *MARHE*.

Interesting observations hold for the total heat release (*tHR*) and the effective heat of combustion presented in Table 3. The *tHR* value was $68 \pm 2 \text{ MJ m}^{-2}$ for the neat PVC compound. With the LDH derivative incorporated, the *tHR* increased even though less fuel is available for combustion. The *tHR* was $72 \pm 3 \text{ MJ m}^{-2}$ for the LDH compound and the highest value was $74 \pm 2 \text{ MJ m}^{-2}$ recorded for the magnesium hydroxide. The effective heat of combustion for the PVC was $16.7 \pm 0.1 \text{ MJ kg}^{-1}$. Values for the filled compounds were similar or even higher. It is interesting to compare the relative heats of combustion scaled with respect to the organic combustible content of the compounds. These are also presented in Table 3. They show values that are 25 % higher for the LDH-filled compound and 14 % higher for the other two fillers. Thus while the fire performance improved with respect to the peak heat release rate, it deteriorated when the total heat release (*tHR*) or effective heat of combustion is considered. These apparent increases are tentatively attributed to the chlorine preferentially interacting and reacting with the fillers. Less halogen present in the vapour phase to inhibit the combustion of the volatile fuel fragments could have resulted in more efficient combustion and hence an increase in the total heat release.

The fire growth rate (*FIGRA*) is an estimator for the fire spread rate and size of the fire (45, 46). The *FIGRA* is defined as the maximum quotient of $HRR(t)/t$. According to Hirschler (47), the fire performance index (*FPI*) is possibly the best single indicator of the overall fire hazard posed by a material. It is defined as the ratio of the time-to-ignition to the peak heat release rate ($FPI = t_{ign}/pHRR$). There is a connection between

FPI and the time to flashover, i.e. the change from small to large-scale fire (47). A lower *FPI* value is associated with a shorter time to flashover suggesting that a shorter time is available for escape in a full-scale fire situation.

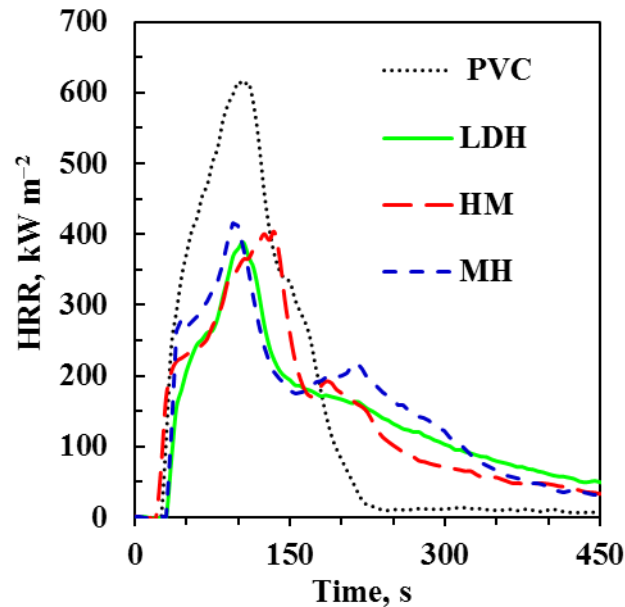


Figure 3.7: Representative cone calorimeter heat release rate curves for the plasticised PVC compound and its composites with the hydrated fillers. Key: PVC = no additive; HM= hydromagnesite; MH = magnesium hydroxide, and LDH = layered double hydroxide.

Figure 3.8 shows the *FIGRA* and *FPI* indices with the latter expressed as its inverse as it then has the same units. Relative to the neat PVC compound, the presence of the LDH markedly decreased the *FIGRA* (>55 %). The $pHRR/t_{ign}$ for the neat PVC was $26 \pm 1 \text{ kW m}^{-2} \text{ s}^{-1}$. It was lowered to $14.4 \pm 0.3 \text{ kW m}^{-2} \text{ s}^{-1}$ in the presence of the LDH while the other PVC compounds featured intermediate values.

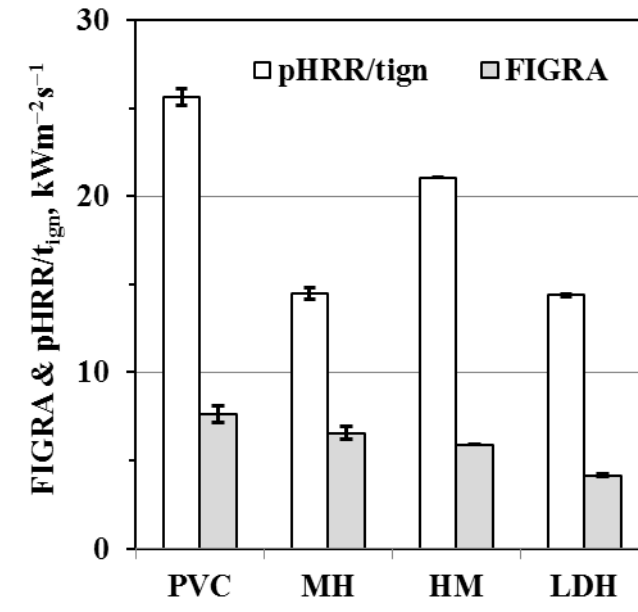


Figure 3.8: The effect of the hydrated fillers on the FIGRA and pHRR/t_{ign} of PVC composites. Key: PVC = no additive; HM= hydromagnesite; MH = magnesium hydroxide, and LDH = layered double hydroxide.

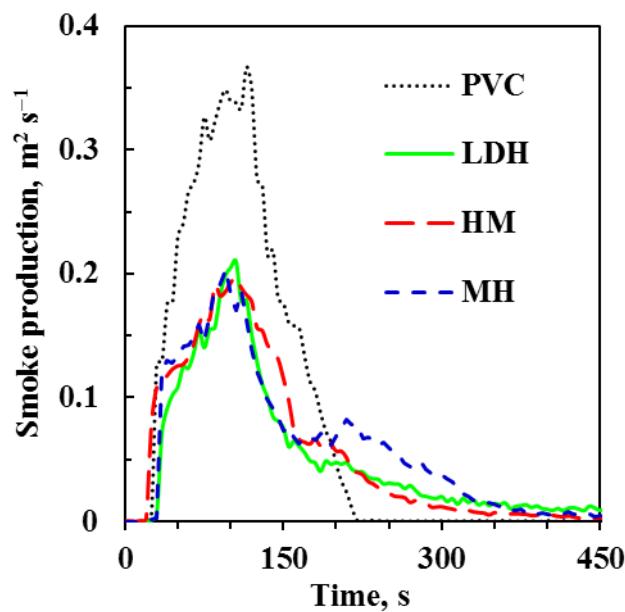


Figure 3.9: Cone calorimeter smoke production rates for the plasticized PVC compound and its composites with LDH derivatives. Key: PVC = no additive; HM = hydromagnesite; MH = magnesium hydroxide, and LDH = layered double hydroxide.

Figure 3.9 and Figure 3.10 show and compare the smoke production rates (SPR) and the smoke production of the composites with that for the neat PVC compound. The

peak smoke production rate was virtually the same for all the filler additives. However, overall LDH reduced the total smoke production more so than the other hydrated fillers.

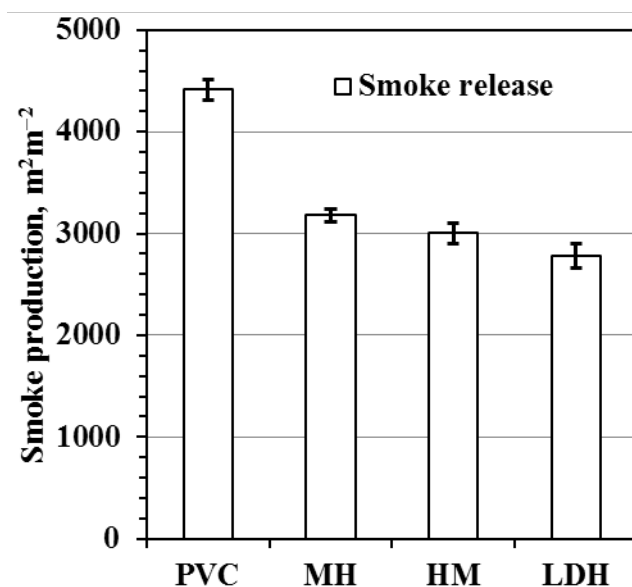


Figure 3.10: Comparing the smoke production of the plasticized PVC compound with that from its composites with LDH derivatives. Key: PVC = no additive; HM = hydromagnesite; MH = magnesium hydroxide, and LDH = layered double hydroxide.

3.5 Discussion

The performance of the LDH can be explained in the context of the PVC degradation mechanism that occurs in two stages: Crosslinking of the polymer chains and dehydrochlorination reactions promote char formation (37). Chain cleavage and cracking reactions lead to the formation of volatile aromatic molecules that promote smoke generation. The hydrogen chloride gas generated by the degradation reaction catalyses the chain propagation reaction. The carbonated LDH improves the heat stability of the PVC by scavenging this corrosive gas. Initially this occurs via the formation of chloride intercalated LDH. However, later on the acid attacks the LDH

structure leading to the formation of metal chlorides. These salts act as Lewis bases that can also promote dehydrochlorination via a carbonium ion mechanism (8). According to Zhu *et al.* (48) LDH acts as a Lewis acids and induces cationic crosslinking (Friedel–Craft reaction) of neighbouring polyene backbones. Metal chlorides also catalytically favour crosslinking and dehydrochlorination reactions at the expense of cracking reactions (48). These actions improve char formation and reduce smoke generation in accordance with the present experimental results.

The release of the HCl by the decomposing PVC inhibits flaming combustion in the cone calorimeter tests. The halogen entering the gas phase contributes to a “flame poisoning effect”, i.e. the slowing down of the free radical chain reactions occurring in the flame (9). In the presence of the LDH, the HCl is efficiently scavenged especially in the early stages of degradation. Less halogen is present in the volatile organics released in the beginning making them easier to ignite. This may explain the shorter time to ignition found for the hydromagnesite compound compared to neat PVC.

Compared to the neat PVC, all the filler additives decreased the peak heat release rate in the cone calorimeter tests. This may be due to a combination of vapour phase and solid phase effects. High heat decomposes the fillers releasing water or water and carbon dioxide. The decomposition is endothermic in nature which means that it cools the polymer substrate. At lower temperature the degradation reactions that generate fuel proceeds more slowly. This explains in part the rate of lower mass loss observed for the LDH compound in the cone calorimeter tests. In addition the inert gases liberated have a dilution effect on the air-fuel mixture in the gas phase. This cools the

flame reducing the rate of heat generation. The inorganic residues may form a protective layer on the surface of the substrate. It may act as a barrier to heat transfer to the underlying polymer and also to mass transfer of degradation products migrating to the gas phase. Finally the inorganic residues may effectively reflect incoming infrared radiation that would otherwise have heated the substrate to higher temperatures. All these effects may contribute to the lowering of the heat release rate observed in the cone calorimeter tests.

Finally, at elevated temperature and in the presence of oxygen, the metal oxide residues from the decomposition of the LDH catalyse the oxidation of the carbonaceous char residues. This explains the absence of organic residues above 600 °C in the TGA runs conducted in an air atmosphere.

3.6 Conclusion

Layered double hydroxide (LDH) $[\text{Mg}_4\text{Al}_2(\text{OH})_{12}\text{CO}_3 \cdot 4\text{H}_2\text{O}]$ and hydromagnesite $[4\text{MgCO}_3 \cdot \text{Mg}(\text{OH})_2 \cdot 4\text{H}_2\text{O}]$ (HM) flame retardant fillers were successfully synthesised using hydrothermal methods. Characterisation using XRD, ICP-MS and FTIR confirmed that the products approached these idealised compositions.

Emulsion grade PVC was plasticised with 100 phr of diisononyl phthalate and filled with 30 phr layered double hydroxide (LDH), hydromagnesite or magnesium hydroxide as combination stabiliser-flame retardant additives. It was found that LDH showed good performance in a static heat stability test. Analysis of the Thermomat data suggests that this additive actually modifies the PVC degradation mechanism. The hydromagnesite and magnesium hydroxide improved heat stability too but only

marginally. Analysis of the Thermomat data suggests that, unlike the LDH, these basic additives did not affect the intrinsic rate at which the PVC matrix degraded. They retarded the degradation process primarily by scavenging the hydrochloric acid liberated during the initial phase of the PVC degradation. The addition of LDH also significantly improved the fire resistance of the plasticised PVC. The LDH filler performed better than magnesium hydroxide and hydromagnesite with respect to most fire retardant performance indices e.g. the fire growth rate (FIGRA) the maximum average rate of heat emission (*MARHE*) and the fire performance index (FPI). It lowered the peak heat release rate (*pHRR*), from $623 \pm 8 \text{ kW m}^{-2}$ to $389 \pm 9 \text{ kW m}^{-2}$ but increased the total heat release from $68 \pm 2 \text{ MJ m}^{-2}$ to only $72 \pm 3 \text{ MJ m}^{-2}$. The LDH filler was also more effective at reducing the total smoke production. It is concluded that LDH is a promising functional filler for plasticised PVC that imparts both heat stability and improved fire performance.

3.7 References

1. Miyata S, Kumura T. Synthesis of new hydrotalcite-like compounds and their physico-chemical properties. *Chemistry Letters*. 1973;2(8):843-8.
2. Sato T, Fujita H, Endo T, Shimada M, Tsunashima A. Synthesis of hydrotalcite-like compounds and their physico-chemical properties. *Reactivity of Solids*. 1988;5(2-3):219-28.
3. Bellotto M, Rebours B, Clause O, Lynch J, Bazin D, Elkaïm E. A Reexamination of Hydrotalcite Crystal Chemistry. *The Journal of Physical Chemistry*. 1996;100(20):8527-34.
4. White WB. Infrared characterization of water and hydroxyl ion in the basic magnesium carbonate minerals. *American Mineralogist*. 1971;56:46-53.
5. Coaker AW. Fire and flame retardants for PVC. *Journal of Vinyl and Additive Technology*. 2003;9(3):108-15.
6. Otani S. On the carbon fiber from the molten pyrolysis products. *Carbon*. 1965;3(1):31-8.
7. Folarin OM, Sadiku ER. Thermal stabilizers for poly(vinyl chloride): A review. *International Journal of Physical Sciences*. 2011;6(18):4323-30.
8. Levchik SV, Weil ED. Overview of the recent literature on flame retardancy and smoke suppression in PVC. *Polymers for Advanced Technologies*. 2005;16(10):707-16.
9. Weil ED, Levchik S, Moy P. Flame and smoke retardants in vinyl chloride polymers - Commercial usage and current developments. *Journal of Fire Sciences*. 2006;24(3):211-36.

10. Hornsby PR. The application of hydrated mineral fillers as fire retardant and smoke suppressing additives for polymers. *Macromolecular Symposia*. 1996;108(1):203-19.
11. Hornsby PR. Fire retardant fillers for polymers. *International Materials Reviews*. 2001;46(4):199-210.
12. Xu ZP, Saha SK, Braterman PS, D'Souza N. The effect of Zn, Al layered double hydroxide on thermal decomposition of poly(vinyl chloride). *Polymer Degradation and Stability*. 2006;91(12):3237-44.
13. Wang X, Zhang Q. Effect of hydrotalcite on the thermal stability, mechanical properties, rheology and flame retardance of poly(vinyl chloride). *Polymer International*. 2004;53(6):698-707.
14. Gao Y, Wu J, Wang Q, Wilkie CA, O'Hare D. Flame retardant polymer/layered double hydroxide nanocomposites. *Journal of Materials Chemistry A*. 2014;2(29):10996-1016.
15. Hornsby PR, Watson CL. A study of the mechanism of flame retardance and smoke suppression in polymers filled with magnesium hydroxide. *Polymer Degradation and Stability*. 1990;30(1):73-87.
16. Laoutid F, Bonnaud L, Alexandre M, Lopez-Cuesta JM, Dubois P. New prospects in flame retardant polymer materials: From fundamentals to nanocomposites. *Materials Science and Engineering: R: Reports*. 2009;63(3):100-25.
17. Braun D. Poly(vinyl chloride) on the Way from the 19th Century to the 21st Century. *Journal of Polymer Science, Part A: Polymer Chemistry*. 2004;42(3):578-86.

18. Starnes Jr WH, Ge X. Mechanism of autocatalysis in the thermal dehydrochlorination of poly(vinyl chloride). *Macromolecules*. 2004;37(2):352-9.
19. Starnes Jr WH. Structural and mechanistic aspects of the thermal degradation of poly(vinyl chloride). *Progress in Polymer Science (Oxford)*. 2002;27(10):2133-70.
20. Lin Y-J, Li D-Q, Evans DG, Duan X. Modulating effect of Mg–Al–CO₃ layered double hydroxides on the thermal stability of PVC resin. *Polymer Degradation and Stability*. 2005;88(2):286-93.
21. van der Ven L, van Gemert MLM, Batenburg LF, Keern JJ, Gielgens LH, Koster TPM, et al. On the action of hydrotalcite-like clay materials as stabilizers in polyvinylchloride. *Applied Clay Science*. 2000;17(1–2):25-34.
22. Lin Y, Wang J, Evans DG, Li D. Layered and intercalated hydrotalcite-like materials as thermal stabilizers in PVC resin. *Journal of Physics and Chemistry of Solids*. 2006;67(5-6):998-1001.
23. Gupta S, Agarwal DD, Banerjee S. Role of hydrotalcites cations in thermal stabilization of poly (vinyl chloride). *International Journal of Polymeric Materials and Polymeric Biomaterials*. 2012;61(2):124-35.
24. Labuschagné FJWJ, Giesekke EW, Van Schalkwyk JD, inventors SA Patent 2007/09947 Production of hydrotalcite. South Africa2007.
25. ISO. *Plastics - Determination of the tendency of compounds and products based on vinyl chloride homopolymers and copolymers to evolve hydrogen chloride and any other acidic products at elevated temperatures Part 3: Conductometric method*1993.
26. ISO. *ISO/TS 5660-3:2012 Reaction-to-fire tests - Heat release, smoke production and mass loss rate. Part 3: Guidance on measurement*. Geneva: ISO; 2012.

27. ISO. ISO 5660-2:2002 Reaction-to-fire tests - Heat release, smoke production and mass loss rate. Part 2: Smoke production rate (dynamic measurement). Geneva: ISO; 2002.
28. ISO. ISO 5660-1:2015 Reaction-to-fire tests - Heat release, smoke production and mass loss rate. Part 1: Heat release rate (cone calorimeter method) and smoke production rate (dynamic measurement). Geneva: ISO; 2015.
29. Wang Z, Huang, P., Fan, W.C., Wang, Q., editor Measurements on the fire behaviour of PVC sheets using the cone calorimeter. Proceedings of the Asia-Oceania Symposium on Fire Science & Technology; 1988: International Association for Fire Safety Science.
30. Klopogge JT, Wharton D, Hickey L, Frost RL. Infrared and Raman study of interlayer anions CO_3^{2-} , NO_3^- , SO_4^{2-} and ClO_4^- in Mg/Al-hydrotalcite. *American Mineralogist*. 2002;87(5-6):623-9.
31. Choudhary VR, Pataskar SG, Gunjekar VG, Zope GB. Influence of preparation conditions of basic magnesium carbonate on its thermal analysis. *Thermochimica Acta*. 1994;232(1):95-110.
32. Sawada Y, Yamaguchi J, Sakurai O, Uematsu K, Mizutani N, Kato M. Thermogravimetric study on the decomposition of hydromagnesite $4 \text{MgCO}_3 \cdot \text{Mg}(\text{OH})_2 \cdot 4 \text{H}_2\text{O}$. *Thermochimica Acta*. 1979;33(C):127-40.
33. Ren H, Chen Z, Wu Y, Yang M, Chen J, Hu H, et al. Thermal characterization and kinetic analysis of nesquehonite, hydromagnesite, and brucite, using TG-DTG and DSC techniques. *Journal of Thermal Analysis and Calorimetry*. 2014;115(2):1949-60.

34. Vágvölgyi V, Frost RL, Hales M, Locke A, Kristóf J, Horváth E. Controlled rate thermal analysis of hydromagnesite. *Journal of Thermal Analysis and Calorimetry*. 2008;92(3):893-7.
35. Rey F, Fornes V, Rojo JM. Thermal decomposition of hydrotalcites. An infrared and nuclear magnetic resonance spectroscopic study. *Journal of the Chemical Society, Faraday Transactions*. 1992;88(15):2233-8.
36. Bera P, Rajamathi M, Hegde MS, Kamath PV. Thermal behaviour of hydroxides, hydroxysalts and hydrotalcites. *Bull Mater Sci*. 2000;23(2):141-5.
37. Bacaloglu R, Stewen U. Study of PVC degradation using a fast computer scanning procedure. *Journal of Vinyl and Additive Technology*. 2001;7(3):149-55.
38. Malík J, Kröhnke C. Polymer stabilization: present status and possible future trends. *Comptes Rendus Chimie*. 2006;9(11–12):1330-7.
39. Šimon P. Considerations on the single-step kinetics approximation. *Journal of Thermal Analysis and Calorimetry*. 2005;82(3):651-7.
40. Dente M, Bozzano G, Faravelli T, Marongiu A, Pierucci S, Ranzi E. Kinetic Modelling of Pyrolysis Processes in Gas and Condensed Phase. In: Guy BM, editor. *Advances in Chemical Engineering*. Volume 32: Academic Press; 2007. p. 51-166.
41. Anderson HL, Kemmler A, Höhne GWH, Heldt K, Strey R. Round robin test on the kinetic evaluation of a complex solid state reaction from 13 European laboratories. Part 1. Kinetic TG-analysis. *Thermochimica Acta*. 1999;332(1):33-53.

42. Pospíšil J, Horák Z, Pilař J, Billingham NC, Zweifel H, Nešpůrek S. Influence of testing conditions on the performance and durability of polymer stabilisers in thermal oxidation. *Polymer Degradation and Stability*. 2003;82(2):145-62.
43. Kamal MR, Sourour S. Kinetics and thermal characterization of thermoset cure. *Polymer Engineering & Science*. 1973;13(1):59-64.
44. Labuschagne F, Molefe DM, Focke WW, van der Westhuizen I, Wright HC, Royeppen MD. Heat stabilising flexible PVC with layered double hydroxide derivatives. *Polymer Degradation and Stability*. 2015;113:46–54.
45. Scharrel B, Hull TR. Development of fire-retarded materials—Interpretation of cone calorimeter data. *Fire and Materials*. 2007;31(5):327-54.
46. Sacristán M, Hull TR, Stec AA, Ronda JC, Galià M, Cádiz V. Cone calorimetry studies of fire retardant soybean-oil-based copolymers containing silicon or boron: Comparison of additive and reactive approaches. *Polymer Degradation and Stability*. 2010;95(7):1269-74.
47. Hirschler MMS, S., editor. *Flame Retardants 92*; 1992; London/New York: Elsevier Applied Science.
48. Zhu H, Wang W, Liu T. Effects of copper-containing layered double hydroxide on thermal and smoke behavior of poly(vinyl chloride). *Journal of Applied Polymer Science*. 2011;122(1):273-81.

Chapter 4: Layered double hydroxide derivatives as flame retardant for flexible PVC³

4.1 Introduction

PVC is a very versatile polymer used in diverse applications including flooring, rigid pipes, flexible hoses, conveyor belting, wire- and cable-insulation. Neat PVC has a relatively high chlorine content of 56.7 wt.%, that makes it more resistant to ignition and burning than most organic polymers (Coaker, 2003). Furthermore, pyrolysis of PVC yields an isotropic carbon char residue (Otani, 1965) and this contributes to the mechanisms of flame retardant action (Folarin and Sadiku, 2011). However, the conventional plasticisers used in the manufacture of flexible PVC detract from this outstanding fire resistance and therefore flame-retardant (FR) and smoke-suppressant (SS) additives must be incorporated in order to meet product test specifications such as limiting oxygen index (LOI), heat release rate, smoke evolution, smoke toxicity, etc. (Coaker, 2003). Levchik and Weil (2005) and Weil *et al.*, (2006) reviewed the chemical additives that have been considered to achieve acceptable fire properties in the principal PVC application areas.

Neat PVC is thermally unstable (Braun, 2004) and prone to autocatalytic dehydrochlorination (Starnes Jr and Ge, 2004). The hydrogen chloride assumes a catalytic role in the degradation mechanism (Starnes Jr, 2002). In practice the processing problems associated with the use of PVC are overcome through the use of heat stabiliser additives (Braun, 2004). Scavenging the liberated HCl generated by the

³ This Chapter has been submitted to Journal of Thermal Analysis and Calorimetry and is reproduced here in the form in which it was submitted for review.

degradation reaction is a way to arrest the degradation. Layered double hydroxides (LDHs) are promising heat stabilisers for PVC owing to their intrinsically high capacity to react with HCl (Lin *et al.*, 2005, Van der Ven *et al.*, 2000, Lin *et al.*, 2006). LDHs are anionic clays with a brucite-like structure (Jones and Newman, 1998). They consist of stacks of positively charged mixed metal (Mg and Al) hydroxide layers that require the presence of interlayer anions to maintain overall charge neutrality. Unlike most metallic salts, LDHs are readily incorporated into PVC resins to provide translucent PVC articles. The thermal stabilisation action of LDHs involves two steps. Initially HCl (formed during thermal dehydrochlorination) displaces the carbonate interlayer anions to afford LDHs with chloride anions in the interlayer. As further dehydrochlorination takes place, the HCl reacts with the clay itself, ultimately destroying its structure and forming metal chlorides, metal hydroxy-chlorides and hydrates of magnesium and aluminium. (van der Ven *et al.*, 2000)

On heating LDH decomposes endothermically, releasing CO₂ and water vapour as inert gases. Hence it is a potential flame retardant additive for plasticised PVC as well as other polymers (Xu *et al.*, 2006, Wang and Zhang, 2004, Gao *et al.*, 2014). In addition LDH is also a good smoke suppressant (Kuang *et al.*, 2010, Zhang *et al.*, 2006). This makes LDHs a favourable material to be used in plasticised PVC as additive to act as both heat stabiliser and flame retardant. However, current industrial solutions are based on conventional MgAl-LDH. This communication considered LDH modifications related to partial or full substitution of the magnesium or aluminium constituents of conventional LDH with other metals. The effect of these modifications on the fire retardancy and smoke suppression of plasticised PVC was studied using a cone calorimeter.

4.2 Experimental

4.2.1 Materials

Preparation of LDH-derivatives

The LDH-derivatives listed in Table 1 were synthesised according to the method described by Labuschagné *et al.*, (2007). All samples were coated with stearic acid. A detailed description of the procedures was reported in a previous communication (Labuschagné *et al.*, 2015). The composition, specific surface area and d_{50} particle size of the LDH-derivatives are given in Table 1.

Preparation of PVC-composites

Diisononyl phthalate (DINP) plasticiser (130 g) was weighed into a 600 mL beaker. Next small portions of the PVC powder (up to a total of 130 g) were added and mixed-in using a high-speed Anvil milkshake mixer. The dispersion was de-aerated for about 30 min in a Speedvac vacuum chamber. Then the LDH filler powder (39 g) was incorporated. The dispersion was again de-aerated but this time for about 1 h. These plastisol samples were used as is to test the dynamic heat stability and also to cast solid sheets for other characterisation procedures, e.g. mechanical testing.

Cast PVC composite sheets were made in a three step pressing process. The paste mixture was poured into a mould measuring 100 mm × 100 mm × 3.5 mm. The mould was closed and placed in convection oven set at a temperature of 130 °C for 10 min. Then it was hot pressed at a pressure of 10 MPa at 150 °C for 5 min. The mould was then removed from the press and a heavy weight placed on the top plate. The moulding was allowed to cool down at ambient conditions before it was removed.

Table 4.1: LDH derivatives: Apparent elemental composition calculated from ICP-OES, BET surface area and particle size

Sample	Formula	BET, m ² g ⁻¹	d ₅₀ , μm
MgAl-LDH	[Mg _{2.092} Al _{0.908} (OH) ₆](CO ₃) _{0.454}	18.3	3.08 ± 0.03
CaAl-LDH	[Ca _{2.275} Al _{0.725} (OH) ₆](OH) ₂ CO ₃) _{0.182}	5.44	6.25 ± 0.12
MgFeAl-LDH	[Mg _{2.062} Fe _{0.198} Al _{0.740} (OH) ₆](CO ₃) _{0.370}	9.83	1.87 ± 0.02
MgCuAl-LDH	[Mg _{1.570} Cu _{0.597} Al _{0.833} (OH) ₆](CO ₃) _{0.417}	13.3	2.00 ± 0.09
MgZnAl-LDH	[Mg _{1.527} Zn _{0.554} Al _{0.918} (OH) ₆](CO ₃) _{0.459}	12.4	2.30 0.11

4.3 Characterisation

All characterisations were performed on the moulded sheets.

4.3.1 Mechanical Properties

Tensile testing was carried out on a Lloyds Instruments LRX Plus machine according to the ASTM D 638 method. The crosshead speed was 50 mm min⁻¹. Type IV dumbbells were cut from the sheets. Five specimens were tested at each composition.

4.3.2 Thermogravimetric Analysis (TGA)

Thermogravimetric analysis (TGA) using the dynamic method on a Mettler Toledo A851 TGA/SDTA instrument was performed on all the samples. About 10-15 mg sample was placed in an open 150 μL alumina pan. Temperature was scanned from 25 °C to 900 °C at a scan rate of 10 °C min⁻¹ with air or nitrogen flowing at a rate of 50 mL min⁻¹.

4.3.3 Cone calorimeter test

The ISO 5660 standards (2002a, 2002b, 2003) were followed in performing the cone calorimeter tests using a Dual Cone Calorimeter (Fire Testing Technology (UK) Ltd.).

Three specimens of each composition were tested. The sheet dimensions were $100 \text{ mm} \times 100 \text{ mm} \times 3.4 \pm 0.1 \text{ mm}$. They were placed on aluminium foil and exposed horizontally to an external heat flux of 35 kW m^{-2} . This heat flux was chosen on the basis of the study conducted by Wang *et al.* (1988). They studied 3 mm to 10 mm thick PVC sheets at heat fluxes of 25 kW m^{-2} , 35 kW m^{-2} and 50 kW m^{-2} and found that the time to ignition varied linearly with the inverse of the cone calorimeter heat flux. Furthermore, the minimum heat flux for ignition of sheets in this thickness range was found to be about 19 kW m^{-2} .

4.4 Results

4.4.1 Physical appearance

Figure 4.1 shows images of the moulded sheets. The discoloration of the PVC sample is attributed to the fact that no stabiliser was used at all. Strong pigmentation effects were observed with the MgFeAl-LDH (red) and the MgCuAl-LDH (black) additives.

4.4.2 Mechanical Properties

Table 4.2 shows the effect of the additives on the tensile properties of plasticised PVC. A marginal reinforcing effect was observed for MgAl-LDH and MgZnAl-LDH but the stiffness of the sample containing CaAl-LDH was actually lower than that of the neat PVC compound. The latter sample also showed a reduced tensile strength although the elongation to break was in the range of those observed for the other compounds. The poor performance of this sample is not currently understood. Otherwise the mechanical properties were similar to those for the base PVC compound.



Figure 4.1: Physical appearance of the pressed PVC sheets

Table 4.2: Mechanical properties (tensile strength, Young's modulus and elongation to break) of the PVC compounds filled with the LDH derivatives

Sample	σ , MPa	E, MPa	ϵ , %
PVC	4.16 ± 0.13	2.8 ± 0.3	250 ± 7
MgAl-LDH	4.46 ± 0.09	3.3 ± 0.2	316 ± 7
CaAl-LDH	2.82 ± 0.14	2.4 ± 0.2	226 ± 11
MgFeAl-LDH	4.28 ± 0.12	2.7 ± 0.2	316 ± 11
MgCuAl-LDH	3.55 ± 0.26	3.0 ± 0.2	222 ± 25
MgZnAl-LDH	3.73 ± 0.18	3.3 ± 0.5	262 ± 22

4.4.3 Thermogravimetric Analysis (TGA) of the LDH-PVC composites

Figure 4.2 shows TGA traces for the LDH-PVC compounds recorded in air and in nitrogen atmospheres. In a nitrogen atmosphere the flexible PVC apparently suffers major mass loss in two main steps. However, the derivative curves (DTG not shown) showed multiple peaks in the first mass loss stage. The first stage commences at

240 °C, reaches a maximum rate at 315 °C and ends at 370 °C. At this point the residue is 20.7 wt.%. The second stage starts at 420 °C, reaches a maximum rate at 467 °C and ends at 510 °C with a residue of 7.0 wt.% remaining. The initial mass loss is due a combination of PVC degradation (mainly dehydrochlorination) events and volatilisation of the plasticiser. The second stage is attributed to pyrolysis reactions that ultimately lead to a carbonaceous char residue (4.3 wt.% at 900 °C). The shape of the mass loss curves for the LDH-PVC composites mirror those of PVC. The mass loss onset temperatures are virtually identical but mass loss occurs over a narrower temperature range and the residue after each stage is greater than found for the neat PVC. The ranking for initial mass loss rate, from fastest to slowest, for the additives is:

$\text{MgZnAl-LDH} \gg \text{MgFeAl-LDH} > \text{MgCuAl-LDH} > \text{CaAl-LDH} \approx \text{MgAl-LDH}$

The MgZnAl-LDH, in particular, significantly accelerated the mass loss during the first stage. The initial decomposition yields ZnCl_2 which autocatalytically accelerates the dehydrochlorination reaction according to the mechanism reported by Levchik and Weil (2005). The higher char yield is also attributed to catalytic effects that favour crosslinking and aromatisation reactions at the expense of cracking reactions that yield volatiles.

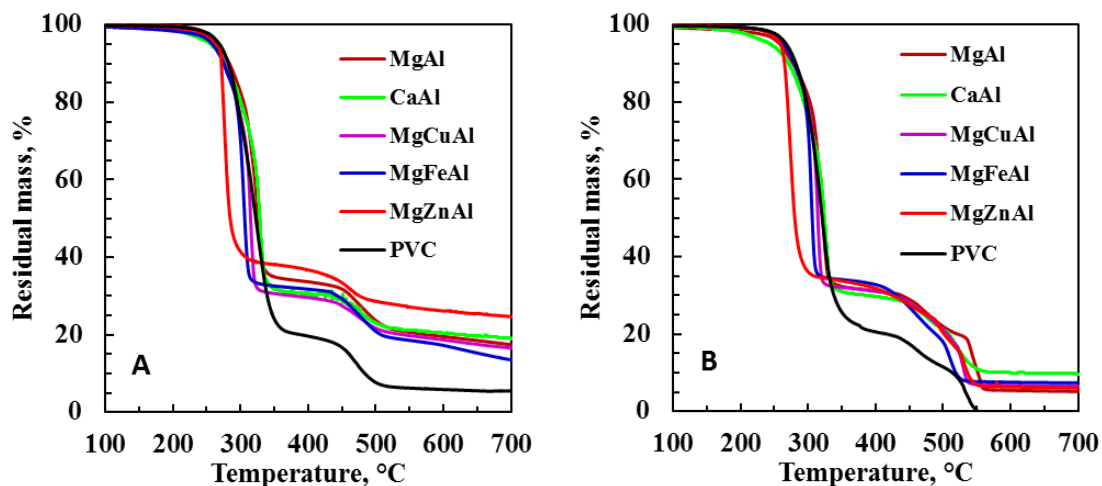


Figure 4.2: TGA traces for the PVC-LDH composites in (A) nitrogen and (B) air atmospheres. The temperature was scanned from 25 °C to 900 °C at a scan rate of 10 °C min⁻¹ with gas flowing at a rate of 50 mL min⁻¹.

The initial part of the mass loss curves (below 300 °C) found in an air atmosphere is similar to that in a nitrogen atmosphere. However, at higher temperatures additional mass loss occurs owing to the oxidation of the carbonaceous char. The PVC sample residue decreases to zero at ca. 550 °C. The other samples show a greater residue but this represents non-volatile inorganic matter.

4.4.4 Flammability

The cone calorimeter results are presented in Figure 3 to Figure 9 and they are summarised in Table 4.3. All the samples ignited after a short but similar induction period. They burned producing a large amount of smoke. For purposes of readability and clarity, some of the figures show only the data obtained for the neat PVC, the compound containing the reference additive MgAl-LDH and the compound that provided the best performance in each category.

Table 4.3: Cone calorimeter data summary

Parameter	Units	PVC	MgAl LDH	CaAl LDH
Time to ignition (t_{ign})	S	23.0 ± 2.1	27.7 ± 1.2	18.0 ± 0.1
Time to flame out	S	306 ± 137	654 ± 51	442 ± 21
Time to $pHRR$	S	103 ± 10	105 ± 1	145 ± 9
Peak heat release rate ($pHRR$)	kW m^{-2}	623 ± 8	389 ± 9	381 ± 24
Total heat release (tHR)	MJ m^{-2}	68 ± 2	72 ± 3	78 ± 3
$FIGRA$	$\text{kW m}^{-2} \text{s}^{-1}$	6.1 ± 0.6	3.7 ± 0.1	2.6 ± 0.2
$MAHRE$	kW m^{-2}	367 ± 11	208 ± 2.2	241 ± 13.1
$pHRR/t_{ign}$	$\text{kW m}^{-2} \text{s}^{-1}$	26.0 ± 0.8	14.4 ± 0.3	21.2 ± 1.4
Smoke release	$\text{m}^2 \text{m}^{-2}$	4413 ± 97	2780 ± 121	3153 ± 292
		MgFeAl LDH	MgCuAl LDH	MgZnAl LDH
Time to ignition (t_{ign})	S	24.0 ± 1.0	21.7 ± 1.5	23.7 ± 0.6
Time to flame out	S	649 ± 41	482 ± 56	638 ± 27
Time to $pHRR$	S	45 ± 0	107 ± 3	40 ± 0
Peak heat release rate ($pHRR$)	kW m^{-2}	253 ± 5	383 ± 22	319 ± 7
Total heat release (tHR)	MJ m^{-2}	72 ± 3	64 ± 4	74 ± 7
$FIGRA$	$\text{kW m}^{-2} \text{s}^{-1}$	5.6 ± 0.1	3.7 ± 0.3	8.0 ± 0.2
$MAHRE$	kW m^{-2}	176 ± 1.3	208 ± 7.5	195 ± 3.3
$pHRR/t_{ign}$	$\text{kW m}^{-2} \text{s}^{-1}$	10.9 ± 0.2	17.2 ± 1.9	13.3 ± 0.3
Smoke release	$\text{m}^2 \text{m}^{-2}$	2468 ± 15	2244 ± 216	2971 ± 136

Figure 4.3 plots the times to ignition and time to flame out for the various samples.

The time to ignition (t_{ign}) was 23 ± 2 s for the neat PVC compound. It was longest for the MgAl-LDH containing compound (28 ± 1 s) and shortest for CaAl-LDH (18 ± 0 s). The time to flame out was 306 ± 137 s for the neat PVC compound. It increased by between 44 % and 112 % with LDH added.

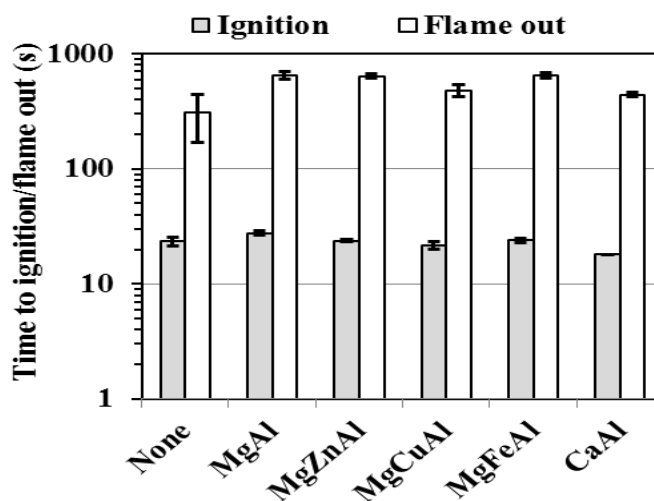


Figure 4.3: Cone calorimeter time to ignition and flame out for the plasticised PVC compound and its composites with LDH derivatives.

Figure 4.4 shows representative mass loss curves obtained during the cone calorimeter tests. Directly after ignition, the neat PVC compound showed rapid mass loss and this was virtually complete by 200 s. Thereafter there was a very slow steady decline in the residue amount with the char yield in the order of 3 wt.% at the end of the test. The LDH composites lost mass at a much slower rate over a longer time. Up to about 150 s into the test, the mass loss curves virtually coincided. After this time they diverged with CaAl-LDH showing the greatest mass loss and MgZnAl-LDH the least. These compounds spanned the char yields of the others with ca. 13 wt.% and 20 wt.% respectively. The faster initial mass loss and the higher ultimate char yield found for the MgZnAl-LDH agrees with behaviour observed in the TGA pyrolysis run in a nitrogen atmosphere.

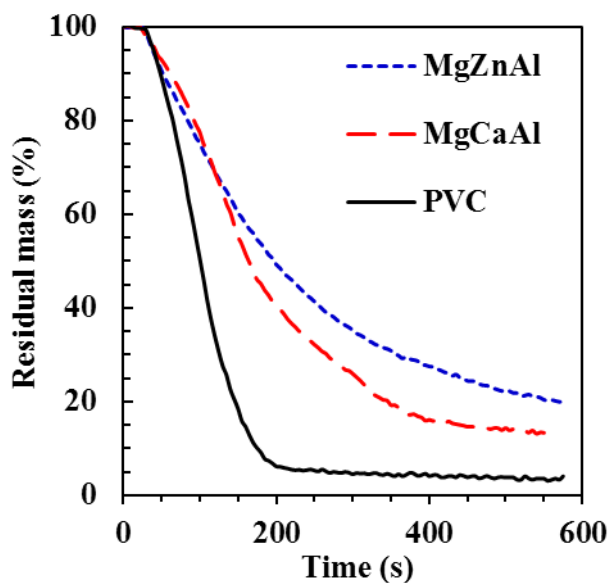


Figure 4.4: Representative cone calorimeter mass loss curves for the plasticised PVC compound and its composites with LDH derivatives. The sample sheets were backed by aluminium foil and their dimensions were $100 \text{ mm} \times 100 \text{ mm} \times 3.5 \pm 0.1 \text{ mm}$. They were exposed horizontally to an external heat flux of 35 kW m^{-2} .

Figure 4.5 shows representative heat release rate (*HRR*) curves obtained from the cone calorimeter tests. The heat release curves for the neat plasticised PVC compound exhibited the shape characteristic of a thermally thin sample (Schartel and Hull, 2007). Thermally thin samples are identified by a sharp peak in their *HRR* curves as the whole sample is pyrolysed nearly at once. The *HRR* curves for the filled compounds were flatter and broader than that for the neat PVC. *HRR* curves characteristic of thermally thick, char-producing samples show a sudden rise to a plateau value (Schartel and Hull, 2007). However, the *HRR* curves for the samples containing LDH derivatives were more complex. They showed a sudden rise to a peak value with a slow but steady decline over a longer time period. The CO_2 and CO release rates (not shown graphically) curves mirrored those observed for the *HRR* (Figure 4.5) almost perfectly.

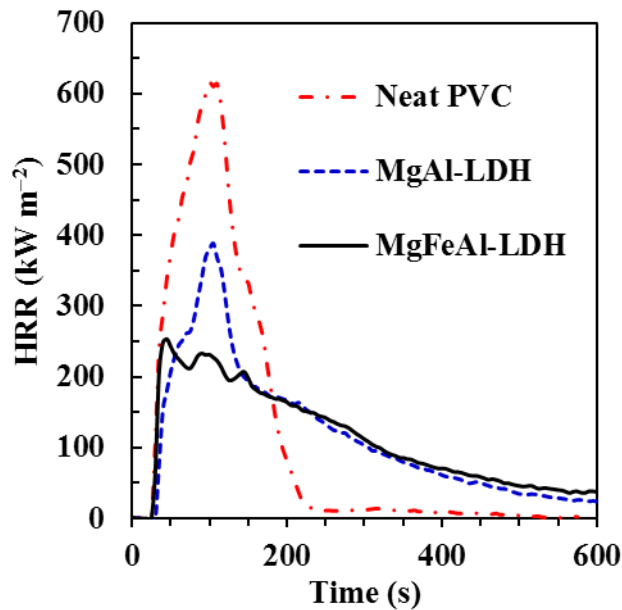


Figure 4.5: Representative cone calorimeter heat release rate curves for the plasticised PVC compound and its composites with LDH derivatives. The sample sheets were backed by aluminium foil and their dimensions were 100 mm × 100 mm × 3.5 ± 0.1 mm. They were exposed horizontally to an external heat flux of 35 kW m⁻².

Figure 4.6 shows the effect of adding the LDH fillers to the PVC on the peak heat release rates (*pHRR*) and the maximum average rate of heat emission (*MARHE*). The *pHRR* for the neat PVC compound was 623 ± 8 kW m⁻². Incorporating LDH derivatives at the 13 wt.% level caused a significant lowering of the *pHRR*. MgAl-LDH lowered the *pHRR* value to 389 ± 9 kW m⁻² but the best result was obtained with MgFeAl-LDH (253 ± 5 kW m⁻²).

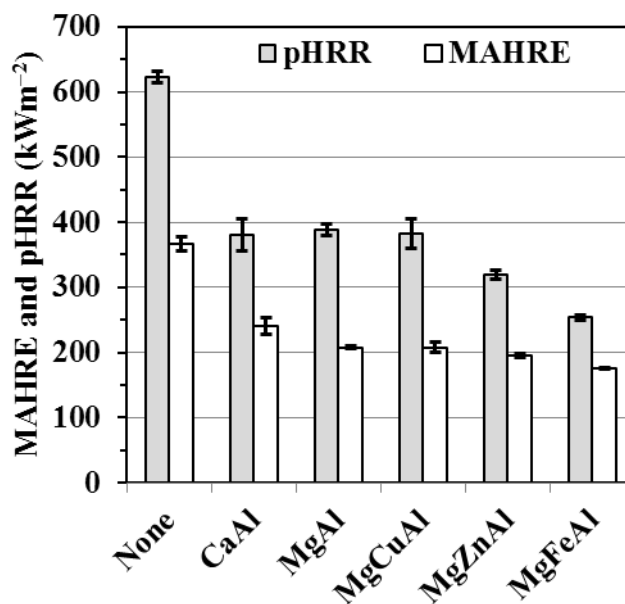


Figure 4.6: Cone calorimeter peak heat release rates and total heat release for the plasticised PVC compound and its composites with LDH derivatives. The sample sheets were backed by aluminium foil and their dimensions were 100 mm × 100 mm × 3.5 ± 0.1 mm. They were exposed horizontally to an external heat flux of 35 kW m⁻².

An important index used to interpret cone calorimeter data is the maximum average rate of heat emission (*MARHE*) (Schartel and Hull, 2007, Sacristán et al., 2010). The *MARHE* parameter is defined as the peak value of the cumulative heat emission divided by time (Sacristán et al., 2010). It provides a measure of the propensity for fire development under full scale conditions. The addition of the LDH derivatives significantly reduced the *MARHE*. On the whole the reduction follows the same trend that was observed for the peak heat release rate. The *MARHE* for the neat PVC was 367 ± 11 kW m⁻² and this was reduced to 176 ± 1 kW m⁻² with the MgFeAl-LDH as stabiliser-flame retardant.

Interesting observations hold for the total heat release (*tHR*). It was 68 ± 2 MJ m⁻² for the neat PVC compound (Table 4.3). With the LDH derivatives incorporated, the *tHR*

increased even though less fuel is actually available. The $pHRR$ was $72 \pm 3 \text{ MJ m}^{-2}$ for the MgAl-LDH compound and the highest value was $78 \pm 3 \text{ MJ m}^{-2}$ recorded for the CaAl-LDH. Thus while the fire performance improved with respect to the peak heat release rate, it deteriorated when the total heat release is considered. The apparent increase in the total heat release (tHR) is tentatively attributed to the chlorine preferentially interacting and bonding with the LDH. This means that more of the carbon became available as fuel.

The fire growth rate ($FIGRA$) is an estimator for the fire spread rate and size of the fire (Schartel and Hull, 2007, Sacristán et al., 2010). Strictly speaking the $FIGRA$ is defined as the maximum quotient of $HRR(t)/t$. The fire performance index (FPI) is possibly the best single indicator of the overall fire hazard posed by a material (Hirschler, 1992). It is defined as the ratio of the time-to-ignition to the peak heat release rate ($FPI = t_{ign}/pHRR$). There is a connection between FPI and the time to flashover, i.e. the change from small to large-scale fire (Hirschler, 1992). A lower FPI value is associated with a shorter time to flashover suggesting that a shorter time is available for escape in a full-scale fire situation. Figure 4.7 shows the $FIGRA$ and FPI indices with the latter expressed as its inverse as it then has the same units as the $FIGRA$. Relative to the neat PVC compound, the presence of the MgAl-LDH or the CaAl-LDH markedly decreased the $FIGRA$ (>50 %). However, a significant higher value was found for the MgZnAl-LDH. The $pHRR/t_{ign}$ for the neat PVC was $26 \pm 1 \text{ kW m}^{-2} \text{ s}^{-1}$. It was lowered to $10.9 \pm 0.2 \text{ kW m}^{-2} \text{ s}^{-1}$ in the presence of MgFeAl-LDH while the other PVC compounds featured intermediate values.

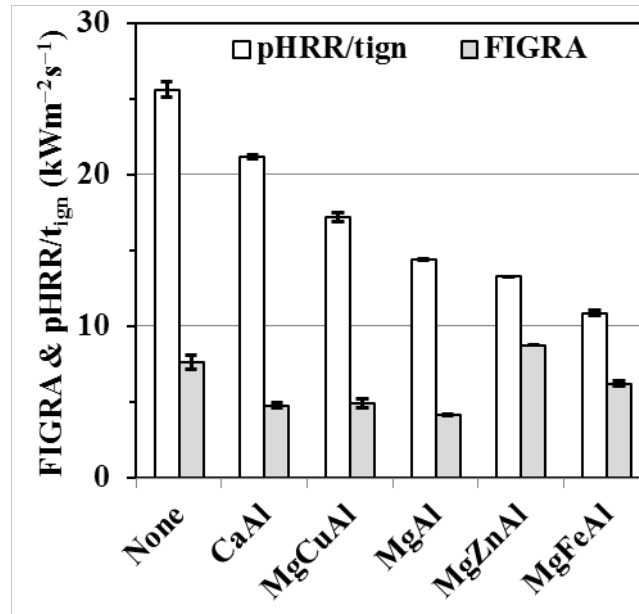


Figure 4.7: The effect of the LDH derivatives on the FIGRA and $pHRR/t_{ign}$ of PVC composites. The sample sheets were backed by aluminium foil and their dimensions were $100\text{ mm} \times 100\text{ mm} \times 3.5 \pm 0.1\text{ mm}$. They were exposed horizontally to an external heat flux of 35 kW m^{-2} .

Figure 4.8 shows representative smoke production rates (*SPR*) and Figure 4.9 compares the smoke production of the composites with that for the neat PVC compound. The LDH derivatives composites featured lower *SPR* in comparison to the neat PVC just as they also featured reduced rates of mass loss under flaming conditions. The lowest peak value was observed with MgFeAl-LDH (Figure 4.8) but the lowest overall amount was obtained with MgCuAl-LDH (Figure 4.9).

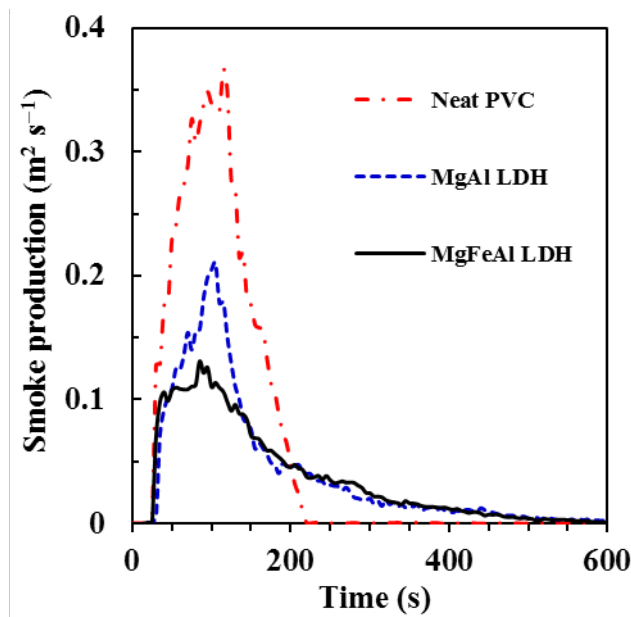


Figure 4.8: Cone calorimeter smoke production rates for the plasticised PVC compound and its composites with LDH derivatives. The sample sheets were backed by aluminium foil and their dimensions were 100 mm × 100 mm × 3.5 ± 0.1 mm. They were exposed horizontally to an external heat flux of 35 kW m⁻².

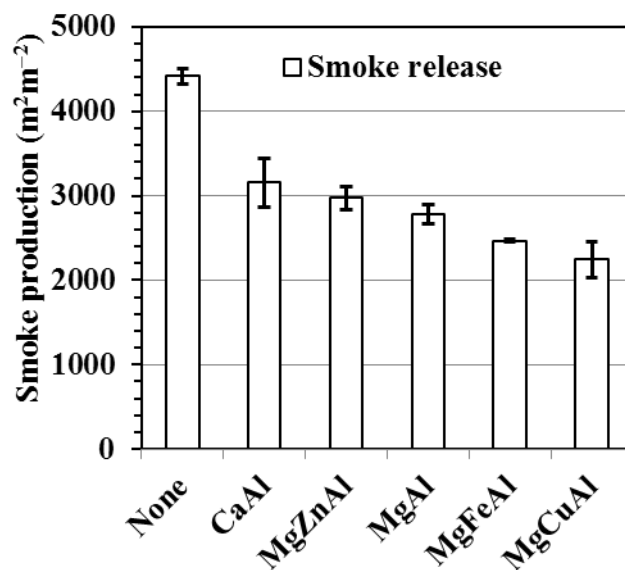


Figure 4.9: Comparing the smoke production of the plasticised PVC compound with that from its composites with LDH derivatives. The sample sheets were backed by aluminium foil and their dimensions were 100 mm × 100 mm × 3.5 ± 0.1 mm. They were exposed horizontally to an external heat flux of 35 kW m⁻².

4.5 Discussion

Compared to the neat PVC, the LDH-stabilised PVC samples showed different behaviour in the TGA and cone calorimeter tests. There was also a clear LDH composition effect. The MgZnAl-LDH accelerated the initial TGA mass loss in both air and nitrogen atmospheres but led to relatively high char yields at higher temperatures. In the cone calorimeter tests, they generally decreased the time to ignition and increased the time to flame out. They also increased the total fire load, but proved to be effective flame retardants with respect to all other fire performance indices. MgFeAl-LDH was most effective at reducing the peak heat release rate (*pHRR*), the maximum average rate of heat emission (*MARHE*) and the fire performance index (*FPI*). MgAl-LDH led to the lowest fire growth rate (*FIGRA*) while MgCuAl-LDH showed the lowest smoke production.

The performance of the LDH-derivatives can be explained in the context of the PVC degradation mechanism. Neat PVC degradation occurs in two stages. The first stage proceeds as an autocatalytic dehydrochlorination of the PVC backbone with the liberated hydrogen chloride assuming a catalytic role (Starnes Jr, 2002). The degradation reaction is initiated at defect sites (e.g., internal allylic chloride and tertiary chloride structural flaws). The mechanism of autocatalysis involves a free-radical process that converts ordinary polymer repeat units into chloroallylic structures of low thermal stability (Starnes Jr and Ge, 2004). It also leads to the formation of sequences of conjugated double bonds along the polymer chain. In the second stage of degradation these highly reactive defects undergo secondary reactions. Crosslinking of the polymer chains and dehydrochlorination reactions promote char formation (Bacaloglu and Stewen, 2001). Chain cleavage and cracking

reactions led to the formation of volatile aromatic molecules that promote smoke generation.

The hydrochloric acid generated by the degradation reaction catalyses the chain propagation reaction. The carbonated LDHs improve the heat stability of the PVC by scavenging this corrosive gas. Initially this occurs via the formation of chloride intercalated LDHs. However, later on the acid attacks the LDH structure leading to the formation of metal chlorides. These salts act as Lewis acids that can also promote dehydrochlorination via a carbonium ion mechanism (Levchik and Weil, 2005). ZnCl_2 in particular appears to be a more active catalyst than HCl. This explains the faster mass loss observed for the MgZnAl-LDH compound during the initial stages of the degradation and recorded in both the cone calorimeter and in the TGA experiments.

According to Zhu *et al.* (2011) the LDHs act as Lewis acids and induce cationic crosslinking (Friedel–Craft reaction) of neighbouring polyene backbones. Metal chlorides also catalytically favour crosslinking and dehydrochlorination reactions at the expense of cracking reactions (Zhu *et al.*, 2011). These actions improve char formation and reduce smoke generation in accordance with the present experimental results. Copper ions acts as reductive crosslinking agent and this may explain the observation that the MgCuAl-LDH compound was a particularly effective smoke suppressant.

The release of the HCl by the decomposing PVC inhibits flaming combustion in the cone calorimeter tests. The halogen entering the gas phase contributes to a “flame poisoning effect”, i.e. the slowing down of the free radical chain reactions occurring

in the flame (Weil *et al.*, 2006). In the presence of the LDHs, the HCl is efficiently scavenged especially in the early stages of degradation. Less halogen is present in the volatile organics released in the beginning, making them easier to ignite. This may explain the shorter time to ignition found for some LDH compounds compared to neat PVC.

Compared to the neat PVC, all the LDH compounds decreased the peak heat release rate in the cone calorimeter tests. This may be due to a combination of vapour phase and solid phase effects. High heat decomposes the LDHs, releasing water and carbon dioxide. The decomposition is endothermic in nature which means that it cools the polymer substrate. At lower temperature the degradation reactions that generate fuel proceeds more slowly. This explains, in part, the lower rate of mass loss observed for the LDH compounds in the cone calorimeter tests. In addition, the inert gases liberated have a dilution effect on the air-fuel mixture in the gas phase. This cools the flame and reduces the rate of heat generation. The inorganic residues may also form a protective layer on the surface of the substrate. They may act as a barrier to heat transfer to the underlying polymer and also as a barrier to mass transfer of degradation products migrating to the gas phase. Finally the inorganic residues may effectively reflect incoming infrared radiation that would otherwise have heated the substrate to higher temperatures. All these effects may contribute to the lowering of the heat release rate observed in the cone calorimeter tests.

Finally, at elevated temperature and in the presence of oxygen, the metal oxide residues from the decomposition of the LDHs catalyse the oxidation of the

carbonaceous char residues. This explains the absence of organic residues above 600 °C in the TGA runs conducted in an air atmosphere.

4.6 Conclusions

Emulsion grade PVC was plasticised with 100 phr of diisononyl phthalate (DINP) and filled with 30 phr layered double hydroxides (LDHs) as combination stabiliser-flame retardant. The MgAl-LDH with approximate composition $[\text{Mg}_4\text{Al}_2(\text{OH})_{12}](\text{CO}_3)\cdot 3\text{H}_2\text{O}$ was chosen as reference additive. Derivatives in with partial substitution of the magnesium or the aluminium with zinc, copper, iron or calcium were also evaluated. The thermal decomposition was studied by thermogravimetric analysis and the fire behaviour determined in a cone calorimeter. The addition of LDH derivatives significantly improved the fire resistance of the plasticised PVC. Partial substitution of the aluminium by Fe(III) in the LDH lowered the peak heat release rate (*pHRR*), from $623 \pm 8 \text{ kW m}^{-2}$ to $253 \pm 5 \text{ kW m}^{-2}$ but increased the total heat release from $68 \pm 2 \text{ MJ m}^{-2}$ to $72 \pm 3 \text{ MJ m}^{-2}$. This MgFeAl-LDH also improved other fire resistance indices, e.g. the maximum average rate of heat emission (*MARHE*) and the fire performance index (*FPI*). MgAl-LDH showed the lowest fire growth rate (*FIGRA*) while the MgCuAl-LDH showed the lowest smoke production.

4.7 Acknowledgements

Financial support from the *THRIP* programme of the Department of Trade and Industry and the National Research Foundation as well as Greenfield Innovation, Engelbrecht & Mentz and Blue Sky Venture Partners is gratefully acknowledged.

4.8 References

- 2002a. ISO 5660-1: 2002 Reaction to fire tests. Heat release, smoke production and mass loss rate. Part 1: Heat release rate (cone calorimeter method) and smoke production rate (dynamic measurement). ISO, Geneva, Switzerland.
- 2002b. ISO 5660-2: 2002. Reaction to Fire Tests. Heat Release, Smoke Production and Mass Loss Rate. Part 2: Smoke Production Rate (Dynamic Measurements). ISO, Geneva, Switzerland.
2003. ISO/TR 5660-3: 2003. Reaction to Fire Tests. Heat Release, Smoke Production and Mass Loss Rate. Part 3: Guidance on Measurement. ISO, Geneva, Switzerland.
- BRAUN, D. 2004. Poly(vinyl chloride) on the Way from the 19th Century to the 21st Century. *Journal of Polymer Science, Part A: Polymer Chemistry*, 42, 578-586.
- COAKER, A. W. 2003. Fire and flame retardants for PVC. *Journal of Vinyl and Additive Technology*, 9, 108-115.
- FOLARIN, O. M. & SADIKU, E. R. 2011. Thermal stabilizers for poly(vinyl chloride): A review. *International Journal of Physical Sciences*, 6, 4323-4330.
- GAO, Y., WU, J., WANG, Q., WILKIE, C. A. & O'HARE, D. 2014. Flame retardant polymer/layered double hydroxide nanocomposites. *Journal of Materials Chemistry A*, 2, 10996-11016.
- HIRSCHLER, M. M., SHAKIR, S., 1992, Measurements of cable fire properties by using heat release equipment, *Flame Retardants '92, Plastics and Rubber Institute Fire Retardants Tech. Mtg*, 22-23 Jan 1992, , 77-99.
- KUANG, Y., ZHOA, L., ZHANG, S., ZHANG, F., DONG, M., XU, S., 2010. Morphologies, Preparations and Applications of Layered Double Hydroxide Micro-/Nanostructures. *Materials*, 3, 5220-5235.

LABUSCHAGNÉ, F. J. W. J., GIESEKKE, E.W., VAN SCHALKWYK, J.D. 2007. Production of Hydrotalcite. South Africa patent application no 2007/09947.

LABUSCHAGNÉ, F. J. W. J., MOLEFE, D. M., FOCKE, W. W., VAN DER WESTHUIZEN, I., WRIGHT, H. C., ROYEPPEN, M. D., 2015, Heat stabilising flexible PVC with layered double hydroxide derivatives. *Polymer Degradation and Stability*, 113, 46-54.

LEVCHIK, S. V. & WEIL, E. D. 2005. Overview of the recent literature on flame retardancy and smoke suppression in PVC. *Polymers for Advanced Technologies*, 16, 707-716.

LIN, Y.-J., LI, D.-Q., EVANS, D. G., DUAN, X. 2005. Modulating effect of Mg–Al–CO₃ layered double hydroxides on the thermal stability of PVC resin. *Polymer Degradation and Stability*, 88, 286-293.

LIN, Y., WANG, J., EVANS, D. G., LI, D. 2006. Layered and intercalated hydrotalcite-like materials as thermal stabilizers in PVC resin. *Journal of Physics and Chemistry of Solids*, 67, 998-1001.

OTANI, S. 1965. On the carbon fiber from the molten pyrolysis products. *Carbon*, 3, 31-38.

SACRISTÁN, M., HULL, T. R., STEC, A. A., RONDA, J. C., GALIÀ, M., CÁDIZ, V. 2010. Cone calorimetry studies of fire retardant soybean-oil-based copolymers containing silicon or boron: Comparison of additive and reactive approaches. *Polymer Degradation and Stability*, 95, 1269-1274.

SCHARTEL, B., HULL, T. R. 2007. Development of fire-retarded materials— Interpretation of cone calorimeter data. *Fire and Materials*, 31, 327-354.

STARNES JR, W. H. 2002. Structural and mechanistic aspects of the thermal degradation of poly(vinyl chloride). *Progress in Polymer Science (Oxford)*, 27, 2133-2170.

STARNES JR, W. H., GE, X. 2004. Mechanism of autocatalysis in the thermal dehydrochlorination of poly(vinyl chloride). *Macromolecules*, 37, 352-359.

VAN DER VEN, L., VAN GEMERT, M. L. M., BATENBURG, L. F., KEERN, J. J., GIELGENS, L. H., KOSTER, T. P. M., FISCHER, H. R. 2000. On the action of hydrotalcite-like clay materials as stabilizers in polyvinylchloride. *Applied Clay Science*, 17, 25-34.

WANG, X., ZHANG, Q. 2004. Effect of hydrotalcite on the thermal stability, mechanical properties, rheology and flame retardance of poly(vinyl chloride). *Polymer International*, 53, 698-707.

WANG, Z., HUANG, P., FAN, W.C., WANG, Q., 1998, Measurements on the fire behaviour of PVC sheets using the cone calorimeter. *Proceedings of the Asia-Oceania Symposium on Fire Science & Technology. International Association for Fire Safety Science*, 221-227.

WEIL, E. D., LEVCHIK, S., MOY, P. 2006. Flame and smoke retardants in vinyl chloride polymers - Commercial usage and current developments. *Journal of Fire Sciences*, 24, 211-236.

XU, Z. P., SAHA, S. K., BRATERMAN, P. S., D'SOUZA, N., 2006. The effect of Zn, Al layered double hydroxide on thermal decomposition of poly(vinyl chloride). *Polymer Degradation and Stability*, 91, 3237-3244.

ZHANG, Z., ZHU, M., SUN, B., ZHANG, Q., YAN, C., FANG, S., 2006. *Journal of Macromolecular Science, Part A: Pure and Applied Chemistry*, 43(11), 1807-1814

ZHU, H., WANG, W., LIU, T. 2011. Effects of copper-containing layered double hydroxide on thermal and smoke behavior of poly(vinyl chloride). *Journal of Applied Polymer Science*, 122, 273-281.

Chapter 5: Heat stabilising flexible PVC with layered double hydroxide derivatives⁴

5.1 Introduction

Hydrotalcite $[\text{Mg}_6\text{Al}_2(\text{OH})_{16}]\text{CO}_3 \cdot 4\text{H}_2\text{O}$ is a naturally occurring anionic clay mineral. Layered double hydroxides (LDH) $([\text{M}^{\text{II}}_{(1-x)}\text{M}^{\text{III}}_x(\text{OH})_2]^{x+}(\text{A}^{n-}_{(x/n)})_m \cdot m\text{H}_2\text{O})$ are synthetic analogues [1, 2]. The structure of these compounds consists of trioctahedral metal hydroxide sheets that alternate with interlayers containing anions and water. The brucite-like sheets have a net positive charge x per formula unit owing to isomorphic substitution of some of the divalent cations ($\text{M}^{\text{II}} = \text{Mg}, \text{Ca}, \text{Zn}, \text{Fe}, \text{Co}, \text{Ni}, \text{Cu}, \text{etc.}$) by trivalent ones ($\text{M}^{\text{III}} = \text{Al}, \text{Fe}, \text{Cr}, \text{Mn}, \text{etc.}$). This net positive charge is balanced by an equal negative charge from the interlayer anions ($\text{A}^{n-} = \text{CO}_3^{2-}, \text{Cl}^-, \text{NO}_3^-, \text{OH}^-, \text{etc.}$). Carbonate anions in LDH- CO_3 do not readily ion exchange owing to strong electrostatic and hydrogen-bonding interactions [3]. However, others such as nitrate, hydroxides and chloride ions are exchangeable and this facilitates incorporation of many different anions [1, 4, 5]. The number of co-intercalated (associated) water molecules (m) depends on environmental conditions [6]. The stoichiometric coefficient (x) can be varied over a wide range, giving rise to a large class of same structural materials [3, 7].

Poly(vinyl chloride) (PVC) is a commodity polymer with numerous industrial and consumer applications. PVC processing is associated with many practical difficulties owing to its relatively low thermal stability [8]. Thermal degradation during

⁴ This paper was published as Polymer Degradation and Stability. 2015;113:46–54

processing is a common problem in polymer processing. In the case of PVC, a unique feature is the release of free hydrochloric acid. The reaction is initiated at defect sites (e.g., internal allylic chloride and tertiary chloride structural flaws). It proceeds as an autocatalytic dehydrochlorination of the PVC backbone with the liberated hydrogen chloride assuming a catalytic role [9]. The mechanism of autocatalysis involves a free-radical process that converts ordinary polymer repeat units into chloroallylic structures of low thermal stability [10]. Apart from liberating a corrosive gas, this degradation reaction also results in the formation of polyene sequences of π -conjugated double bonds along the polymer chain. Besides causing severe discoloration, the net effect is a loss of desirable physical and mechanical properties [8].

In practice the processing problems associated with the use of PVC are overcome through the use of heat stabiliser additives[8]. Three main heat stabiliser types are recognised, i.e. preventive, suppressive and curative heat stabilisers [11]. Preventive stabilisers substitute labile chlorine atoms for more stable groups and thus act during the initial stages of PVC thermal degradation. Suppressive stabilisers are HCl scavengers, and act by removing the acidic dehydrochlorination catalyst. Curative stabilisers are able to add to double bonds in the PVC backbone. Stabilisers that react with allylic chlorides are called primary stabilisers, e.g. zinc stearate, lead- and tin compounds. These reactions shorten the π -conjugated polyene sequence and thereby reduce the discoloration of degrading PVC. Furthermore they also retard the auto-acceleration process by transforming highly labile allylic chloride structures into more stable groups [11]. HCl generated by the degradation catalyses the chain propagation reaction. Scavenging it is a way to stop the further degradation of PVC. The diffusion

of HCl is a slow process so that this approach cannot prevent dehydrochlorination in its early stages. However, heat stabilisers that scavenge HCl help to avoid autocatalytic degradation and consequently the rate of degradation is slower. These secondary stabilisers give good long term stabilisation. They include calcium stearate, lead compounds and layered double hydroxides (LDHs).

Some of the most effective heat stabilisers for PVC are based on Pb, Cd and Sn compounds [8]. For environmental reasons these toxic heavy metal-based complexes are being phased out. Layered double hydroxides (LDHs) are promising alternatives for lead-containing suppressive heat stabilisers owing to their intrinsically high capacity to react with HCl [12-14]. Unlike most metallic salts, the conventional LDH is readily incorporated into the PVC resin to provide translucent articles. The thermal stabilisation action of LDH involves two steps. Initially, HCl formed during thermal dehydrochlorination, displaces the carbonate interlayer anions to afford LDHs with Cl^- anions in the interlayer. As further dehydrochlorination takes place, the HCl reacts with the clay itself, ultimately destroying its structure and forming metal chlorides, metal hydroxy-chlorides and hydrates of magnesium and aluminium [13].

The present interest is to explore ways to improve the heat stabilisation effect of LDH in PVC. This communication considers LDH modifications related to partial or full substitution of the magnesium or aluminium components of conventional LDH with other metals. The effect of these modifications on the heat stability of plasticised PVC was studied. Heat stability was evaluated by tracking the temporal progression of PVC degradation. It was quantified by following the evolution of HCl, the development of colour due to formation of conjugated double bond sequences and the

change of the apparent melt viscosity caused by crosslinking or cleavage of the polymer chain [15].

5.2 Experimental

5.2.1 Materials

Al(OH)₃ was an industrial grade supplied by Chemical Initiatives. All other reagents used were analytical grade reagents supplied by Merck. TPC Paste Resin Co., Ltd. supplied poly(vinyl chloride) emulsion grade PG680. It was a free flowing powder with a K-value of 69. The diisononyl phthalate (DINP) plasticiser was supplied by Isegen.

5.2.2 Synthesis of LDH-derivatives

The LDH-derivatives were synthesised according to the method previously described by Labuschagné *et al.*, [16]. A typical procedure for MgAl-LDH i.e., [Mg_{0.667}Al_{0.333}(OH)₂](CO₃)_{0.167}·*m*H₂O, was as follows: Light MgO and Al(OH)₃ powders were mixed in the required 2:1 stoichiometric ratio. The powder mix was slowly added, while stirring, to one litre of distilled water in a 1.6 L Parr autoclave. The final solids concentration of the slurry was 15 wt.%. A 60 mol.% excess of NaHCO₃ was added to the mixture as the source for the intercalate anion. The reaction was conducted under vigorous stirring at a temperature of 180 °C and a pressure of approximately 14 bar. The autoclave was kept at this temperature and pressure for approximately 5 h. Thereafter heating was discontinued and the reaction mixture was allowed to cool overnight while stirring. The solid product was removed from the autoclave, filtered and washed several times with distilled water to remove residual NaHCO₃. Finally it was dried in an oven at 80 °C for at least 48 h.

The substituted layered double hydroxides, i.e. LDH-derivatives, were synthesised following a similar procedure. The target was either to substitute part of the aluminium with iron(III) or part of the magnesium with copper(II) or zinc(II). For MgFeAl-LDH, 25 mol.% of the $\text{Al}(\text{OH})_3$ was substituted with Fe_2O_3 . For MgCuAl-LDH and the MgZnAl-LDH 25 mol.% of the MgO was substituted by an equivalent molar amount of the corresponding oxide. For CaAl-LDH, all of the MgO was substituted with an equal molar amount of CaO and a proprietary carbonation procedure was employed. The compound synthesized was calcium hemicarboaluminate [17] ($[\text{Ca}_4\text{Al}_2(\text{OH})_{12}][\text{OH}(\text{CO}_3)_{0.5}\cdot 4\text{H}_2\text{O}]$). In this clay half the interlayer carbonate ions are substituted by hydroxyl ions.

5.2.3 Surface coating of the LDH-derivatives

All samples were coated with stearic acid as follows: The dried solids were milled into a fine powder using a coffee grinder. They were then suspended in 1 L distilled water and heated to 75 °C. The solids content of all the slurries was less than 20 wt.%. The slurries were vigorously agitated with a Silverson disperser. Stearic acid, equivalent to 2.0 wt.% based on the total dry uncoated solid sample, was added to the hot slurry. The suspension was stirred for 15 min at 6 000 rpm. The coated powders were recovered by filtering. They were dried in a convection oven set at 60 °C and ground to a fine powder.

5.2.4 Preparation of PVC-composites

DINP plasticiser (130 g) was weighed into a 600 mL beaker. Next small portions of the PVC powder (up to a total of 130 g) were added and mixed-in using a high-speed Anvil milkshake mixer. The dispersion was de-aerated for about 30 min in a Speedvac

vacuum chamber. Then the LDH filler powder (39 g) was incorporated. The dispersion was again de-aerated but this time for about 1 h.

Cast PVC composite sheets were made in a three-step pressing process. The paste mixture was poured into a mould measuring 100 mm × 100 mm × 3.5 ± 0.1 mm. The mould was closed and placed in convection oven set at a temperature of 130 °C for 10 min. Then it was hot pressed at a pressure of 10 MPa at 150 °C for 5 min. The mould was then removed from the press and a heavy weight placed on the top plate. The moulding was allowed to cool down at ambient conditions before it was removed.

5.3 Characterisation

5.3.1 Particle size and BET surface area determination

The particle size distributions were determined with a Mastersizer Hydrosizer 2000MY (Malvern Instruments, Malvern, UK). The specific surface areas of the powders were measured on a Nova 1000e BET instrument in N₂ at 77 K.

5.3.2 Scanning Electron Microscopy (SEM)

A small quantity of the powdered product or the LDH precursor was placed onto carbon tape on an aluminium sample holder. Excess powder was removed using a single compressed air blast. The samples were then coated five times with carbon under argon gas using the Polaron Equipment E5200 SEM auto-coating sputter system. The powder samples were viewed on a Zeiss Ultra plus FEG SEM scanning electron microscope.

5.3.3 X-ray diffraction (XRD)

X-ray diffraction analysis was performed on a PANalytical X-pert Pro powder diffractometer fitted with an X'celerator detector using Fe filtered CoK α radiation ($\lambda = 0.17901$ nm). The instrument featured variable divergence and receiving slits. X'Pert High Score Plus software was used for data manipulation and phase identification.

5.3.4 Inductively coupled plasma optical emission spectrometry (ICP-OES)

The elemental composition of the LDH derivatives was determined with a Spectro Arcos model inductively coupled plasma optical emission spectrometer (ICP-OES). Firstly, about 0.5 g of the clay was dissolved in 50 mL Aqua Regia. After cooling down, the reaction mixture was diluted with 50 mL of distilled water and filtered through ashless filter paper. Before performing the ICP-OES analysis, 1 mL of solution was added to 99 mL of distilled water. The analysis was then performed, analysing for copper, magnesium, aluminium, calcium, zinc, iron and sodium. The insoluble fraction was determined by ashing the filter paper.

5.3.5 Fourier transform infrared spectroscopy (FTIR)

FTIR spectra were recorded on a Perkin Elmer 100 Spectrophotometer. Powder samples were pressed onto the Zn/Se plate of a MIRacle ATR attachment. The spectra were obtained over the range 650 – 4 000 cm^{-1} and represent the average of 32 scans at a resolution of 2 cm^{-1} .

5.3.6 Thermogravimetric Analysis (TGA)

Thermogravimetric analysis (TGA) was performed using the dynamic method on a Mettler Toledo A851 TGA/SDTA instrument. About 11 – 15 mg sample was placed in an open 150 μL alumina pan. Temperature was scanned from 25 $^{\circ}\text{C}$ to 900 $^{\circ}\text{C}$ at a scan rate of 10 $^{\circ}\text{C min}^{-1}$ with air or nitrogen flowing at a rate of 50 mL min^{-1} .

5.4 Heat stability assessment

5.4.1 Dynamic heat stability (Rheomix)

The dynamic stability of the PVC compositions was investigated at 200 $^{\circ}\text{C}$ using the torque rheometer technique [18-20] on a Haake Polylab OS with Rheomix 600p OS Lab Mixer using roller rotors. The plastisol paste mixture (70 g) was loaded into the internal mixing chamber. The samples were processed at a rotor speed of 60 rpm and the torque was recorded as a function of time.

5.4.2 Metrastat thermal stability

The static heat stability was determined in triplicate using sample strips measuring ca. 200 mm \times 20 mm \times 3.5 \pm 0.1 mm that were cut from the pressed sheets. A Metrastat heat stability oven was used. The strips were placed in the Metrastat trays of length 256 mm in random positions for each of the three runs. The machine automatically retracts the trays from the oven at a constant rate of 300 mm in 180 min. The oven temperature was set at 200 $^{\circ}\text{C}$ and the air flow was 10 $\text{m}^3 \text{min}^{-1}$. After testing the strips were photographed. The change in colour along the strips was quantified using imaging software and the change in the grey scale is reported as a function of oven time.

5.4.3 Thermomat thermostability

The thermostability of the PVC compounds was evaluated on a Metrohm 895 Professional PVC Thermomat according to ISO 182 Part 3. The method is based on the fact that PVC releases HCl when it decomposes at high temperatures. The evolved hydrochloric acid is flushed with a stream of nitrogen gas and passed through a measuring vessel where it is absorbed in purified water. The progress of the decomposition is tracked by measuring the change in the conductivity of this water. Performance is quantified in terms of either the induction time (i.e. the time that is required to reach the break point in the conductivity curve) or a stability time, i.e. the time until a conductivity difference of $50 \mu\text{S cm}^{-1}$ is reached. The PVC compound sample amount tested was 0.50 ± 0.05 g. The samples were cut into small pieces less than 1 mm in size. The stability was determined at $200 \text{ }^\circ\text{C}$. Nitrogen flow was controlled at 7 L h^{-1} and 50 mL deionised water was used to trap the HCl.

Table 5.1: LDH particle sizes and BET surface area

Sample	BET surface area		Particle size, μm		
	$\text{m}^2 \text{ g}^{-1}$	D_{10}	D_{50}	D_{90}	
MgAl-LDH	18.3	0.68 ± 0.00	3.08 ± 0.03	13.10 ± 0.26	
MgZnAl-LDH	12.4	0.67 ± 0.01	2.30 ± 0.11	13.93 ± 1.36	
MgCuAl-LDH	13.3	0.62 ± 0.00	2.00 ± 0.09	9.84 ± 1.61	
MgFeAl-LDH	9.83	0.61 ± 0.01	1.87 ± 0.02	4.03 ± 0.06	
CaAl-LDH	5.44	1.94 ± 0.04	6.25 ± 0.12	18.43 ± 0.12	

5.5 Results

5.5.1 LDH Particle size and BET surface area

Table 5.1 reports the particle sizes and the BET specific surface areas for the LDH-derivatives. The median (d_{50}) particle size varied from 1.9 μm to 6.25 μm . BET surface was highest for MgAl-LDH (18.3 $\text{m}^2 \text{g}^{-1}$) and lowest for CaAl-LDH (5.44 $\text{m}^2 \text{g}^{-1}$).

Figure 5.1 shows FEG SEM micrographs of some LDH-derivative powders. The individual powder particles are made up of highly agglomerated flake-shaped crystals. The primary flakes were smallest for MgCuAl-LDH and largest for CaAl-LDH. The micrograph for the latter actually shows an edge-on view whereas the other micrographs show a top view.

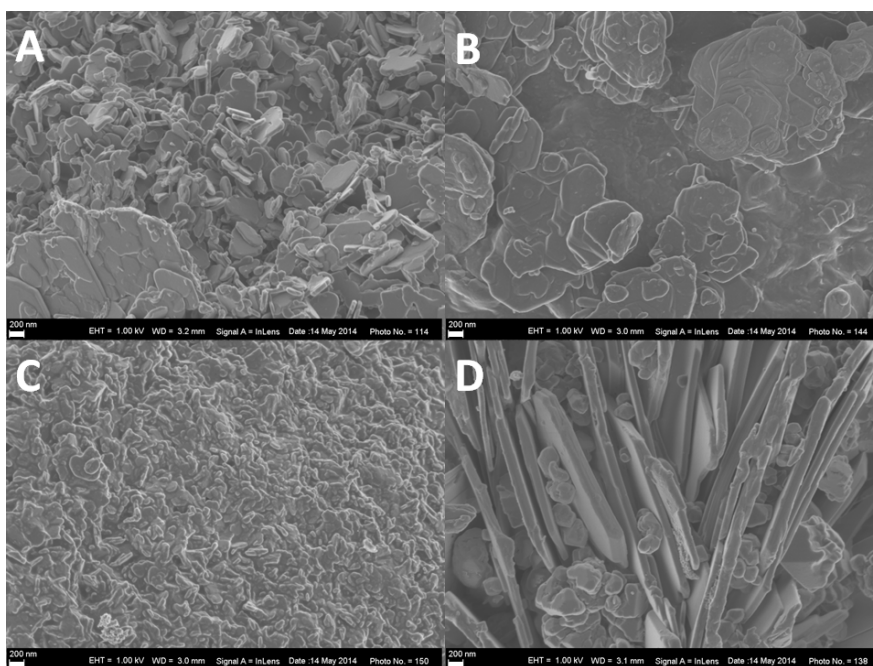


Figure 5.1: SEM micrographs of (A) MgZnAl-LDH; (B) MgFeAl-LDH; (C) MgCuAl-LDH, and (D) CaAl-LDH. The size bar indicates a length of 200 nm.

The XRD patterns shown in Figure 5.2 feature reflections characteristic of LDHs [3]. The reflections at $2\theta = 13.474^\circ$ and $2\theta = 27.125^\circ$ in the XRD diffractogram for MgAl-LDH are consistent with a brucite layer basal spacing of 0.761 nm. The d-spacing values for the other compounds are listed in Table 5.2. It was slightly larger (0.768 nm) for the MgFeAl-LDH and slightly lower (0.755 nm) for CaAl-LDH than the value for MgAl-LDH (0.761 nm) but consistent with literature reports [17, 21, 22]. The sharp nature of the reflections points to a high crystallinity of the corresponding powders.

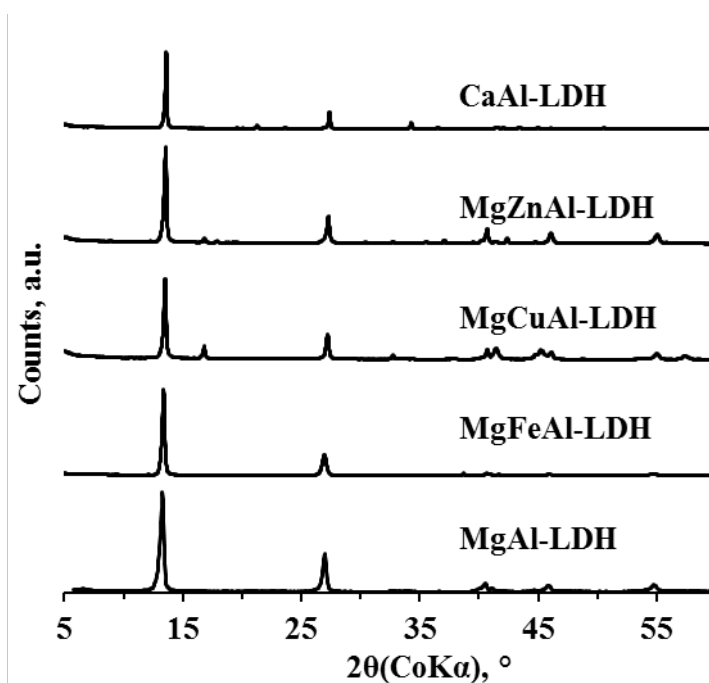


Figure 5.2: X-ray diffraction patterns for the various LDH derivatives

Table 5.2 reports the ICP-OES chemical composition results in terms of the general formula: $[Mg_{2+\alpha}Al_{1-\alpha}(OH)_6](CO_3)_{(1-\alpha)/2} \cdot xH_2O$. The apparent α value varied from 0.08 (MgZnAl-LDH) to 0.28 (CaAl-LDH).

Table 5.2: LDH derivatives: Apparent elemental composition calculated from ICP-OES, TGA residue at 900 °C and d-spacing from XRD results.

Sample	Apparent composition	Residue,	d-spacing,
		%	nm
MgAl-LDH	$[\text{Mg}_{2.092}\text{Al}_{0.908}(\text{OH})_6](\text{CO}_3)_{0.454}$	57.0	0.761
MgCuAl-LDH	$[\text{Mg}_{1.570}\text{Cu}_{0.597}\text{Al}_{0.833}(\text{OH})_6](\text{CO}_3)_{0.417}$	65.6	0.761
MgZnAl-LDH	$[\text{Mg}_{1.527}\text{Zn}_{0.554}\text{Al}_{0.918}(\text{OH})_6](\text{CO}_3)_{0.459}$	61.9	0.758
MgFeAl-LDH	$[\text{Mg}_{2.062}\text{Fe}_{0.198}\text{Al}_{0.740}(\text{OH})_6](\text{CO}_3)_{0.370}$	56.3	0.768
CaAl-LDH	$[\text{Ca}_{2.275}\text{Al}_{0.725}(\text{OH})_6](\text{OH})_2\text{CO}_3)_{0.182}$	59.2	0.755

Figure 5.3 shows that all the FTIR spectra, except the one for CaAl-LDH, were very similar. The presence of the stearic acid coating is evident from the two small peaks observed between 2993 cm^{-1} and 2961 cm^{-1} for CaAl-LDH, MgZnAl-LDH, MgCuAl-LDH and MgFeAl-LDH respectively. The broad band that is observed at ca. 3470 cm^{-1} is attributed to $-\text{OH}$ stretching vibrations in the octahedral layer and the free and hydrogen bonded water molecules present in the interlayer. The strong sharp peaks near 1366 cm^{-1} are due to the CO_3^{2-} ν_3 antisymmetric vibrations. The CaAl-LDH shows two strong peaks here, suggesting the presence of two different environments for carbonate ions.

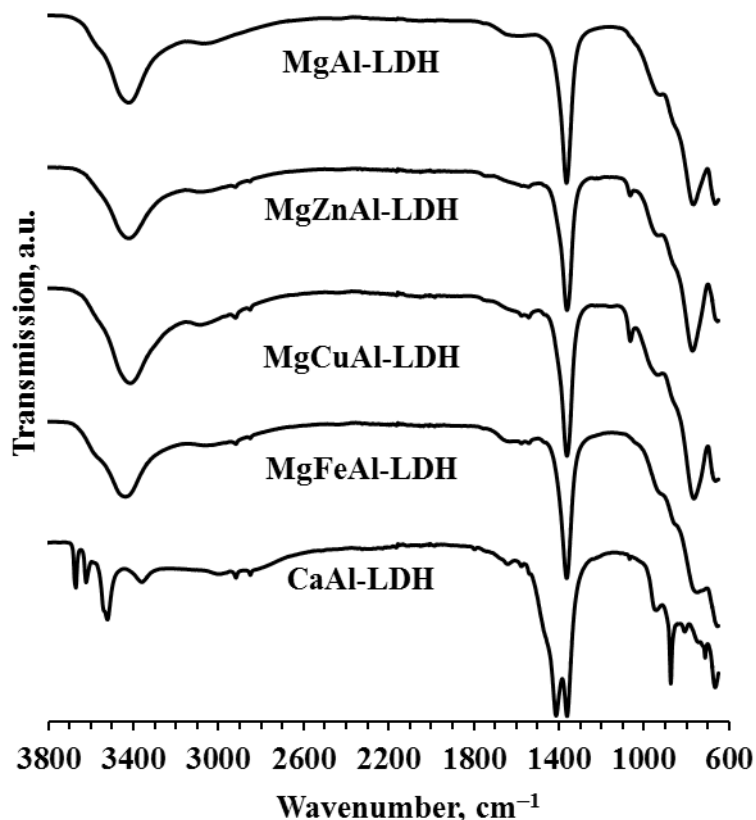


Figure 5.3: FTIR spectra of the various LDH derivatives

Figure 5.4 summarises the TGA mass loss curves for various LDH samples as obtained in an air atmosphere. All the derivatives showed the three distinct mass loss steps expected for LDH during thermal decomposition.[23, 24] They correspond to dehydration, dehydroxylation and finally the removal of the interlayer carbonate anion. The first step is usually the loss of physisorbed and interlayer water, which commences at about 50 °C and is complete by 150 °C [25]. Mass loss commenced earlier and was initially more pronounced for CaAl-LDH. It lost about 12 wt.% by 190 °C. However, between 460 °C and 700 °C the cumulative mass loss was less than that found for the other LDH derivatives. Above the latter temperature, CaAl-LDH showed mass loss behaviour reminiscent of that expected for calcium carbonate. CaAl-LDH showed a total mass loss of 41 % at 900 °C. The initial mass loss for

MgAl-LDH, MgZnAl-LDH, MgCuAl-LDH and MgFeAl-LDH were quite similar. However, compared to the other compounds, the TGA mass loss curve of MgCuAl-LDH appeared shifted to higher temperatures. The first mass loss event commenced at around 130 °C and was complete by about 250 °C showing a mass loss of ca. 12 %. The second mass loss event is more or less complete by 350 °C at which point the mass loss had reached about 30 %. Mass loss was effectively complete by about 700 °C. The residues, recorded at 900 °C, are listed in Table 5.2.

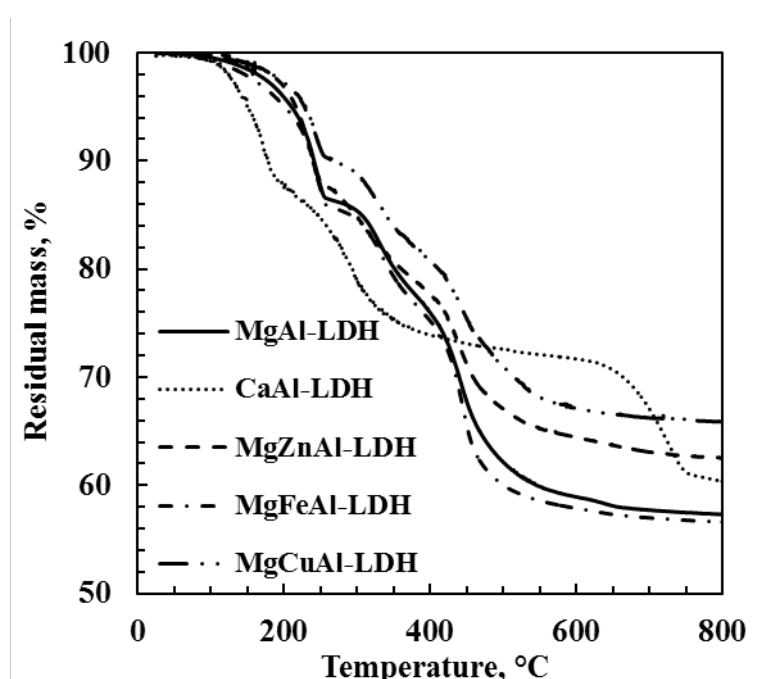


Figure 5.4: TGA traces in air for the LDH derivatives. Temperature was scanned from 25 °C to 900 °C at a scan rate of 10 °C min⁻¹ with air flowing at a rate of 50 mL min⁻¹.

5.5.2 Heat stability of the PVC composites

During the primary stage of degradation, discoloration of the PVC is observed. It is caused by the formation of conjugated polyene sequences of double bonds along the polymer chain. These defects are highly reactive and they undergo secondary reactions that lead to crosslinking or cleavage of the polymer chains [15]. Thus the progression of PVC degradation may be quantified by the following three approaches:

(i) The evolution of HCl; (ii) The development of colour due to formation of conjugated double bond sequences, and (iii) the changing of physical properties such as the melt viscosity due to crosslinking or cleavage of the polymer chain [15]. The Thermomat method tracks HCl evolution from a small sample of stabilised PVC. This method favours additives that preferentially react with HCl such that it begins to evolve only when the additives are completely consumed. Torque rheometer tests that simulate industrial processing conditions have the advantage that they measure the degradation under dynamic conditions. However, they react to changes in material consistency which is more sensitive to crosslinking or cleavage of the polymer chains. The viscosity changes are caused by the secondary degradation processes that commence relatively late in comparison to the primary PVC degradation (observed as discolouration). According to Bacaloglu and Stewen [15] by the time the viscosity starts to change, the PVC material has already been degraded to such an extent that it can no longer be used because of important appearance and mechanical property alterations. They conclude that discoloration monitoring offers the most sensitive procedure for following the PVC degradation. Owing to their very high molecular absorptivity in the visible region, conjugated polyenes with seven and more double bonds can be observed even for a degree of degradation as low as 5 ppm of the monomer units [15].

The thermogravimetric analysis performed on the PVC compounds provided basic information on the intrinsic heat stability of the PVC compounds. Apart from the TGA, three additional heat stability tests were performed. Two were static tests and one a dynamic test. These test differed with respect to the nature of the atmosphere, the sample size and the parameter (as well as its trigger level) used to define the

failure point. The Thermomat and TGA tests were performed in a nitrogen atmosphere while oxygen was present in the Metrostat and dynamic Rheomix experiments. The presence of oxygen is known to affect the rate of degradation in torque rheometer-like tests [18].

The large charge size employed in the Rheomix tests made it possible to retain a considerable amount of the evolved HCl. The presence of higher concentrations of dissolved HCl affects the rate of degradation because it catalyses the dehydrochlorination reactions. In the TGA and Thermomat experiments the sample size was quite small while thin sheets were used in the Metrostat experiments. The higher surface to volume ratios, the shorter diffusion paths and the use of gas streams to sweep away the evolved gaseous degradation products clearly should affect their concentration in the samples themselves. Finally, the parameter chosen, as well as its trigger level, to define the end point was different in each case. Owing to these dissimilarities it should not be surprising that the heat stability ranking of the various samples was not the same in all these tests.

5.5.3 TGA of the LDH-PVC composites

Figure 5.5 shows TGA traces for the LDH-PVC compounds recorded in a nitrogen atmosphere. The flexible PVC apparently suffers two major mass loss stages. The first commences at 240 °C, reaches a maximum rate at 315 °C and ends at 370 °C. At this point the residue is 20.7 wt.%. The second stage starts as 420 °C, reaches a maximum rate at 467 °C and ends at 510 °C with a residue of 7.0 wt.% remaining. However, the derivative curves (DTG not shown) show multiple peaks in the mass loss stage. The initial mass losses are due a combination of PVC degradation (mainly

dehydrochlorination) events and volatilisation of the plasticiser. The second stage is attributed to pyrolysis reactions that ultimately lead to a carbonaceous char residue (4.3 wt.% at 900 °C). The shape of the mass loss curves for the LDH-PVC composites mirror those of PVC. The mass loss onset temperatures are virtually identical but mass loss occurs over a narrower temperature range. The residue after each stage is greater than found for the neat PVC. The ranking for initial mass loss rate, from fastest to slowest, for the additives at peak decomposition is:

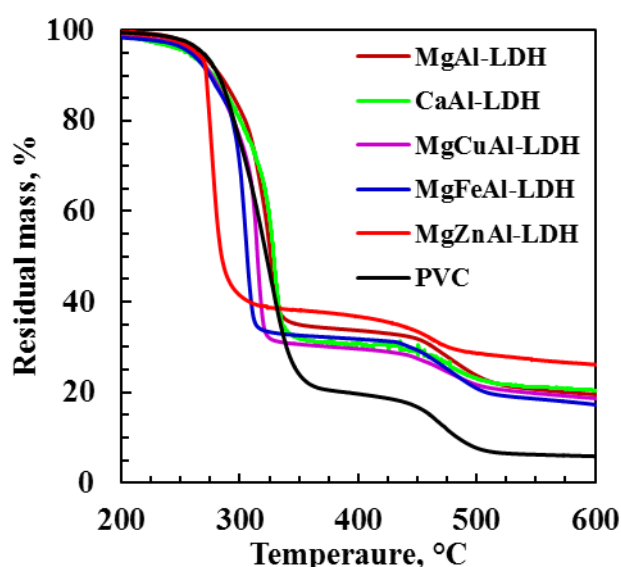


Figure 5.5: TGA traces in air for the PVC-LDH composites. Temperature was scanned from 25 °C to 900 °C at a scan rate of 10 °C min⁻¹ with nitrogen flowing at a rate of 50 mL min⁻¹.

The MgZnAl-LDH, in particular, significantly accelerated the mass loss during the first stage. The initial decomposition yields ZnCl₂ which autocatalytically accelerates the dehydrochlorination reaction according to the mechanism reported by Levchik and Weil [26]. This is also known as zinc poisoning in industry. The higher char yield is also attributed to catalytic effects that favour crosslinking and aromatisation reactions at the expense of cracking reactions that yield volatiles.

5.5.4 Dynamic heat stability test (Rheomix)

Representative torque vs. time curves are shown in Figure 5.6. The characteristics of the torque vs. time curves can be explained as follows: The high mixer chamber wall temperature and the friction imparted by the mixer blades cause rapid fusion of the plastisol into a high consistency viscous mass. This results in the very rapid rise to a peak value in the torque. As the temperature of the mix increases, the melt viscosity decreases and thus the torque decreases to a low plateau value. Over time as the material degradation proceeds, the molar mass increases because of crosslinking processes and the torque rises again. Initially the torque rises moderately but eventually the increase becomes much more pronounced. In the torque rheometer test the thermal stability is usually associated with the time necessary to reach the fast torque increase after the gelation process. Ideally it is measured as the time for the appearance of the inflection point in the torque-time curve. Even though these different stages of the torque curves were clearly evident in each measurement, the transitions between them were continuous.

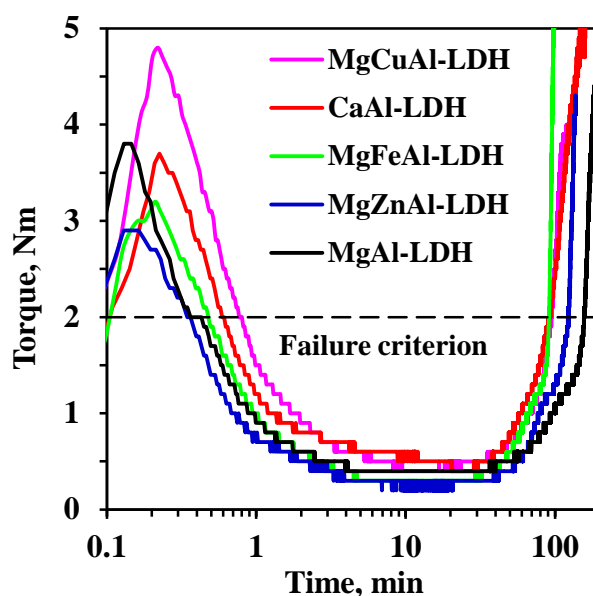


Figure 5.6: Representative torque vs. time curves obtained with the Rheomix. The rotor speed was 60 rpm and the mixing chamber temperature was set at 200 °C.

Furthermore, the curves showed considerable superimposed noise and it was not possible to determine unequivocally the location of an inflection point. Therefore the time to reach a torque of 2 N was arbitrarily chosen as the heat stability measure. It is indicated by the broken horizontal line in Figure 5.6. The corresponding dynamic heat stability times are shown in Figure 5.10. The ranking of the additives from fastest to slowest degrading was as follows:

$\text{MgFeAl-LDH} \approx \text{CaAl-LDH} > \text{MgCuAl-LDH} \gg \text{MgZnAl-LDH} \gg \text{MgAl-LDH}$

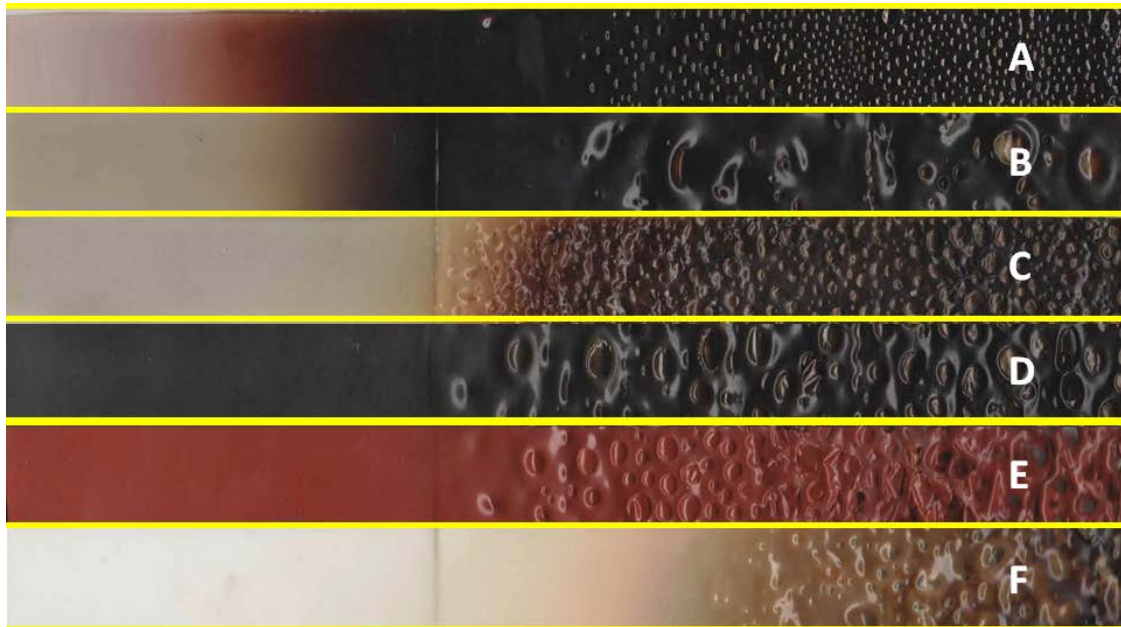


Figure 5.7: Metrastat sample appearances. (A) Neat PVC; (B) MgAl-LDH; (C) CaAl-LDH; (D) MgCuAl-LDH; (E) MgFeAL-LDH, and (F) MgZnAl-LDH

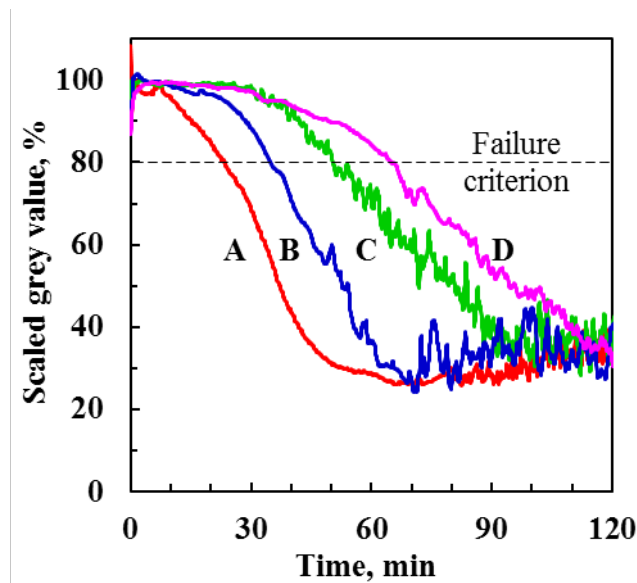


Figure 5.8: “Normalised” Metrastat grey value test results. (A) Neat PVC; (B) MgAl-LDH; (C) CaAl-LDH; (D) MgZnAl-LDH. The broken horizontal line defines the failure criterion that was adopted.

5.5.5 Metrastat thermal stability

The appearance of the flexible PVC after exposure in the Metrastat heat stability oven is shown in Figure 5.7. The grey scale colour variation along the strips was normalised to 100 units of the original sheet colour and the results are plotted in Figure 5.8. An arbitrary failure criterion was defined by a 20 % change in this normalised grey scale. This was used to obtain the heat stability times that are listed in Figure 8. Unfortunately the original colours of the MgCuAl-LDH and MgFeAl-LDH composites were too dark to allow a reliable assessment. Of the remaining composites, the one based on the MgZnAl-LDH had the highest Metrastat heat stability time (72 ± 20 min). The ranking of the additives with respect to the Metrastat heat stability times was (from fastest to slowest degrading):



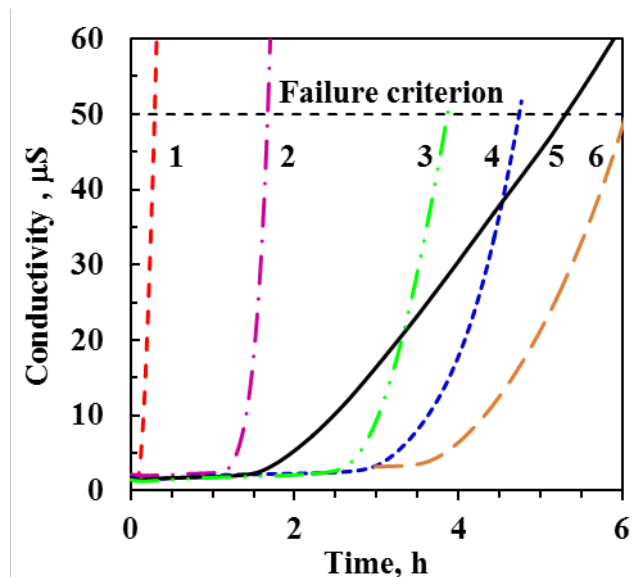


Figure 5.9: Representative Thermomat conductivity curves for the PVC compounds: 1. Neat PVC; 2. MgZnAl-LDH; 3. MgFeAl-LDH; 4. MgAl-LDH; 5. CaAl-LDH; 6. MgCuAl-LDH. The broken horizontal line defines the failure criterion.

5.5.6 Thermomat heat stability

Representative Thermomat conductivity response curves are shown in Figure 5.9. The induction time corresponds to the onset time while the stability time is defined by the time required to reach a conductivity of $50 \mu\text{S cm}^{-1}$. Interestingly, while the CaAl-LDH containing compound has a lower induction time than the MgAl-LDH compound, it outperformed the latter if the stability time is taken as the failure criterion. The ranking of the stabilisers in terms of the worst to best induction times was as follows:

MgZnAl-LDH >> MgFeAl-LDH > MgAl-LDH > CaAl-LDH > MgCuAl-LDH

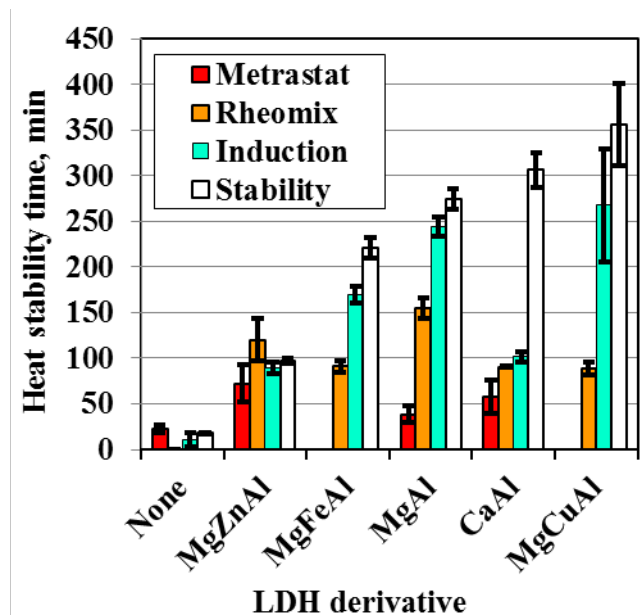


Figure 5.10: Static and dynamic heat stability times measured at 200 °C using the torque rheometer technique (Rheomix); following the development of colour with heating time (Metrastat), and tracking the evolution of hydrochloric acid (Thermomat induction and stability times).

The effect of the LDH derivatives on the Thermomat stability times of the flexible PVC compounds are shown in the Figure 5.10. The neat PVC compound had a stability time of 0.31 ± 0.01 h. All the LDH derivatives improved the stability time with MgCuAl-LDH giving the best result of 5.93 ± 0.76 h. As expected from the TGA results, the stability time improvement was least for MgZnAl-LDH. The ranking of the stabiliser stability times from worst to best was as follows:

$$\text{MgZnAl-LDH} > \text{MgFeAl-LDH} > \text{MgAl-LDH} > \text{CaAl-LDH} > \text{MgCuAl-LDH}$$

This differs from that found for the acceleration of the initial TGA mass loss and also with respect to the Thermomat induction times. The ranking of the CaAl-LDH system has improved to second best.

5.6 Discussion

The SEM, FTIR, XRD and TGA data for the CaAl-LDH compound appeared odd. The FTIR spectrum (Figure 5.3) indicates the presence of two different carbonate ion containing compounds. The SEM micrograph (Figure 5.1) shows large flat flakes with smaller crystals located between them. This also suggests the presence of two different phases. The TGA mass loss curve in Figure 5.4 also looks very different from that usually seen for LDHs. Inspection of the TGA data initially led to the suspicion that the sample might have been contaminated with calcium carbonate. However, with respect to the XRD diffractogram there is no match with calcite or any other calcium carbonate phase in Figure 5.2. In fact it indicates that the product is a “pure” crystalline phase. The d-spacing calculated for the compound shown in Figure 2 is 0.755 nm and this matches that reported for the compound calcium monocarboaluminate perfectly [21, 22]. The structure of this compound is that of a “pure” CaAl-LDH and the formula is: $[\text{Ca}_4\text{Al}_2(\text{OH})_{12}]\text{CO}_3 \cdot 5\text{H}_2\text{O}$.

However, there is another compound called calcium hemicarboaluminate [17] with the structural formula: $[\text{Ca}_4\text{Al}_2(\text{OH})_{12}] \text{OH}(\text{CO}_3)_{0.5} \cdot 4\text{H}_2\text{O}$ in which half the interlayer carbonate ions are substituted by hydroxyl ions. Cement curing studies revealed that this hemicarboaluminate forms during the early stages of hydration and as the hydration progresses, a gradual conversion of the hemicarboaluminate into the monocarboaluminate occurs [27]. The conundrum is resolved if one accepts that the present CaAl-LDH sample is actually a mixture of about equal amounts of calcium monocarboaluminate and calcium hemicarboaluminate. Basically the carbonate ions in the latter compound will have slightly different electronic environments owing to the presence of the hydroxyl groups. This explains the presence of two carbonate ion

absorption bands in the FTIR spectrum. Finally, these two compounds may be expected to have virtually identical XRD diffractograms.

These heat stability results were quite surprising, especially those for the LDH materials containing iron and copper. It is well known that transition metal oxides (especially those of Fe and Cu) promote the degradation of PVC composites [28-30]. At the cost of thermal stability, they reduce the fire risk posed by PVC by increasing char yield and reducing smoke production during fire situations [29]. The present results indicate that the effect of the transition metals on thermal stability of PVC is changed when it they were incorporated into the LDH lattice.

The actual PVC degradation and stabilisation processes occur via multiple primitive reaction steps, each with their own characteristic temperature-dependent rate constant. In addition, mass transfer effects play a significant role. Thus the exact mechanisms are possibly too complicated to be mathematically tractable. Malík and Kröhnke [31] declared: “Present theoretical understanding of polymer degradation and stabilisation principles does not yet sufficiently cover the full chemical and physical complexity of polymer stabilisation ...” Thus, for simplicity and convenience such systems are frequently modelled using the so-called single step reaction approximation [32, 33]. It is assumed that the process can be described by an apparent first order differential equation analogous to the kinetic expression for a single homogeneous chemical reaction [33, 34]. Obviously such an equation would in fact apply when the overall kinetics is chemically controlled by a single primitive reaction, e.g. stabiliser consumption during the induction period [35]. A central feature of PVC degradation is its autocatalytic nature [9, 10]. This implies that an autocatalytic reaction

mechanism, e.g. the general form suggested by Kamal and Sourour [36] could be considered:

$$\frac{d\alpha}{dt} = k\alpha^m(1-\alpha)^n \quad (1)$$

where α is the degree of conversion that defines the extent of degradation of the polymer [-]; t is the time [s]; k is the rate constant [s^{-1}] and m [-], n [-] are dimensionless constants defining the reaction orders. A modification that reduces the number of parameters to two is obtained by setting $m = 1 - 1/\theta$ and $n = 1 + 1/\theta$ with $\theta \geq 1$. Equation (1) then reduces to:

$$\frac{d\alpha}{dt} = k\alpha^{1-1/\theta}(1-\alpha)^{1+1/\theta} \quad (2)$$

Note that this equation provides a parametric interpolation formula between the predictions of the logistic equation ($\theta \rightarrow \infty$) describing classic autocatalytic behaviour and second order kinetics ($\theta = 1$). The general solution for isothermal conditions is

$$\left(\frac{\alpha}{1-\alpha}\right)^{1/\theta} = 1 + \frac{k}{\theta}(t - t_1) \quad (3)$$

where t_1 serves as an integration constant with units of time. The degree of conversion can be expressed explicitly as a function of time:

$$\alpha = 1 - \frac{1}{1 + \left[1 + (k/\theta)(t - t_1)\right]^\theta} \quad (4)$$

For $\theta \rightarrow \infty$ Equation (4) reduces to the familiar Proud-Tompkins kinetic expression [37]. For $1 \leq \theta < \infty$ it is possible to enforce the initial condition $\alpha = 0$ at $t = 0$ by setting $t_1 = \theta/k$. With this condition the equation simplifies to

$$\alpha = 1 - \left[1 + (t/\tau)^\theta\right]^{-1} \quad (5)$$

This equation predicts a rate maximum at a time equal to $[\theta/k][(\theta-1)/\theta+1]^{1/\theta}$. This means that the S-shaped conversion curve shifts to higher times with increasing θ and decrease in the rate constant k . Note that the apparent reaction rate constant can be calculated from $k = \theta/\tau$. It was assumed that the conductivity is directly proportional to the degree of degradation of the polymer sample. The parameters τ and θ were obtained by least squares fitting of Equation (5) to the Thermomat conductivity vs. time curves. Typical fits are shown in Figure 11.

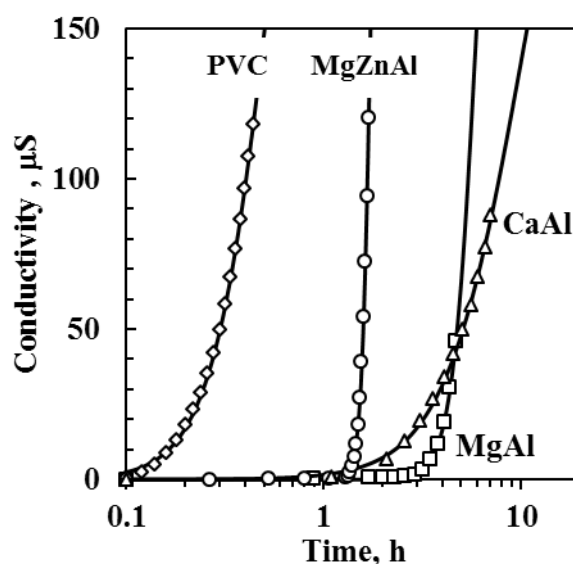


Figure 5.11: Thermomat conductivity curves showing typical curve fits of equation (5).

Figure 5.12 shows a plot of the rate constant k vs. the reaction order parameter θ . The order parameter for the neat PVC was $\theta = 2.92 \pm 0.12$ and the degradation rate constant was $k = 5.07 \pm 0.26$ h. Except for MgZnAl-LDH, the incorporation of the LDH stabilisers lowered the degradation rate constant. The reaction order parameter for the CaAl-LDH was lower (2.53 ± 0.27) while for all the other LDH-based compounds it was higher. Interestingly and rather unexpectedly, these two parameters

appeared to be strongly correlated for the LDH-stabilised PVC compounds. In fact, the relationship can be expressed by $k \approx 0.196 e^{\theta/4}$. This shows that the rate constant k increases rapidly with increase in the reaction order parameter θ . As mentioned above, autocatalytic behaviour is indicated by large values of order the parameter θ . This means that, with the exception of the CaAl-LDH, the presence of the LDH stabilisers emphasised the autocatalytic nature of the degradation process. With exception of the MgZnAl-LDH, the presence of the LDH stabilisers significantly lowered the magnitude of the reaction rate constant k .

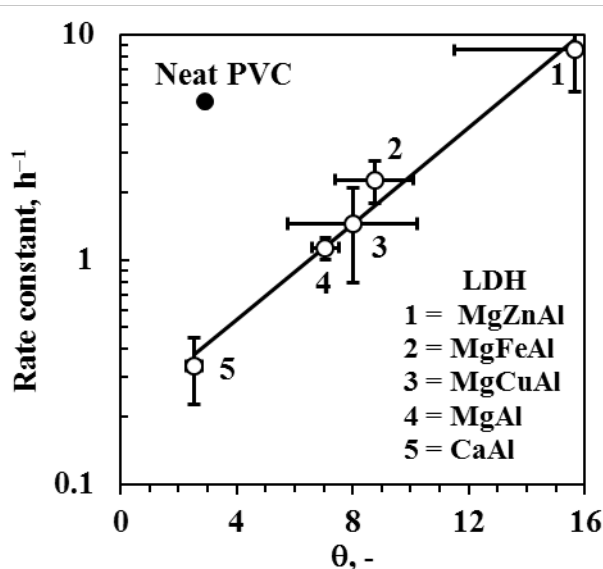


Figure 5.12: The correlation between the parameters of equation (5) for the LDH-stabilised PVC compounds. The solid line is described by the relation $k = 0.196 e^{\theta/4}$.

5.7 Conclusion

Layered double hydroxides (LDHs) derivatives were synthesised using a hydrothermal method. Apart from the conventional LDH ($[\text{Mg}_4\text{Al}_2(\text{OH})_{12}]\text{CO}_3 \cdot 4\text{H}_2\text{O}$) used as heat stabiliser for PVC the synthesis efforts targeted the following compounds: $[\text{Mg}_3\text{ZnAl}_2(\text{OH})_{12}]\text{CO}_3 \cdot 4\text{H}_2\text{O}$; $[\text{Mg}_3\text{CuAl}_2(\text{OH})_{12}]\text{CO}_3 \cdot 4\text{H}_2\text{O}$; $[\text{Mg}_4\text{AlFe}(\text{OH})_{12}]\text{CO}_3 \cdot 4\text{H}_2\text{O}$ and $[\text{Ca}_4\text{Al}_2(\text{OH})_{12}]\text{CO}_3 \cdot 5\text{H}_2\text{O}$. Characterisation using

XRD, ICP-MS and FTIR confirmed that the products approached these idealised compositions. The exception was the calcium based LDH (calcium hemicarboaluminate). This product turned out to be a mixture of the target compound and calcium hemicarboaluminate with the structural formula: $[\text{Ca}_4\text{Al}_2(\text{OH})_{12}]\text{OH}(\text{CO}_3)_{0.5}\cdot 4\text{H}_2\text{O}$.

It was found that the best performance in dynamic heat stability tests was achieved with the conventional product $[\text{Mg}_4\text{Al}_2(\text{OH})_{12}]\text{CO}_3\cdot 4\text{H}_2\text{O}$. However, $[\text{Mg}_3\text{ZnAl}_2(\text{OH})_{12}]\text{CO}_3\cdot 4\text{H}_2\text{O}$ improved colour retention in Metrastat static heat stability tests. In addition, $[\text{Mg}_3\text{CuAl}_2(\text{OH})_{12}]\text{CO}_3\cdot 4\text{H}_2\text{O}$ performed better as a HCl scavenger, preventing the release of hydrochloric acid for a longer time in the Thermomat evaluation. The key finding of this study is that different metal substitutions affect performance differently in different heat stability tests. This means that there should be room for fine tuning of LDH heat stabilisers for optimal performance in specific tests and end-use applications.

5.8 Acknowledgements

Financial support from the THRIP programme of the Department of Trade and Industry and the National Research Foundation as well as Greenfield Innovation is gratefully acknowledged.

5.9 References

- [1] Leroux F, Besse J-P. Polymer Interleaved Layered Double Hydroxide: A New Emerging Class of Nanocomposites. *Chemistry of Materials*. 2001;13:3507-15.
- [2] Rives V. *Layered Double Hydroxides: Present and Future*: Nova Science Publishers; 2001.
- [3] Cavani F, Trifirò F, Vaccari A. Hydrotalcite-type anionic clays: Preparation, properties and applications. *Catalysis Today*. 1991;11:173-301.
- [4] Khan AI, O'Hare D. Intercalation chemistry of layered double hydroxides: recent developments and applications. *Journal of Materials Chemistry*. 2002;12:3191-8.
- [5] Miyata S, Kumura T. Synthesis of new hydrotalcite-like compounds and their physico-chemical properties. *Chemistry Letters*. 1973:843-8.
- [6] Ulibarri M, Pavlovic I, Barriga C, Hermosin M, Cornejo J. Adsorption of anionic species on hydrotalcite-like compounds: effect of interlayer anion and crystallinity. *Applied Clay Science*. 2001;18:17-27.
- [7] Taylor H. Crystal structures of some double hydroxide minerals. *Mineral Mag*. 1973;39:377-89.
- [8] Braun D. Poly(vinyl chloride) on the Way from the 19th Century to the 21st Century. *Journal of Polymer Science, Part A: Polymer Chemistry*. 2004;42:578-86.
- [9] Starnes Jr WH. Structural and mechanistic aspects of the thermal degradation of poly(vinyl chloride). *Progress in Polymer Science (Oxford)*. 2002;27:2133-70.
- [10] Starnes Jr WH, Ge X. Mechanism of autocatalysis in the thermal dehydrochlorination of poly(vinyl chloride). *Macromolecules*. 2004;37:352-9.
- [11] Loffeld P. *Novel Synthetic Hydrotalcites for Applications in Polymer Science*: Universiteit Utrecht, Faculteit Scheikunde; 2004.

- [12] Lin Y-J, Li D-Q, Evans DG, Duan X. Modulating effect of Mg–Al–CO₃ layered double hydroxides on the thermal stability of PVC resin. *Polymer Degradation and Stability*. 2005;88:286-93.
- [13] van der Ven L, van Gemert MLM, Batenburg LF, Keern JJ, Gielgens LH, Koster TPM, et al. On the action of hydrotalcite-like clay materials as stabilizers in polyvinylchloride. *Applied Clay Science*. 2000;17:25-34.
- [14] Lin Y, Wang J, Evans DG, Li D. Layered and intercalated hydrotalcite-like materials as thermal stabilizers in PVC resin. *Journal of Physics and Chemistry of Solids*. 2006;67:998-1001.
- [15] Bacaloglu R, Stewen U. Study of PVC degradation using a fast computer scanning procedure. *Journal of Vinyl and Additive Technology*. 2001;7:149-55.
- [16] Labuschagné FJWJ, Giesekke, E.W., Van Schalkwyk, J.D. . Production of Hydrotalcite. South Africa 2007.
- [17] Runčevski T, Dinnebier RE, Magdysyuk OV, Pöllmann H. Crystal structures of calcium hemicarboaluminate and carbonated calcium hemicarboaluminate from synchrotron powder diffraction data. *Acta Crystallographica Section B: Structural Science*. 2012;68:493-500.
- [18] Pukánszky B, Nagy TT, Kelen T, Tüdös F. Comparison of dynamic and static degradation of poly(vinyl chloride). *Journal of Applied Polymer Science*. 1982;27:2615-23.
- [19] Collins EA, Metzger AP, Furgason RR. Relationship between torque and capillary rheometer thermal stability measurements for PVC compounds. *Polymer Engineering & Science*. 1976;16:240-5.
- [20] Collins EA, Krier CA. Poly(vinyl chloride) thermal stability. I. Evaluation by melt rheology. *Journal of Applied Polymer Science*. 1966;10:1573-89.

- [21] François M, Renaudin G, Evrard O. A cementitious compound with composition $3\text{CaO}\cdot\text{Al}_2\text{O}_3\cdot\text{CaCO}_3\cdot 11\text{H}_2\text{O}$. *Acta Crystallographica Section C: Crystal Structure Communications*. 1998;54:1214-7.
- [22] Renaudin G, Francois M, Evrard O. Order and disorder in the lamellar hydrated tetracalcium monocarboaluminate compound. *Cement and Concrete Research*. 1999;29:63-9.
- [23] Reichle WT. Catalytic reactions by thermally activated, synthetic, anionic clay minerals. *Journal of Catalysis*. 1985;94:547-57.
- [24] Moyo L, Focke WW, Heidenreich D, Labuschagne F, Radosch H-J. Properties of layered double hydroxide micro-and nanocomposites. *Materials Research Bulletin*. 2013;48:1218-27.
- [25] Frost RL, Martens W, Ding Z, Kloprogge JT. DSC and high-resolution TG of synthesized hydrotalcites of Mg and Zn. *Journal of Thermal Analysis and Calorimetry*. 2003;71:429-38.
- [26] Levchik SV, Weil ED. Overview of the recent literature on flame retardancy and smoke suppression in PVC. *Polymers for Advanced Technologies*. 2005;16:707-16.
- [27] Ipavec A, Gabrovšek R, Vuk T, Kaučič V, Maček J, Meden A. Carboaluminate phases formation during the hydration of calcite-containing Portland cement. *Journal of the American Ceramic Society*. 2011;94:1238-42.
- [28] Gupta MC, Viswanath SG. Role of metal oxides in the thermal degradation of poly(vinyl chloride). *Industrial and Engineering Chemistry Research*. 1998;37:2707-12.
- [29] Li B. Study of thermal degradation and decomposition of rigid poly(vinyl chloride) with metal oxides using thermogravimetry and cone calorimetry. *Polymer Degradation and Stability*. 2000;68:197-204.

- [30] Blazsó M, Jakab E. Effect of metals, metal oxides, and carboxylates on the thermal decomposition processes of poly(vinyl chloride). *Journal of Analytical and Applied Pyrolysis*. 1999;49:125-43.
- [31] Malík J, Kröhnke C. Polymer stabilization: present status and possible future trends. *Comptes Rendus Chimie*. 2006;9:1330-7.
- [32] Šimon P. Considerations on the single-step kinetics approximation. *Journal of Thermal Analysis and Calorimetry*. 2005;82:651-7.
- [33] Dente M, Bozzano G, Faravelli T, Marongiu A, Pierucci S, Ranzi E. Kinetic Modelling of Pyrolysis Processes in Gas and Condensed Phase. In: Guy BM, editor. *Advances in Chemical Engineering*; Academic Press; 2007. p. 51-166.
- [34] Anderson HL, Kemmler A, Höhne GWH, Heldt K, Strey R. Round robin test on the kinetic evaluation of a complex solid state reaction from 13 European laboratories. Part 1. Kinetic TG-analysis. *Thermochimica Acta*. 1999;332:33-53.
- [35] Pospíšil J, Horák Z, Pilař J, Billingham NC, Zweifel H, Nešpůrek S. Influence of testing conditions on the performance and durability of polymer stabilisers in thermal oxidation. *Polymer Degradation and Stability*. 2003;82:145-62.
- [36] Kamal MR, Sourour S. Kinetics and thermal characterization of thermoset cure. *Polymer Engineering & Science*. 1973;13:59-64.
- [37] Brown ME. The Prout-Tompkins rate equation in solid-state kinetics. *Thermochimica Acta*. 1997;300:93-106.

Chapter 6: Conclusions and Recommendations

6.1 Overall conclusions

The performance of the hydrated fillers magnesium hydroxide, hydromagnesite and layered double hydroxides (LDHs) as heat stabilisers and flame retardants was investigated using plasticised PVC as matrix. These fillers were either obtained from commercial sources or synthesised using hydrothermal techniques. The fillers were comprehensively characterised using a wide range of instrumental techniques. Rheology was used to investigate the effect of stearic acid coating on the dispersability of the powders in a liquid. Emulsion grade PVC was plasticised with 100 phr diisononylphthalate and 30 phr stearic acid-coated hydrated filler. The heat stability and the fire performance properties of the composites were evaluated. It was found that the standard layered double hydroxide outperformed magnesium hydroxide and hydromagnesite with respect to static heat stability (Thermomat method) as well as most fire indices measured on a cone calorimeter. Next modified layered double hydroxides were prepared by (partial) replacement of either the magnesium or the aluminium ions in the clay with zinc, copper, iron or calcium. The effect of such modification on the heat stability and flame retardancy of the plasticised PVC was investigated. These samples were subjected to a wider range of heat stability tests including Metrastat and the torque rheometer dynamic method. It was found that these modifications had a significant effect on both heat stability and fire performance.

The detailed findings were as follows:

The effect of a stearic acid surface coating. The effect of a stearic acid coating on the dispersability of these plate-like powders was investigated. Dilute solutions of

stearic acid in acetone were prepared and used to coat the powders. The presence of the coating was confirmed by diffuse reflectance infrared spectroscopy (DRIFT) and quantified by XPS and thermogravimetric analysis. The coating level almost equivalent to monolayer coverage was achieved when the hydrotalcite and hydromagnesite powders were treated with 20 mL acetone/g filler containing 2.5 g L^{-1} stearic acid. Measured BET surface areas of the hydrotalcite and hydromagnesite powders decreased by as much as 33 % when coated with stearic acid. SEM showed that the hydrotalcite and magnesium hydroxide powders comprised small crystals that are profusely agglomerated. Owing to their fineness and tendency to agglomerate in high porosity structures, both the hydrotalcite and hydromagnesite powders are very effective thickening agents for white oil. The rheology of slurries containing 25 wt.% solids (ca. 11 vol.%) was studied as a function of shear rate. The suspended powders increased the apparent low-viscosity by several orders of magnitude. This substantial thickening effect was attributed to a tendency of the particles to aggregate as high-porosity flocs in the oil. A lower limit for the porosity of the flocs is estimated at 81 vol.% on the assumption that the flocs are spherical in shape and similar in size.

The suspensions also showed considerable shear thinning. This is consistent with the idea that the application of shear causes break-up of the agglomerates and releases the occluded fluid. The significantly lower viscosities observed for the stearic acid treated samples indicate that the surface coating reduced the adhesive forces between the particles. This made it easier to break-up the agglomerates and aids dispersion of individual particles. However, a reduction in the shear rate allowed for the reformation of the agglomerates.

Comparing the utility of the different hydrated fillers. Emulsion grade PVC was plasticised with 100 phr of diisononyl phthalate and filled with 30 phr layered double hydroxides (LDH), hydromagnesite or magnesium hydroxide as combination stabiliser-flame retardant additives. Amongst the three fillers, LDH displayed good performance in a static heat stability test and also significantly enhanced the fire resistance of the plasticised PVC. The other two did enhance the heat stability but only slightly. The LDH filler also outperformed magnesium hydroxide and hydromagnesite with respect to most fire retardancy indices as the fire growth rate (FIGRA), the maximum average rate of heat emission (MAHRE) and the fire performance index (FPI).

Fine tuning the layered double hydroxide for improved PVC heat stability.

Derivative compounds were synthesised and subjected to heat stability testing: $\text{Mg}_3\text{ZnAl}_2(\text{OH})_{12}\text{CO}_3 \cdot 4\text{H}_2\text{O}$; $\text{Mg}_3\text{CuAl}_2(\text{OH})_{12}\text{CO}_3 \cdot 4\text{H}_2\text{O}$; $\text{Mg}_4\text{AlFe}(\text{OH})_{12}\text{CO}_3 \cdot 4\text{H}_2\text{O}$, and $\text{Ca}_4\text{Al}_2(\text{OH})_{12}\text{CO}_3 \cdot 5\text{H}_2\text{O}$. Amongst these, $\text{Mg}_3\text{ZnAl}_2(\text{OH})_{12}\text{CO}_3 \cdot 4\text{H}_2\text{O}$ showed an improvement of colour retention in Metrastat static heat stability tests and $\text{Mg}_3\text{CuAl}_2(\text{OH})_{12}\text{CO}_3 \cdot 4\text{H}_2\text{O}$ showed a better performance as HCl scavenger recording a longer time preventing its release in the Thermomat evaluation. It was found that the best performance in dynamic heat stability tests was achieved with the conventional product ($\text{Mg}_4\text{Al}_2(\text{OH})_{12}\text{CO}_3 \cdot 4\text{H}_2\text{O}$).

Fine tuning the layered double hydroxide for PVC flame retardancy. The same composites were subjected to cone calorimetry fire testing. The addition of LDH derivatives significantly improved the fire resistance of the plasticised PVC. The partial substitution of the aluminium by Fe(III) in the LDH lowered the peak heat

release rate ($pHRR$), from $623 \pm 8 \text{ kW m}^{-2}$ to $253 \pm 5 \text{ kW m}^{-2}$ but increased the total heat release from $68 \pm 2 \text{ MJ m}^{-2}$ to $72 \pm 3 \text{ MJ m}^{-2}$. This MgFeAl-LDH also improved other fire resistance indices, e.g. the maximum average rate of heat emission ($MAHRE$) and the fire performance index (FPI). MgAl-LDH showed the lowest fire growth rate ($FIGRA$) while the MgCuAl-LDH showed the lowest smoke production.

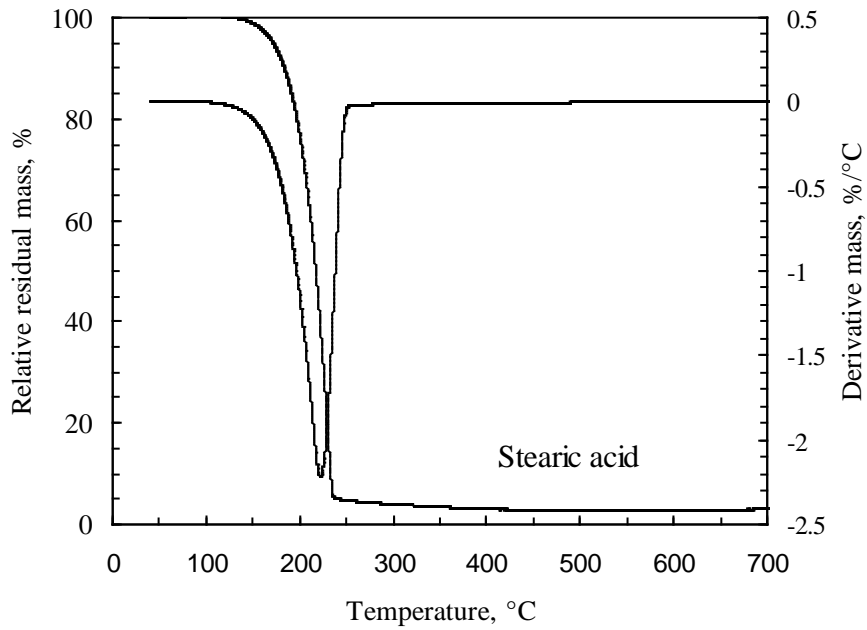
The most significant conclusion of this study is that partial metal substitution of conventional magnesium-aluminium LDH does affect additive performance in plasticised PVC. This means that there is scope for improving and tailoring this additive for particular applications.

6.2 Future Research

Although much research has been done on fire retardants and heat stabilisers, there is much scope for improvement. For example, other partial or full metal substitutions in LDH could be considered. An unexpected finding was that, in the plasticised PVC matrix, the LDH performed better as flame retardant than magnesium hydroxide and hydromagnesite. It would therefore be interesting to determine whether this holds for other polymers as well.

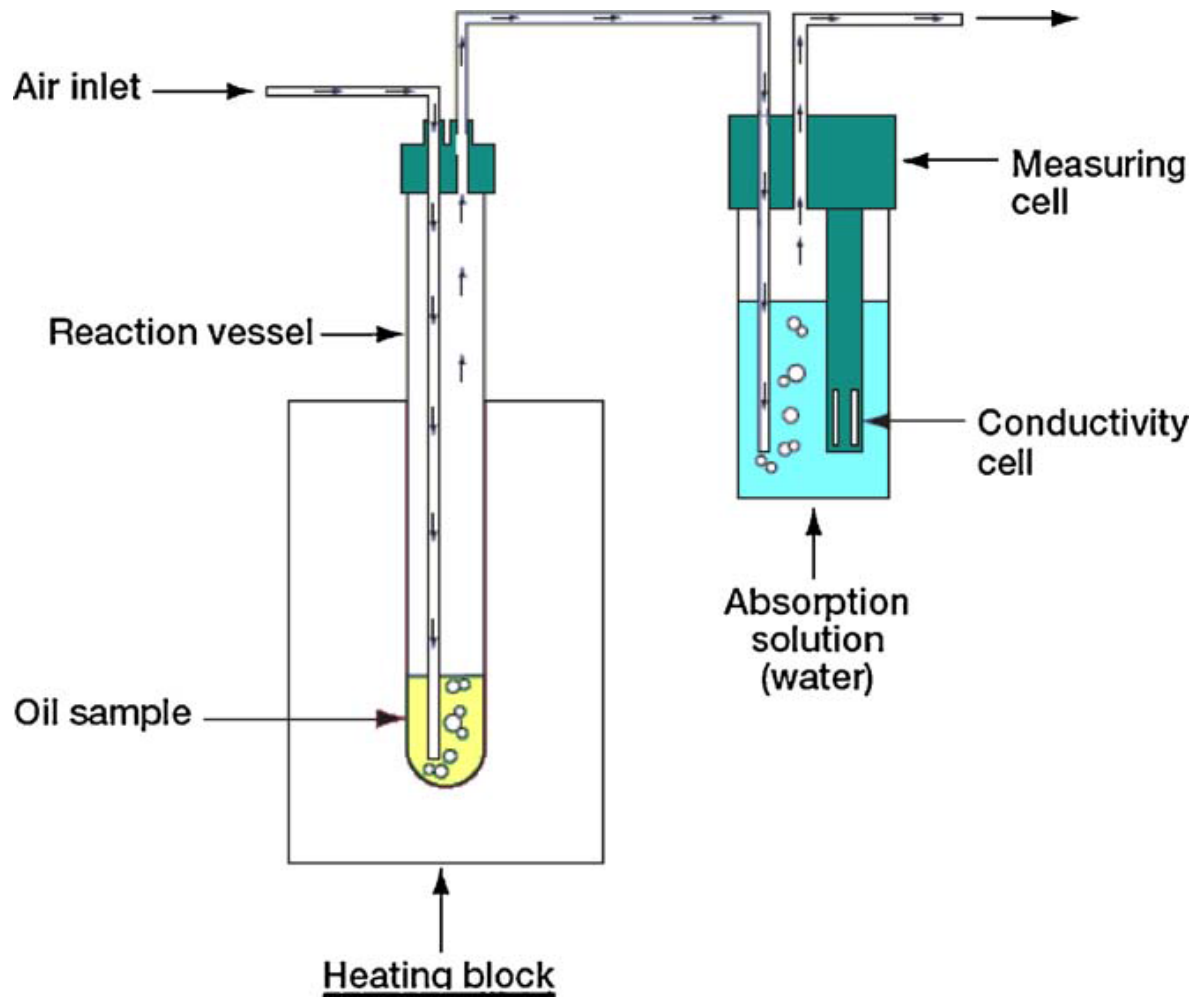
APPENDICES

Appendix A



TGA trace of stearic acid

Appendix B



Schematic of Rancimat test [1].

References

- [1] Jebe TA, Matlock MG, Sleeter RT. Collaborative study of the oil stability index analysis. *J Am Oil Chem Soc* 1993;70(11):1055–61.

Appendix C

Functional description of the Metrastat oven

These tests were performed in accordance to ASTM standards 2115-92, re-approved (2003). The static heat stability was determined in triplicate using sample strips measuring ca. 200 mm × 20 mm × 3.5 ± 0.1 mm. They were cut from the pressed sheets. A Metrastat heat stability oven was used. The strips were placed in the Metrastat trays of length 256 mm in random positions for each of the three runs. The machine automatically retracts the trays from the oven at a constant rate of 300 mm in 180 min. The oven temperature was set at 200 °C whilst maintaining a constant airflow across the samples and the air flow was 10 m³ min⁻¹.

The purpose of the constant airflow is to maintain a uniform temperature throughout the whole oven for all the samples placed on the tray. It also flushes air contaminated with HCl gas from the oven, which would accelerate polymer degradation.



Metrastat thermal stability oven used during this research

Appendix D

Pictures of Cone calorimeter used in this work



The name "Cone Calorimeter" was adopted from the symmetrical configuration of its radiant heater, conical electric heater. The calculations of Huggett [1] validated that the average heat of combustion for a broad range of materials is a constant 13.1 kJ g^{-1} oxygen consumed, with an accuracy of $\pm 5 \%$ or better. This idea is based on the information that the heat output from many combustible materials as well as most natural and synthetic plastics, rubbers and textiles is almost always a constant 13.6 kJ g^{-1} oxygen used up. A small scale apparatus, the Cone Calorimeter, developed and described by Babrauskas [3], utilizes this oxygen consumption principle to determine the rate release rate per unit area q'' . Thus the rate release rate can be determined with good

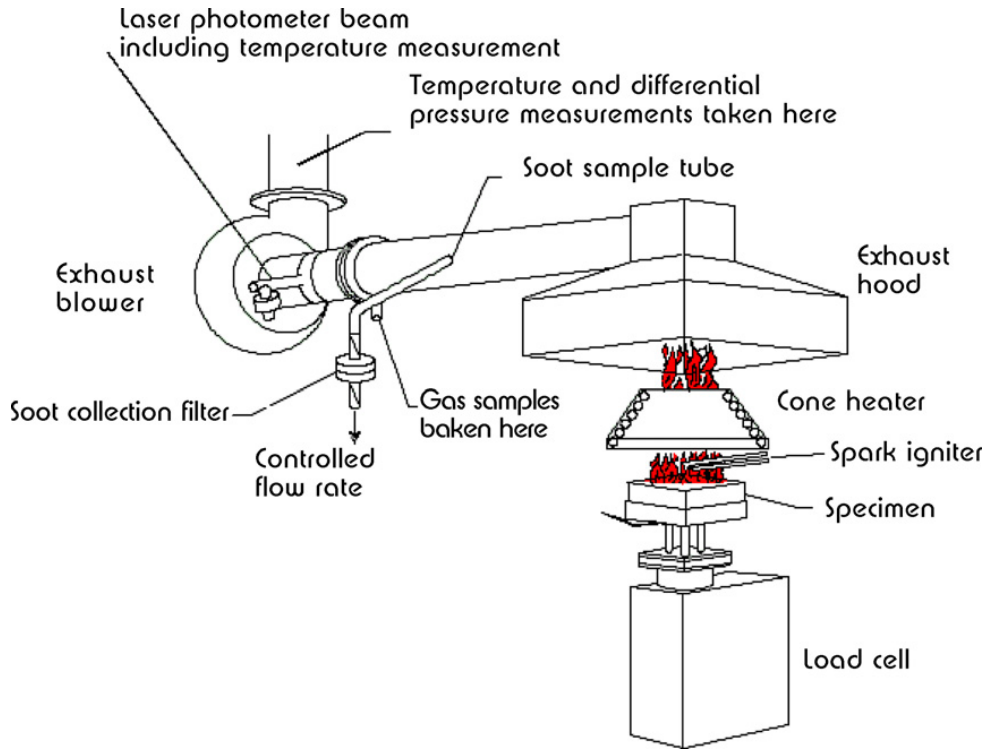
accuracy from two simple measurements, the flow rate of air through the combustion system and the oxygen depletion in this flow [2].

Data from this instrument can be used in research to predict the full-scale fire behaviour of certain furnishings and wall lining materials [4].

References

1. Huggett, C., "Estimation of Rate of Heat Release by Means of Oxygen Consumption Measurements", *Fire and Materials*, **4**, 61 (1980).
2. Parker, W.J., "Calculation of Heat Release by Oxygen Consumption for Various Applications", *J. Fire ScL 1*, 380 (1984).
3. Babrauskas, V., "Development of the Cone Calorimeter - A Bench-Scale Heat Release Apparatus Based on Oxygen Consumption", *Ibid* **8**, 81 (1984).
4. Babrauskas, V., "Bench-Scale Methods for Prediction of Full-Scale Fire Behavior of Furnishings and Wall Linings", Technology Report 84-10, Society of Fire Protection Engineers, Boston, M.A.

Fire Testing Technologies (FTT) cone calorimeter, accompanied by the experimental set up



One-dimensional burning model Detail of the cone calorimeter set-up

Appendix E

Photos of different samples showing the nature of the residue remaining after complete combustion of PVC composites samples during cone calorimeter testing



MOH

PVC

MgAl-LDH



CaAl-LDH

MgZnAl-LDH



MgCuAl-LDH

MgFeAl-LDH